Impacts of short-term climate change and anthropogenic activity on marine ecosystem variability and biogeochemical processes in the Gulf of Taranto (central Mediterranean Sea)

Dissertation with the aim of achieving a doctoral degree at the

Faculty of Mathematics, Informatics and Natural Sciences
Department of Earth Science
Universität Hamburg

Submitted by
Valerie Menke

Hamburg
2017

Datum der Disputation: 02.02.2018

Folgende Gutachter empfehlen die Annahme der Dissertation:

Prof. Dr. Gerhard Schmiedl

Dr. Uwe Mikolajewicz

Abstract

This study examines the variability of benthic ecosystems, depositional environments, biogeochemical processes and water mass dynamics on decadal to multi-decadal timescales in the Gulf of Taranto (central Mediterranean Sea). In the Gulf of Taranto, marine processes are closely linked to large-scale and regional climate patterns because precipitation changes in the Po River catchment and related fluctuations in riverine runoff drive changes in marine nutrient and suspended sediment load, local phytoplankton blooms and organic matter availability at the sea floor. This study focuses on the palaoclimatic and palaoecological evolution of the last millennium and further investigates the environmental impacts of short-term periods of cooling and drying events around 4.2 ka and 8.2 ka BP. The aim is to unravel the links between local environmental processes in the Gulf of Taranto and regional to large-scale climate patterns and its variability. The results will be further used to decipher natural and anthropogenic forcing mechanisms.

High sedimentation rates in the Gulf of Taranto allow for high-resolution paleoclimate studies, which rely on accurate age models. The location of the Gulf of Taranto, east of the Italian volcanic arc with numerous eruptions documented for the Holocene, suggests the use of tephroanalysis for the age assessment of marine sediment cores. Since macroscopically visible tephra layers are absent in Holocene sediments of the Gulf of Taranto, cryptotephrostratigraphy based on electron microprobe analysis of volcanic glass shards was used to characterize marine tephras and identify their source regions. Quantitative analysis of volcanic glass shard abundance identified two tephra layers in the uppermost 50 cm of gravity core GeoB15403-4. Geochemical fingerprinting supported by an AMS ^{14}C-based age model identified the pronounced primary tephra at 36 cm to originate from the felsic 776 AD Monte Pilato Eruption on the island of Lipari. A less pronounced peak of high alkali glasses at 1.5 cm core depth was produced by the 1944 AD Somma-Vesuvius eruption. These tephra layers were used to improve the stratigraphic framework for the investigated core and provide a solid basis for high-resolution palaoclimatic studies in the Gulf of Taranto. The inferred tephra provenance challenges interpretations from previous studies, where pyroclast quantity was tuned to historic eruptions. This underlines the importance of geochemically based tephrostratigraphy in a highly diverse volcanic region such as the eastern Mediterranean.

To examine climate and ecosystem variability as well as to identify anthropogenic influences over the last millennium, sediment cores from two sites in the Gulf of Taranto as well as benthic foraminifera from 43 surface sediment samples from the western Adriatic Sea and the Gulf of Taranto, were investigated. Elevated abundances of modern shallow to intermediate infaunal benthic foraminifera (SIIBF) trace the nutrient-rich Po outflow into the gulf and reflect an organic matter-rich depocenter in the north-eastern part of the gulf in recent times. Decreasing

Ca/Ti ratios, a proxy of terrestrial versus marine origin of sediment input, suggest increasing fluxes of land-derived material at ~1300 AD, which are driven by wetter conditions linked to persistently negative NAO modes. Smectite/Illite ratios record a variable Po river runoff and correlate well with NAO strength for the past ~300 years. The benthic foraminiferal ecosystem variability is closely linked to the Northern Hemisphere temperature record for the past millennium and spectral analysis shows periodicities of 50 to 70 years arguing for an Atlantic Multidecadal Oscillation (AMO) forcing on the hydrology and trophic conditions in the Gulf of Taranto. The effect of rising temperature and nutrient transport during the past 200 years is amplified by increasing anthropogenic activity leading to further enhancement of nutrient and organic matter fluxes. This is evident by increases in SIIBF and a decrease of $\delta^{13}C$ in tests of the infaunal *Uvigerina mediterranea* since ~1800 AD. The SIIBF decrease in the most recent decades likely reflects effects of stricter regulations on fertilizer use in Italy and the reduction of sediment transport due to the stabilization of river banks.

To characterize the centennial and multi-decadal variability of benthic ecosystems, water mass circulation and sediment transport during the 4.2 ka and 8.2 ka climate events, gravity core GeoB15403-4 and 44 surface sediment samples from the western Adriatic Sea and the Gulf of Taranto were investigated. High abundance of SIIBF before 8.5 ka BP and after 8 ka BP record the relatively eutrophic boundary conditions during eastern Mediterranean sapropel S1 formation. These eutrophic conditions are punctuated by a ~500 year long period of more oligotrophic conditions evident in rising abundance of epifaunal benthic foraminifera (EBF). The more oligotrophic conditions likely display overall colder and drier conditions with reduced river input during the 8.2 ka event. Short-term variability likely corresponds to variations of AMO driven temperature and precipitation patterns. The stable isotope records of EBF exhibit higher-amplitude variations around the 8.2 ka event compared to the 4.2 ka event. A positive correlation between epifaunal $\delta^{13}C$ and $\delta^{18}O$ values as well as the comparison with the isotope pattern of modern epifaunal foraminifera from the Gulf of Taranto and the Adriatic Sea identify water mass dynamics as the main driver for the observed early Holocene stable isotope variability at the deeper shelf. The observed shifts between a highly saline and nutrient-poor water mass (high $\delta^{18}O$ and $\delta^{13}C$) and a relatively fresh and nutrient-rich water mass (low $\delta^{18}O$ and $\delta^{13}C$) argue for changes in water mass provenance, most likely between the more oligotrophic Ionian Sea and the more eutrophic river-influenced Adriatic waters. The shelf environments of the eastern Gulf of Taranto during the 4.2 ka cold and dry event appear relatively stable and there is no evidence for major shifts in water mass dynamics but for centennial-scale changes in food fluxes on a generally low trophic level. Comparison of the trophic levels before 8.5 ka BP and modern environments of the Gulf of Taranto suggests, that human-induced eutrophication after ~1800 AD reaches similar magnitudes than the eutrophic conditions during early Holocene sapropel boundary conditions.

Kurzfassung

Im Rahmen dieser Arbeit wurden dekadische bis multidekadische Schwankungen in der Zusammensetzung benthischer Ökosysteme in marinen Ablagerungsräumen sowie in der Dynamik von Wassermassen im Golf von Tarent (zentrales Mittelmeer) untersucht. Im Golf von Tarent sind marine Prozesse eng an regionale und großräumige Klimaphänomene gekoppelt da zeitlich variable Niederschlagsmengen im Einzugsgebiet des Po dessen Abflussraten bestimmen und dadurch den Eintrag von Nährstoffen, Sedimentsuspension, Planktonblüten und die Verfügbarkeit von organischem Material am Meeresboden beeinflussen. Die vorliegende Arbeit konzentriert sich auf die paläoklimatische und paläoökologische Entwicklung während der letzten tausend Jahre und untersucht darüber hinaus die Auswirkungen kurzfristiger Kälte- und Trockenphasen um 4.2 ka und 8.2 ka vor heute. Das Ziel der Arbeit ist es die Verbindung zwischen den lokalen ökologischen Prozessen im Golf von Tarent und übergeordneten globalen Klimamustern im Hinblick auf ihre zeitliche Variabilität zu charakterisieren und die Auswirkungen von natürlichen und anthropogenen Einflüssen zu verstehen.

Die hohen Sedimentationsraten im Golf von Tarent ermöglichen Paläoklimastudien in sehr hoher zeitlicher Auflösung welche präzise Altersmodelle erfordern. Durch die Lage des Golfes, östlich der italienischen Vulkangebiete in denen während des Holozäns zahlreiche Vulkanausbrüche stattfanden, bietet sich dort dieTephrotratigraphie zur Altersbestimmung mariner Sedimentkerne an. Da in den holozänen Sedimentablagerungen im Golf von Tarent keine makroskopisch sichtbaren Tephralagen vorhanden sind, wurde sich auf die Kryptotephrostratigraphie konzentriert. Hierbei werden durch den Einsatz einer Elektronenmikrosonde mikroskopisch kleine vulkanische Gläsern auf ihre Elemenzusammensetzung hin analysiert und die Ergebnisse dazu verwendet, einzelne Tephralagen zu charakterisieren um ihre Herkunftsregion zu identifizieren. Die quantitative Analyse von Aschenpartikeln ließ auf zwei tephralagen in den oberen 50cm des Schwerelotkerns GeoB15403-4 schließen. Geochemisches *fingerprinting* unterstützt durch ein auf AMS^{14}C-Messungen basierende Altersmodel ergab, dass die primäre Aschenlage bei 36 cm von der felsichen Monte Pilato Eruption des Jahres 776 AD auf der Insel Lipari stammt. Die weniger deutliche Aschenlage bei 1.5 cm stammt von der Somma-Vesuv-Eruption von 1944 AD. Diese Tephralagen wurden genutzt um die Stratigraphie des untersuchten Sedimentkerns zu verbessern und bieten eine Referenz für weitere paleoklimatische Studien im Golf von Tarent. Die ermittelte Herkunft dieser Tephralagen stellt die Interpretationen zur Herkunft von Aschenlagen vorheriger Studien im hier untersuchten Zeitfenster in Frage. In diesen Studien wurde das Vorkommen von pyroklastischem Material semiqualitativ ermittelt und mit historischen Eruptionen korreliert. Dies unterstreicht die Wichtigkeit einer geochemisch

basierten Tephrostratigrapie vor allem in Regionen wie dem Mittelmeer mit seinen zahlreichen aktiven Vulkangebieten während des Holozäns.

Um die Variabilität des Klimas und der marinen Ökosysteme sowie anthropogene Einflüsse während des letzten Jahrtausends zu untersuchen wurden Sedimentkerne von zwei Stationen aus dem Golf von Tarent sowie Oberflächenproben von 43 Stationen aus dem westlichen Adriatischen Meer und dem Golf von Tarent analysiert. Die Untersuchung der Rezentfaunen ergab einen hohen Anteil von flach- bis mittel-infaunalen benthischen Foraminiferen (SIIBF) an der Gesamtfauna. Dieser Befund lässt auf einen Einfluss des nährstoffreichen Po-Ausflusses auf die benthischen Ökosysteme in der Adria und dem Golf von Tarant schließen. Darüber hinaus zeigt das räumliche Verteilungsmuster der rezenten SIIBF, dass sich im nordöstlichen Bereich des Golfes von Tarant ein Hochakkumulationsgebiet befindet, welches durch einen erhöhten Eintrag an organischen Material gekennzeichnet ist. Bei der Untersuchung der Sedimentkerne zeigten abnehmende Ca/Ti-Verhältnisse, die mithilfe von XRF-Messungen festgestellt worden sind, einen verstärkten Eintrag terrestrischen Materials um 1300. Dieser verstärkte Eintrag terrestrischen Materials kann in Verbindung mit feuchteren Klimaphasen während eines anhaltenden negativen Modus der Nordatlantischen Oszillation (NAO) in Verbindung gebracht werden. Die Smectit/Illit-Verhältnisse, die in der Tonmineralfraktion ermittelt wurden, deuten auf temporäre Schwankungen im Po-Abfluss hin und korrelieren mit der Stärke der NAO während der letzten ~300 Jahre. Die Schwankungen in den benthischen Foraminiferen-Vergesellschaftungen während des letzten Jahrtausends sind eng an die Temperaturvariabilität der Nordhalbkugel gekoppelt. Hierbei zeigten sich bei einer Spektralanalyse quasi-periodische Schwankungen von ~50 bis ~70 Jahren, die auf einen Einfluss der Atlantischen Multidekadischen Oszillation (AMO) auf die Hydrologie und das trophische Niveau im Golf von Tarent hinweisen. Es hat sich außerdem gezeigt, dass der Effekt von steigenden Temperaturen und einer verstärkten Nährstoffzufuhr während der letzten 200 Jahre durch den zunehmenden anthropogenen Einfluss im Einzugsgebiet des Pos und anderer Flüsse zusätzlich potenziert wird. Dies wird neben der Zunahme an infaunalen Arten auch durch abnehmende δ^{13}C-Werte in den Gehäusen der infaunal lebenden Foraminifere *Uvigerina mediterranea* seit etwa 1800 AD deutlich. Der beobachtete Rückgang der infaunalen Arten während der letzten Jahrzehnte ist wahrscheinlich ein Ergebnis der strengeren Reglementierung von Düngemitteln und einer Verminderung von Sedimenttransport durch die Stabilisierung von Flussbetten.

Um Schwankungen der benthischen Ökosysteme, der Meeresströmungen und des Sedimenttransports während der 4.2 ka und 8.2 ka Klimaevents zu untersuchen, wurden Proben des Schwerelotkerns GeoB15403-4 sowie 44 Oberflächenproben aus dem Adriatischen Meer und dem Golf von Tarent untersucht. Hohe Anteile von infaunalen Arten vor 8.5 ka vor heute und nach 8.0 ka vor heute reflektieren die relativ eutrophen

Rahmenbedingungen während der Ablagerung des Sapropels S1 im östlichen Mittelmeer. Diese eutrophen Bedingungen wurden von einer ~500 Jahre andauernden Phase von eher oligotrophen Bedingungen unterbrochen, die durch einen Anstieg epifaunaler benthischer Foraminiferen (EBF) angezeigt wird. Diese oligotrophen Bedingungen reflektieren wahrscheinlich generell kältere und trockenere Bedingungen während des 8.2 ka-Events, die mit verringerten Eintragsraten der Flüsse einhergingen. Die beobachte, kurzfristige Ökosystemvariabilität steht wahrscheinlich mit Schwankungen in der AMO und damit mit einer temperaturbedingten Niederschlagsveränderung während dieser Zeit in Verbindung. Die Verhältnisse der stabilen Sauerstoffisotope, die in Gehäusen von epifaunalen Foraminiferen gemessen wurde, zeigen größere Schwankungen während des 8.2 ka-Events als während des 4.2 ka-Events an. Die positive Korrelation zwischen den epifaunalen $\delta^{13}C$- und $\delta^{18}O$-Werten sowie der Vergleich mit rezenten Verteilungsmustern von Isotopenwerten epifaunaler benthischer Foraminiferen weist auf einen starken Einfluss unterschiedlicher Wassermassen auf den tieferen Schelf im Golf von Tarent während des frühen Holozäns hin. Die Schwankungen lassen zwischen einer salzreichen und nährstoffarmen (erhöhtes $\delta^{18}O$ und $\delta^{13}C$) Wassermasse aus dem ionischen Meer und einer relativ salzarmen und nährstoffreichen (niedriges $\delta^{18}O$ und $\delta^{13}C$) Wassermasse aus der eutrophen Adria unterscheiden. Die Schelfökosysteme lassen auf wesentlich stabilere Bedingungen während des 4.2-Events schließen. Es ergab sich kein Hinweis auf längerfristige Veränderungen der Wassermassendynamik. Kurzfristige Schwankungen im $\delta^{13}C$-Isotopensignal weisen jedoch auf eine dekadische Variabilität in der Nahrungsverfügbarkeit unter generell oligotropheren Bedingungen am Meeresboden ihn. Der Vergleich zwischen den trophischen Bedingungen vor 8.5 ka vor heute und den Ökosystemen während der letzten rund 1000 Jahre deutet darauf hin, dass die anthropogene Eutrophisierung seit etwa 1800 ähnliche Größenordnungen erreicht wie die eutrophen Bedingungen während der Sapropel-Ablagerung im östlichen Mittelmeer.

Table of contents

1 Introduction

Against the background of a warming climate, it is crucial to understand the forcing factors of past climate change and their impact on marine and terrestrial ecosystems (IPCC, 2014). Over the past decade there has been considerable progress in both, proxy data reconstruction of large-scale trends and climate modelling to assess natural and anthropogenic forcing (e.g., Chevalier et al., 2017; Donders et al., 2008; Grimm et al., 2015; Tierney et al., 2011). However, high-resolution proxy records on decadal to multi-decadal time scales are still sparse but necessary to assess causal factors and spatial patterns of the observed changes, and to validate the results of modelling studies. In this context, the Holocene is of particular interest for climate research since its relatively stable conditions are interrupted by several periods of short-term climate change, which impacted the large-scale ocean circulation, precipitation patterns, terrestrial and marine ecosystems as well as human population.

The Mediterranean Sea is especially sensitive to climate variability because it is a semi-enclosed basin located at the transition between the temperate mid- to high- latitudes and the subtropical low-pressure belt. Furthermore, for the past millennia, the Mediterranean borderlands have been subject to intense land use and agricultural activity altering the discharge of nutrients and suspended sediment to near-coastal waters (e.g., Holmgren et al., 2016; Lamb 2013; Pongratz et al., 2008). This makes the Mediterranean Sea a highly complex system where distinguishing between natural and anthropogenic forcing is particularly complicated. It is therefore crucial to decipher the Mediterranean Sea's response to orbital and suborbital climate dynamics and abrupt shifts, and its large-scale teleconnections.

Among these short-term Holocene climate events, the 8.2 ka BP cold event is the most prominent climate perturbation causing a severe drought that lead to a fundamental societal and cultural reorganization of human populations (Staubwasser and Weiss, 2006; Turney and Brown, 2007; Weis and Bradley, 2001; Weninger et al., 2006). It interrupted a period of relatively wet and warm conditions and resulted in a basin-wide anoxia of the eastern Mediterranean Sea, the collapse of benthic ecosystems at the sea floor and the formation of the sapropel layer S1 (De Rijk et al., 1999; Emeis et al., 2000; Rohling and Hilgen, 2007).

In comparison to the 8.2 ka event that is mostly prominent in northern Hemisphere records, the 4.2 ka event is characterized by a severe drought in the semiarid regions of the North African Monsoon margin (Grootes and Stuiver, 1997; Schulz and Paul, 2002). This drought in the Mediterranean and the Near East was cited as one main reason for the collapse of the Old Egyptian Kingdom and the Akkadian Empire in Mesopotamia (Arz et al., 2006; Drysdale et al., 2006; Weiss et al., 1993). Even though severe environmental changes, like a decline in Nile River discharge and an increase in dust fluxes from the Sahara desert, are reported for the

southern Mediterranean borderlands, its characteristics in the northern Mediterranean borderlands are not well understood (Zanchetta et al., 2016).

Climate anomalies on historic timescales were less pronounced in the Mediterranean region but still had a severe impact on ecosystems and human population. For the past millennium there were two important periods, comprising the Medieval Warm Period (MWP), characterized by warm and relatively dry conditions in central Europe (from ~600 AD to ~ 1400 AD) and the Little Ice Age, a period of low Northern Hemisphere temperatures and wet conditions (from ~1400 AD to ~1850 AD) (e.g. Abrantes et al., 2005; Guiot and Corona et al., 2010; Frisia et al., 2005; Lebreiro et al., 2006).

The faunal and geochemical composition of benthic foraminifera provide an ideal proxy for the reconstruction of climate and circulation changes and trophic conditions (De Rijk et al., 1999; Jorissen et al., 1992, 1995; Schmiedl et al., 2000; Theodor et al., 2016 a, b). Their abundance and faunal composition depends on organic matter fluxes and bottom water oxygen availability, both factors that are linked to surface water productivity, atmospheric circulation, anthropogenic activity and land-sea nutrient fluxes. Benthic foraminifera inhabit different stratified microhabitats. Epifaunal benthic foraminifera live on top of the sediment or even attached to elevated surfaces and are well adapted to oligotrophic conditions with well oxygenated bottom waters (Jorissen et al., 1995). Infaunal benthic foraminifera live up to several centimeters within the sediment and are more tolerant to high organic matter supply and less available oxygen (Fontanier et al., 2002; Koho et al., 2008). In the oligotrophic Mediterranean Sea, near-coastal environments are commonly characterized by high benthic foraminifera standing stocks and diversity especially when river-derived nutrients lead to elevated OM fluxes and productivity (Jorissen et al., 1995; Schmiedl et al., 2000). The stable isotope signature of benthic foraminifera tests on the other hand can be used to reconstruct changes in deep-water ventilation and organic matter fluxes (e.g. Duplessy et al., 1988; Imbrie et al., 1984; Schmiedl at al., 2004; Shackleton 1987; Theodor et al., 2016 a, b). In the Mediterranean Sea, variation in benthic foraminifera $\delta^{13}C$ and $\delta^{18}O$ has proved to be useful to reconstruct varying trophic conditions for example during the last deglaciation, to assess deep water stagnation and reventilation during sapropel formation, as well as to investigate deep water properties on longer timescales (Grimm et al., 2015; Vergnaud-Grazzini and Pierre, 1991; Melki, 2011).

Foraminiferal faunas and their stable isotope composition in the Gulf of Taranto (central Mediterranean Sea) are especially prone to recording short-term climate variability and anthropogenic influence. Here, river input presents a significant organic carbon and nutrient source triggering marine export production but also directly supplying organic matter to the seafloor. This links hydrological changes driven by precipitation over the densely populated Po

Valley to the environmental conditions at the seafloor (Grauel et al., 2013 a; Goudeau et al., 2014; Zonneveld et al., 2012).

In addition to benthic foraminifera records, total organic carbon and nitrogen yields of bulk sediment are a useful proxy for the quantification of organic matter yields and the C/N ratio allows for an estimate of terrestrial versus marine organic matter provenance (e.g. Aksu et al., 1999; Fabiano et al., 1995; Thornton and McManus, 1994).

Clay minerals on the other hand represent a proxy that is independent of sea floor ecology. Their abundance mainly depends on the source rock and the local and large-scale climatic conditions allowing to identify the source area and dispersal pathway (Biscaye 1965; Ehrmann et al., 2007; Venkatarathnam and Ryan, 1971). The relative element composition of bulk sediments from the Gulf of Taranto has successfully been used as a proxy for detrital versus marine biogenic fluxes providing an additional tool for the characterization of environmental variability and provenance of suspended matter in the gulf (Goudeau et al., 2014).

Furthermore, high sedimentation rates in the Gulf of Taranto allow for high resolution studies on marine sediment cores and its location, downwind of several volcanoes that erupted regularly during the Holocene, allows for precise age dating (Bonino et al., 1993; Castangnoli et al., 1990; Taricco et al., 2009).

In light of the above, three research objectives arise and are elaborated in the following section.

1.1 Scientific hypotheses and research objectives

Due to high sedimentation rates in the Gulf of Taranto and its location, downwind of the Italian volcanic arc, tephrostratigraphy provides a high-resolution, ^{14}C- independent stratigraphic framework for the age assessment of marine sediment cores.

During the Holocene, numerous eruptions of the Mt. Vesuvius, the Phlegrean Fields, the Eolian Islands and the Palinuro seamount lead to the deposition of thick distal ash layers in the Mediterranean region (e.g. Siani et al., 2004; Wulf et al., 2008). However, there are no macroscopically visible tephra layers in the uppermost sediment record of the Gulf of Taranto (Goudeau et al., 2014; Menke et al. 2017 a under review). Previous studies from the eastern Gulf of Taranto used the relative abundance of pyroxene grains to identify several tephra layers in marine sediment cores and correlated them to historic volcanic eruptions of the past two millennia (Castangnoli et al., 1990; Bonino et al., 1993; Taricco et al., 2009). However so far, there is no evidence for the source of ash layers based on the geochemistry of the tephra material. This study aims to identify the origin of cryptotephras by applying geochemical fingerprinting of volcanic glass shards. Microprobe analysis can provide evidence for the provenance of eruptive material and allow for the correct correlation of corresponding historic

eruptions. This will improve the stratigraphic framework of sediments from the Gulf of Taranto and adjacent areas and provide a solid basis for further high-resolution paleoclimatic studies.

Italian hydrology, marine sedimentation and benthic ecosystem dynamics in the Gulf of Taranto are closely linked to changes in North Atlantic climate modes and are additionally forced by anthropogenic activity during the past millennium.

On orbital time-scales, the Mediterranean Sea responds to precession-driven changes in African Monsoon strength (Cramp and O'Sullivan, 1999; Emeis et al., 2000; Weldeab et al., 2014). On suborbital time-scales, the North Atlantic climate dynamics are important drivers of Mediterranean temperature and precipitation (Bar-Matthews et al., 1999; Cacho et al., 2001; Rohling and Pälike, 2005, and references therein). On decadal to centennial time scales, the influence of the North Atlantic Oscillation (NAO) and the Atlantic Multidecadal Oscillation (AMO) is evident but spatial and temporal dynamics are not well understood (Beniston et al., 1994; Enfield et al., 2001; Frisia et al., 2003; Knight et al., 2006; Marullo et al., 2011; Hurrel 1995, 2001; Sutton and Hodson, 2005). This natural climate variability is likely overprinted by anthropogenic effects during the past millennium because rising population numbers, the advancement of fertilizing techniques and intensified industrial production also impacted coastal marine ecosystems (Degobbis et al., 2000; Giordani and Angiolini, 1983; Justic, 1987; Lahmeyer, 2006; Lotze et al., 2011, Marchetti et al., 1989; McEverdy and Jones, 1978). This study evaluates new high-resolution records of benthic foraminifera faunal, stable isotopic and bulk sediment biogeochemical changes to gain insights into the dynamics of organic matter fluxes and benthic ecosystems in the Gulf of Taranto during the past millennium. In addition, clay minerals and element ratios derived by X-ray fluorescence characterize the depositional environments independent of ecological processes. This multiproxy approach allows for a comprehensive reconstruction of past environmental and climatic changes, the connection to large scale climate patterns and the identification of the relative contributions of natural and anthropogenic forcing.

Multi-decadal to centennial climate changes are superimposed on the 8.2 ka and 4.2 ka events in the central Mediterranean. Associated variations in circulation and trophic conditions are amplified or attenuated depending on the respective Holocene orbital boundary conditions.

During the relatively stable and warm conditions of the Holocene, the 8.2 ka and 4.2 ka events represent periods of cool and dry conditions that had a severe impact on ecosystems and human populations in the Mediterranean region (Arz et al., 2006; Dansgaard et al., 1993; De

Rijk et al., 1999; Drysdale et al., 2006; Grootes and Stuiver, 1997; Rohling et al., 1997; Staubwasser and Weiss, 2006; Weiss and Bradley, 2001; Weiss et al., 1993; Zanchetta et al., 2016). However, the timing, causes and spatial variation of both events are still subject of debate (e.g. Rohling and Pälike 2005 and references therein; Zanchetta et al., 2016). High sedimentation rates in the Gulf of Taranto allow for the identification of short-term climate perturbations and give insights into the characteristics of both events as well as their internal variability. The combination of benthic foraminiferal fauna data and foraminiferal stable isotope signals with clay mineral ratios allows to identify changes in organic matter fluxes, water mass characteristics and depositional dynamics and to link these changes to large-scale climate forcing and modes of decadal to multi-decadal climate variability.

1.2 Thesis outline and author contributions

The presented thesis is subdivided into six chapters:

Chapter 1 The first chapter provides an introduction into climate variability of the Mediterranean region, explains the general motivation of this study and introduces the research hypotheses and objectives.

Chapter 2 The second chapter gives an overview of the geological development of the Mediterranean Sea as well as the present oceanographic conditions and climate patterns.

Chapter 3 Chapter three is based on a manuscript under review in "Quaternary Research": **Menke V., Kutterolf S., Sievers C., Schindlbeck J. and Schmiedl G.: Cryptotephra from Lipari Volcano in the eastern Gulf of Taranto (Italy) – A ^{14}C- independent time marker for paleoclimatic studies.** In this study, microprobe analysis of volcanic glass shards identifies and characterizes cryptotephra layers in the Gulf of Taranto. The timing of the corresponding volcanic eruptions improves the age assessment of marine sediment cores from this area and provides a stratigraphic framework for further, high-resolution paleoclimate studies. Steffen Kutterrolf and Julie Schindlbeck conducted microprobe analyses and significantly contributed to the data interpretation and discussion. The Bachelor thesis of Carina Sievers served as a pilot study for the applicability of tephroanalysis in the investigated sediment core. Gerhard Schmiedl as my main doctoral advisor contributed to data interpretation and manuscript preparation.

Chapter 4 Chapter four is based on a manuscript under review in "Climate of the Past": **Menke V., Ehrmann W., Milker Y., Brzelinski S., Möbius J., Mikolajewicz U., Zolitschka B., Zonneveld K., Emeis K.C., Schmiedl G.: Combined North Atlantic and anthropogenic forcing of changes in the marine environments in the Gulf of Taranto (Italy) during the last millennium.** This study investigates the multi-decadal to centennial variability of depositional environments, benthic ecosystems and biogeochemical processes over the past millennium in the Gulf of Taranto. Results suggest a link between the clay mineral record and a shift to persistently negative NAO phases. Benthic ecosystems show a link to AMO variability. Eutrophication since ~1800 AD is most likely influenced by anthropogenic activity. Gerhard Schmiedl, Yvonne Milker, Werner Ehrmann, Jürgen Möbius and Uwe Mikolajewicz contributed to the data interpretation, discussion and manuscript preparation. Swaantje Brzelinski conducted the faunal analysis of GeoB15406-4, Yvonne Milker

analyzed the Recent foraminiferal faunas of the surface samples, Werner Ehrmann conducted the clay mineral analyses and Bernd Zolitschka performed the XRF scans. Kay Christian Emeis supported the processing and evaluation of biogeochemical samples and Karin Zonneveld organized the research cruise. All authors contributed to the manuscript preparation.

Chapter 5 Chapter five is based on a manuscript in preparation for submission: **Menke V., Ehrmann W., Mikolajewicz U., Winkelbauer H. A., Theodor M., Mackensen A., Andersen N., Schmiedl G.: Centennial-scale climate modulation of the 8.2 ka and 4.2 ka events in the Central Mediterranean Sea.** This study investigates the climate variability and its influence on the marine environment during the 4.2 and 8.2 climate events. Benthic foraminiferal abundance displays a ~500 year-long shift to oligotrophic conditions corresponding to the 8.2 ka event. Benthic foraminiferal stable isotopes display a centennial-scale variability in water mass dynamics. In contrast, stable isotopes during the 4.2 ka event remain relatively stable and show no pronounced cooling or drying. Werner Ehrmann conducted the clay mineral measurements and evaluation, Andreas Mackensen measured the stable isotopes in foraminiferal tests from the core intervals and Nils Andersen measured the stable isotopes in tests from the surface sediment samples. Helge Arne Winkelbauer helped with sample processing and evaluation of the 4.2 ka stable isotope record. Marc Theodor and Uwe Mikolajewicz contributed to the data interpretation and Gerhard Schmiedl contributed to the data interpretation and manuscript preparation.

Chapter 6 The last chapter concludes the findings of this study with regard to the three research hypotheses. Finally, open questions and further research opportunities are outlined.

2 Study area

2.1 Geography and geology of the Mediterranean Sea

The Mediterranean Sea is a relatively small, semi-enclosed basin nearly landlocked by Africa in the south, Europe in the north and Asia in the east (Fig. 2.1). It extends over 3700 km from east to west and 1600 km from north to south, covering 2.5 million km^2 with an average water depth of 1500 m (Lionello et al., 2006; Tsimplis and Bryden, 2000). The Mediterranean Sea is subdivided into two basins: the western and the eastern Mediterranean basin. The western Mediterranean Sea is connected to the Atlantic Ocean through the 14.5 km wide and ~345 m deep Strait of Gibraltar. It consists of, 1) the Alboran Basin connected to the Atlantic, 2) the Algerian Basin connected to the eastern Mediterranean Sea, 3) the Tyrrhenian Basin bordering Italy, and 4) the Provencal Basin in the center (Wüst, 1960). The western Mediterranean Sea is connected to the eastern Mediterranean basin through the 150 km wide and ~330 m deep Strait of Sicily and the smaller (3- 5 km wide and ~250m deep) Strait of Messina (Robinson et al., 2001; Wüst, 1960). The eastern Mediterranean Sea consists of, 1) the Ionian Basin with the Mediterranean Sea's maximum water depth of 5150 m, 2) the Levantine Basin in the east with the Nile River as its dominant freshwater source, 3) the Aegean Sea in the northeast, connected to the Black Sea through the Dardanelles, Marmara Sea and Bosphorus, and 4) the Adriatic Sea in the north with the Po River as its main freshwater source (Wüst, 1960).

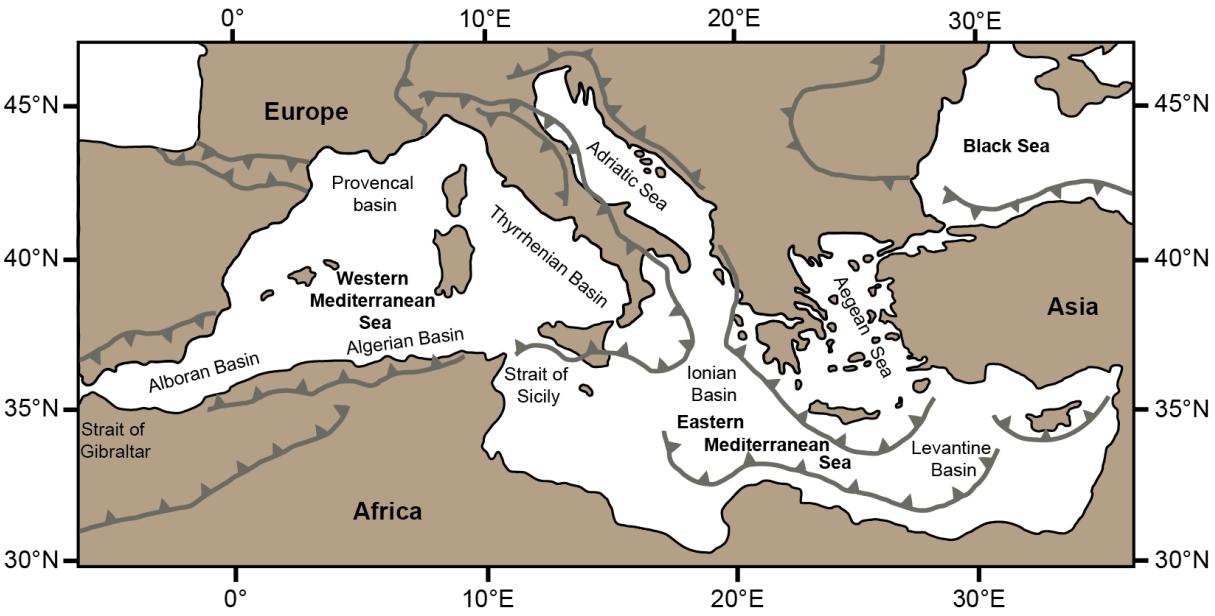

Figure 2.1. Simplified geographic map of the Mediterranean Sea. Grey lines show major thrust faults and subduction zones (modified after Dilek, 2006).

The Mediterranean Sea developed from the Tethys Ocean, a large Mesozoic gulf surrounded by Gondwana and Laurasia. In the Cenozoic, the breakup of Gondwana led to the closure of the Tethys and the development of the Paratethys and the Mediterranean Sea (Rögl, 1999). Northward migration of the African plate closed the Mediterranean Sea's connection to the Atlantic and led to cycles of desiccation between 5.96 and 5.33 million years BP known as the Messinian Salinity Crisis (Hilgen et al., 2007; Hsü et al., 1977). The reopening of the Strait of Gibraltar and the rapid flooding of the Mediterranean basin led to the early Pliocene development of oceanographic conditions close to those prevalent in the modern Mediterranean Sea (Cramp and O'Sullivan, 1999; Rossignol-Strick, 1983).

The present day Mediterranean region remains tectonically highly active. The geodynamic setting of Italy is especially intricate with evidence for regular earthquakes and volcanic eruptions throughout the Quaternary (Keller et al., 1978; Montone et al., 2004).

2.2 Oceanography, climate and productivity of the Mediterranean region

The present Mediterranean Sea is characterized by a generally counterclockwise surface water circulation and an anti-estuarine general circulation caused by a negative water budget (Figs. 2.2 and 2.3). In the Mediterranean Sea, evaporation exceeds precipitation and the Atlantic Water (AW) entering the Mediterranean basin through the Strait of Gibraltar at depths between 75 and 150 m, and with a salinity (S) below 37 psu, becomes warmer and saltier (with up to 39 psu) as it continues eastwards as Modified Atlantic Surface Water (MAW) (Malanotte-Rizzoli and Hecht, 1988) (Fig. 2.3).

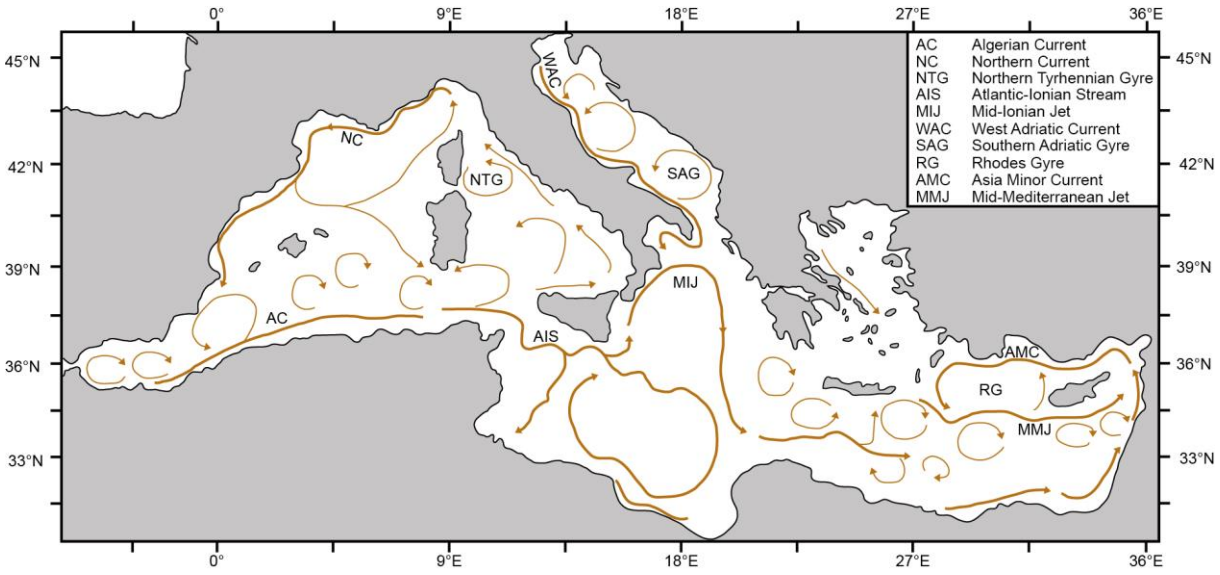

Figure 2.2. Schematized overview of the mean surface circulation patterns in the Mediterranean Sea (redrawn after Poulain et al., 2001).

Winter cooling causes a vertical convection and down-welling in the Levantine Basin forming the Levantine Intermediate Water (LIW) (Robinson et al., 2001; Wüst, 1961). The LIW flows westward at a depth of ~150-600m and enters the Atlantic Ocean as Mediterranean Outflow Water (MOW) (Millot and Taupier-Letage, 2005). The LIW is the source for deep-water formation in both basins. The Western Mediterranean Deep Water (WMDW) is formed in the Gulf of Lyons while the Eastern Mediterranean Deep Water (EMDW) is formed in the Adriatic and the Aegean seas (Millot and Taupier-Letage, 2005; Robinson et al., 2001). Western and eastern Mediterranean deep waters are generally divided by the Strait of Sicily with the exception of a few isolated events when Bernoulli aspiration lifts deep waters above the strait (Béranger et al., 2004).

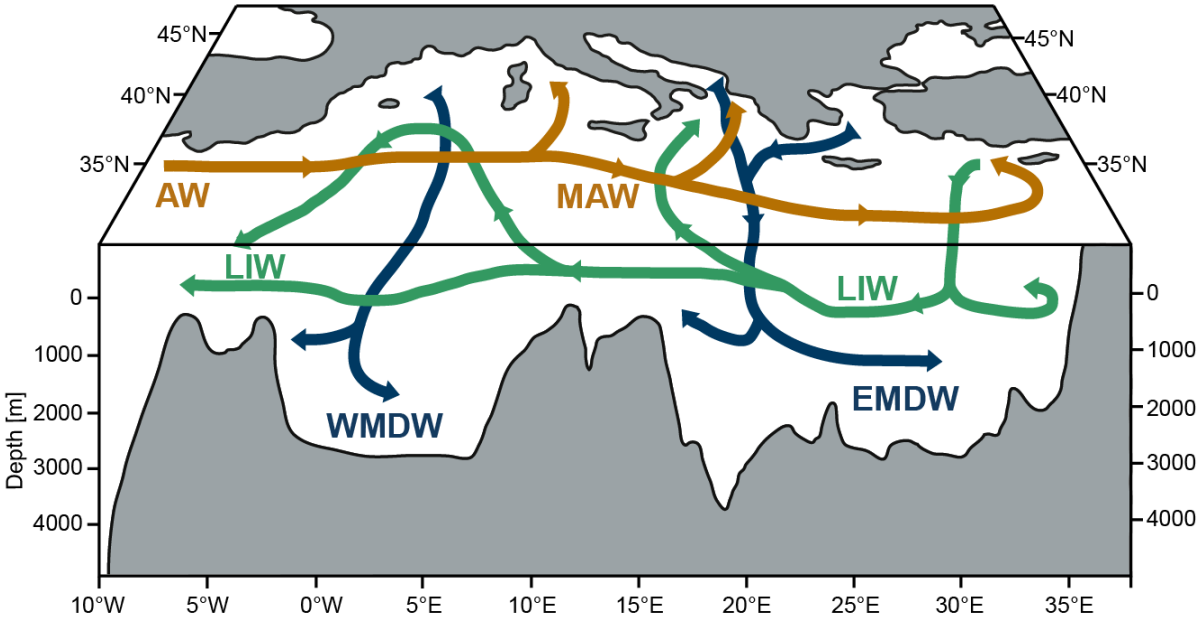

Figure 2.3. Simplified model of the general circulation in the Mediterranean Sea (modified after Tsimplis et al., 2006; Pinardi et al., 2015). Surface water masses (orange) are Atlantic Water (AW) and Modified Atlantic Water (MAW). Levantine Intermediate Water (LIW) is displayed in green. Western Mediterranean Deep Water (WMDW and Eastern Mediterranean Deep Water (WMDW) are shown in blue.

The Mediterranean Sea is located at the transition between the temperate northern high-latitudes (westerlies) and the arid climate of the low-latitudes (subtropical low-pressure belt). Two main drivers of the northern climate systems are the North Atlantic Oscillation (NAO) and the Atlantic Multidecadal Oscillation (AMO). The pathway of the moisture-rich westerlies is closely linked to the NAO (Hurrell, 1995). Fluctuations in the NAO are characterized by the NAO index, a measure for pressure differences between a high-pressure cell over the Azores and a low-pressure cell over Iceland. A positive NAO mode is associated with relatively cold and dry winters, and a negative NAO index corresponds to warm and wet winters in the Mediterranean region (Fig. 2.4) (Luterbacher et al., 2006; Trouet et al., 2009; Xoplaki et al.,

2006). The AMO is correlated to summer temperature and precipitation patterns, especially in North America and Europe, and is found to fluctuate quasi-periodic variability on timescales of 50-70 years (Enfield et al., 2001; Knight et al., 2005; Sutton and Hodson, 2005).

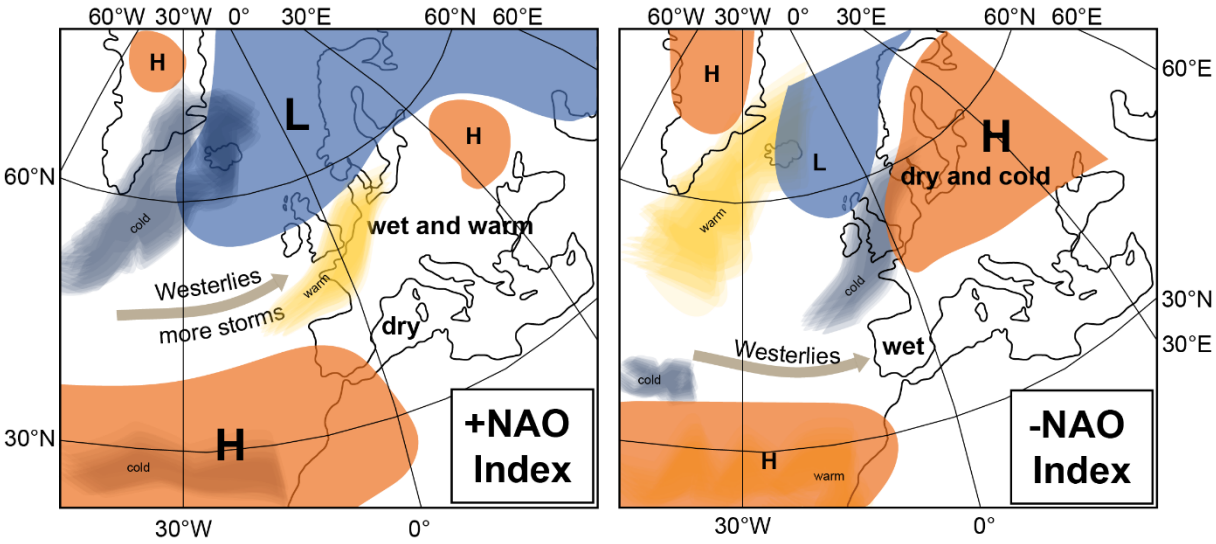

Figure 2.4. Simplified scheme of surface pressure (high pressure H, low pressure L), relative temperature, position of the westerlies, and precipitation during phases of positive NAO index (top) and negative NAO index (after Stenseth et al., 2003, Hurrel et al., 1995, background map from https://www.diercke.de/content/).

Its origin is thought to either be linked to the internal variability of the North Atlantic branch of the thermohaline circulation, or a free oscillation motion of the ocean-atmosphere coupled system (Delworth and Mann, 2000; Jungclaus et al., 2005). The Arctic climate can influence the Mediterranean through cold air outbreaks occurring when there is a high-pressure cell over the polar region and a low pressure zone between ~37° and ~45°N coupled with weak zonal winds. During a negative Arctic Oscillation (AO) polar air travels into mid-latitudes, while during a positive AO mode cold air remains trapped in the polar region by a constant mid-latitude jet stream. In the south, the Mediterranean climate is influenced by shifts in the Intertropical Convergence Zone (ITCZ) (Fig. 2.5). The ITCZ is a low-pressure system between the northern and southern hemisphere Hadley Cells. In northern hemisphere summer, it moves further north resulting in warm and dry conditions in the Mediterranean and in winter it shifts further south, and the westerlies exert a dominant influence on Mediterranean climate. The summer position of the ITCZ drives monsoon intensity in northern Africa most prominently evident in the last African Humid Period (AHD) when a persistent northward position during boreal summer resulted in enhanced rainfall in the Saharan desert between 14.8 and 5.5 kyr BP (e.g. DeMenocal et al. 2000). The northward position of the ITCZ is linked to a maximum in northern hemisphere insolation and ultimately resulted in the formation of the organic rich sediment layer of sapropel S1 in the early Holocene (Rohling et al., 2015). Sapropels are found primarily

in the deeper parts of the eastern Mediterranean basin and are most likely caused by a combination of increased primary production and water column stratification, preventing deep-water formation and fostering the preservation of organic matter (OM) (Emeis et al., 2000; Rohling et al., 2015; Schmiedl et al., 2010).

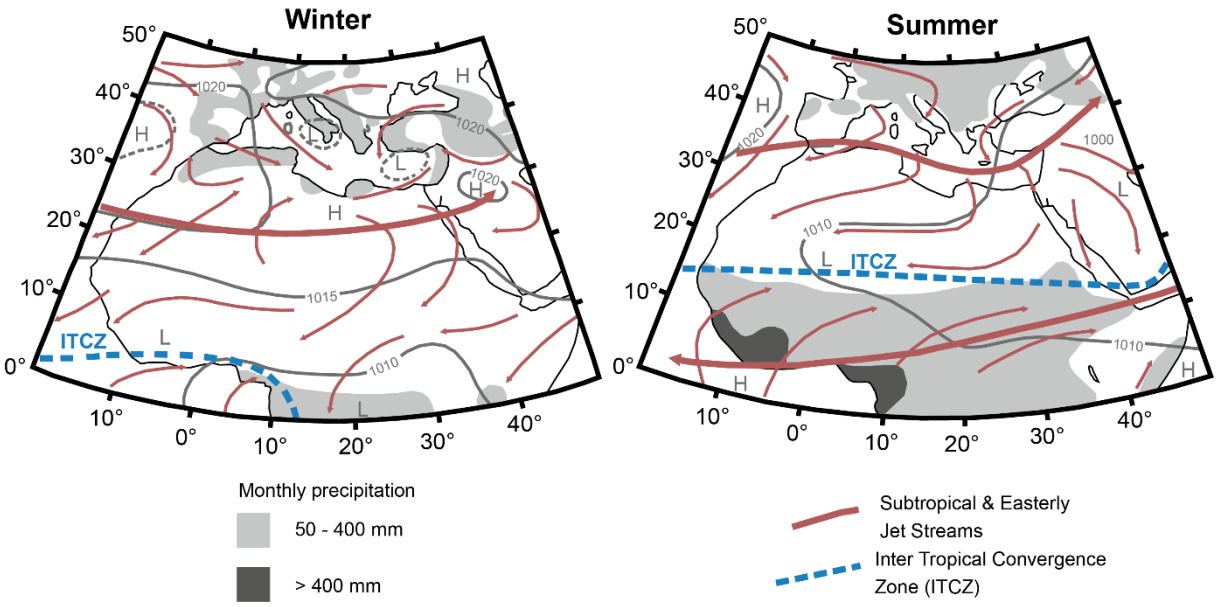

Figure 2.5. Simplified schemes of surface pressure (high pressure H, low pressure L), wind, precipitation and position of the Inter Tropical Convergence Zone (ITCZ) over the Mediterranean and northern Africa for winter (left) and summer (right) (redrawn from Cramp and O'Sullivan, 1999).

The offshore areas of the present Mediterranean Sea are oligotrophic and characterized by low sedimentation rates (Fig. 2.6) (Tanhua et al., 2013). Surface water primary production, derived from chlorophyll *a* data, is higher in the western Mediterranean basin (~160 g C/m^2/year) than in the eastern basin (~110 g C/m^2/year). Highest primary production occurs in near-shore areas and particularly in areas influenced by large river systems like the Po and Nile Rivers where high amounts of nutrients and suspended sediments are introduced into the sea (Fig. 2.6) (Antoine et al., 1995; Barale et al., 2008; Psarra et al., 2000).

2.3 Gulf of Taranto

The Gulf of Taranto is located at the southerneastern tip of Italy in the central Mediterranean Sea. It has a maximum water depth of 2400m and consists of three morphological provinces: the Calabrian Margin, the Taranto Valley and the Apulian Shelf (Rossi et al., 1983). This study focuses on sediments from the eastern Apulian Shelf, a narrow, 15 km wide band (Savini and Corselli, 2010) in the southeastern part of the gulf. In the Gulf of Taranto, river input presents a significant source of nutrients and suspended sediments (Fig. 2.6) (Poulain, 2001). Northern Adriatic rivers draining the eastern Alps, the Po River draining the southwestern Alps and the

Po plain, and several smaller River systems draining the Apennines form a band of relatively fresh surface water in the Adriatic Sea that is pushed against the eastern coastline of Italy by the prevailing anti-cyclonic current system (Trincardi et al., 1994). This southward flowing West Adriatic Current (WAC; S<37 psu) can be traced into the Gulf of Taranto where it leads to high primary production and elevated sedimentation rates allowing for high-resolution Holocene paleoclimate studies (Goudeau et al., 2014; Lipizer et al., 2014; Versteegh et al., 2007; Zonneveld and Siccha, 2016). Maximum extension of the WAC plume along the coast and into the Gulf of Taranto occurs in late spring due to snow melts from the Alps and the northern Apennines, and in fall when enhanced precipitation in the catchment areas leads to increased runoff.

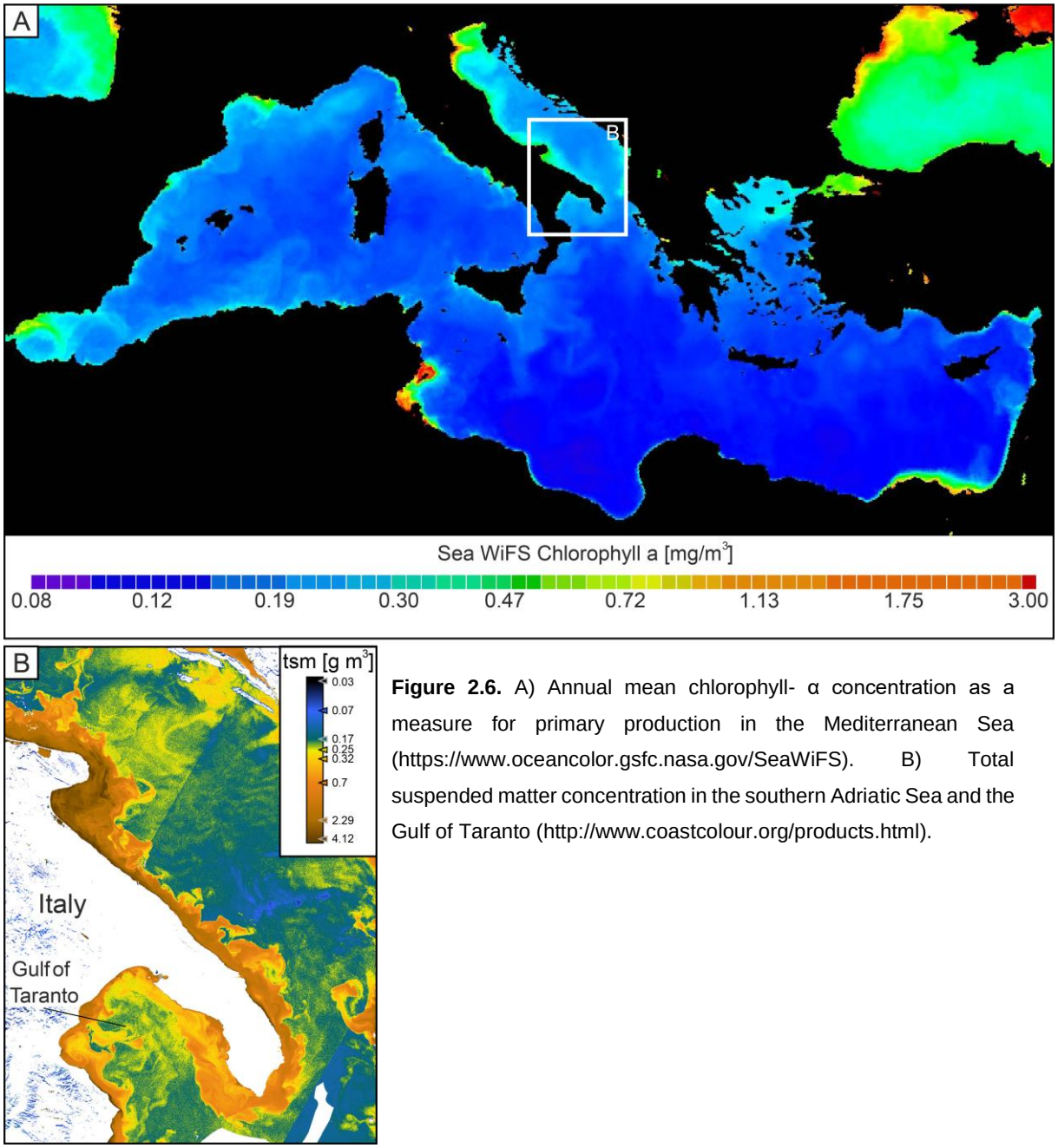

Figure 2.6. A) Annual mean chlorophyll- α concentration as a measure for primary production in the Mediterranean Sea (https://www.oceancolor.gsfc.nasa.gov/SeaWiFS). B) Total suspended matter concentration in the southern Adriatic Sea and the Gulf of Taranto (http://www.coastcolour.org/products.html).

3 Cryptotephra from Lipari Volcano in the eastern Gulf of Taranto (Italy) – A ^{14}C- independent time marker for paleoclimatic studies

Abstract

We present the first tephroanalysis based on geochemical fingerprinting of volcanic glass shards from eastern Apulian shelf sediments in the Gulf of Taranto (Italy). High sedimentation rates in the Gulf are ideal for high-resolution paleoclimate studies, which rely on accurate age models. Cryptotephrostratigraphy is a novel tool for the age assessment of marine sediment cores in the absence of discrete tephra layers. High-resolution quantitative analysis of glass shard abundance in the uppermost 50 cm of a gravity core identified two cryptotephras. Microprobe analysis of glass shards supported by an AMS ^{14}C based age model identified the pronounced primary cryptotephra at 36 cm bsf as the felsic 776 AD Monte Pilato Eruption on the island Lipari, whereas the thinner, mafic tephra layer at 1.5 cm bsf is associated with the 1944 AD eruption of the Somma-Vesuvius. Identifying these tephra layers provides an additional, ^{14}C- independent, stratigraphic framework for further paleoclimatic studies allowing to link Mediterranean climate and hydrology to orbital variation and large scale atmospheric processes. Our results underline the importance of qualitative tephrostratigraphy in a highly geodynamic region, where solely quantitative approaches have demonstrated to bear a high potential for false correlations between tephra layers and eruptions.

This chapter is based on Menke V., Kutterolf S., Sievers C., Schindlbeck J. and Schmiedl G. 2017: Cryptotephra from Lipari Volcano in the eastern Gulf of Taranto (Italy) – A ^{14}C- independent time marker for paleoclimatic studies. Under review in *Quaternary Research*.

3.1 Introduction

Precise age models are of paramount importance for paleoclimatic and paleoenvironmental reconstructions based on marine sediment cores. This is especially true when correlating signatures of climate oscillations to external forcing mechanisms such as solar irradiance or Milankovitch cycles. Tephrochronostratigraphy is an effective dating method since ash layers can be cross-correlated between all types of sedimentary environments including terrestrial, marine and lacustrine archives (e.g., Keller et al., 1978; Kutterolf et al., 2008, 2016; Paterne et al., 1986; Wulf et al., 2004; Neugebauer et al., 2017). Furthermore, in the Mediterranean, tephroanalysis on historical timescales bears minimal temporal uncertainty compared to other common dating methods (AMS ^{14}C dating), since historic documentation exists for major eruptions of the past ~2000 yrs (e.g. Arno et al., 1987). The Gulf of Taranto provides an ideal setting for high-resolution paleoclimatic studies (Zonneveld et al., 2012; Versteegh et al., 2007; Grauel et al., 2013a; Goudeau et al., 2014; Chen et al., 2011; Taricco et al., 2008, 2009, 2015) since it is especially susceptible to both climate variability and human-induced changes in land use, eutrophication and pollution on the Italian mainland. High amounts of nutrients and suspended sediments from the Po and other Italian rivers are transported NW-SE along the Adriatic coast and result in unusually high sedimentation rates in the Gulf of Taranto. Its location downwind of the highly explosive Italian volcanic province suggests the use of tephrostratigraphy to accurately date marine sediment cores (Fig. 3.1 C). Several eruptions of Mt. Vesuvius, the Phlegrean Fields, the Eolian Islands and the Palinuro seamount have emplaced pronounced distal tephra layers in this region (e.g. Siani et al., 2004; Wulf et al., 2008). However, in contrast to thick ash deposits from the eastern Mediterranean Sea that are identifiable by distinct color and grain size changes (e.g. Guichard et al., 1993; Kuzucuoglu et al., 1998; Wulf et al., 2002), there are no macroscopically visible tephra layers in the uppermost sediments of the Gulf of Taranto (e.g., Goudeau et al., 2014; this study). Macroscopic tephra recognition in distal marine or lacustrine sediments as well as soils and ice-cores gets more difficult further away from the source since particle size and amount diminishes with distance (Lowe and Hunt, 2001). These “hidden” distal tephras (Dugmore, 1989) have been named cryptotephras from the Greek word kryptein, meaning “to hide”, and are a relatively new focus for tephrochronological studies in northern Europe, Scandinavia, New Zealand and elsewhere (e.g., Davies et al., 2002; Davies et al., 2012; Davies et al., 2004; Turney et al., 2004; Wohlfarth et al., 2006; Pyne-O'Donnell et al., 2014; Neugebauer et al., 2017). When concentrated in horizons, they can provide valuable insights into eruptive histories as well as significant marker horizons in distal environments where distinct layers are absent.

In the recent past, some authors have microscopically counted the number density of pyroxene grains to identify tephra layers in the Gulf of Taranto (e.g., Castangnoli et al., 1990; Bonino et al., 1993; Taricco et al., 2009). Pyroxene minerals crystalize within the magma chamber

(Schmincke and Sumita, 2013) and can be transported with other pyroclastic material over long distances (Paterne et al., 1988) so peaks in pyroxene grain abundance have been used in the past to tune the sediment record to historical eruptions of the Campanian area. Although this may be a promising first assessment for tephra abundance, it bears a high degree of uncertainty since pyroxene grains 1) can be reworked, 2) can be derived from several eruptions simultaneously, 3) can usually not be allocated to specific eruptions by petrographic features alone or 4) a hiatus in the sediment record can lead to a pyroxene peak being assigned to the wrong eruption. Instead, geochemical fingerprinting of glass shards is a widely used tool to confidently identify the source of ash deposits (e.g. Lowe, 2011; Schindlbeck et al., 2016; Neugebauer et al., 2017), even when using their major element compositions alone (Zanchetta et al., 2011).

In this study, we present a continuous microprobe analysis of glass shards from high-resolution stratigraphic samples of the uppermost 50 cm of a sediment core from the Gulf of Taranto (Fig. 3.1 B). Furthermore, we determine the glass shard abundance within the background sediment to evaluate the nature and systematics of the cryptotephra in a semi-quantitative-compositional approach. The combination of qualitative and quantitative glass shard analyses allows for a reliable correlation of tephra layer(s) to eruptions in this region. This provides an additional stratigraphic framework for further palaeoclimatic studies.

3.2 Geological and environmental setting

Italy is a highly geodynamic region due to its location on the active plate boundary where both the African plate and the Apulian microplate are being subducted under the Eurasian plate (Fig 3.1 A), leading to frequent earthquakes and the only currently active volcanoes in mainland Europe (e.g., D'Antonio et al., 1996, Wortel and Spakman, 2000). Numerous explosive eruptions of the Italian volcanic province have been recorded throughout the Quaternary (Paterne et al., 1990; Keller et al., 1996; Beccaluva et al., 2007; Bourne et al., 2010; Tomlinson et al. 2015). During the Holocene, some of the most active areas were the Phlegrean Fields including the island of Ischia, the Somma-Vesuvius, the Etna on Sicily and the Aeolian Islands with the volcanoes Lipari, Grande Vossa and Stromboli (Fig. 3.1 C). The westward flowing subtropical jet modulates large scale atmospheric circulation patterns over the study area influencing the transport of eruptive material carried into 10 to 20 km height by plinian and subplinian eruptions (Dee et al., 2011; Newhall and Self, 1982). Observational data show, that the predominant wind direction close to the surface is northwest to southeast, following the large-scale circulation (Fig. 3.1 D) (May, 1982) resulting in a preferentially southeast-ward dispersal of pyroclastic material as evident in several tephra layers found in marine sediment cores from the central and eastern Mediterranean Sea (Paterne et al., 1988, 1990; Barberi et al., 1990; Keller et al., 1996; Zanchetta et al., 2011). Similar dispersal pathways are also

predicted in model data, and observed in historic eruptions (e.g., Costa et al., 2006). The Gulf of Taranto, located at the southern tip of Italy in the central Mediterranean Sea, is positioned southeast-ward of the Italian volcanic arc.

Figure 3.1. A) Tectonic overview of the central Mediterranean and adjacent areas (modified after Grünthal und Stromeyer 1992); B) General circulation and dominant water masses of the Gulf of Taranto, and location of gravity core GeoB15403-4 (bathymetry from http://www.gebco.net); C) Italian volcanic provinces (orange) with the Phlegraean Fields (CF) and the Somma Vesuvius (SV) (modified after D'Antonio et al., 1996); D) Annual average surface wind direction and strength over the study area (May, 1982).

The primary water masses controlling the oceanography in the Gulf of Taranto are 1) the West Adriatic Current (WAC) fed by suspension-rich freshwater from the Po river before moving counter clockwise along the western Adriatic coastline into the Gulf (Lipizer et al., 2014) and 2) the Levantine Intermediate Water (LIW) which enters the basin from the Levantine Sea at

depths between 200 and 600m (Turchetto et al., 2007) (Fig. 3.1 B). Due to high nutrient content and suspended loads, relatively high sedimentation rates between 0.52 mm/yr to 2.81 mm/yr have been reported for the shallow eastern Apulian shelf, making it a favorable location for high-resolution climate change studies (e.g. Goudeau et al., 2013 a; Zonneveld et al., 2012; Versteegh et al., 2007) that are in need of precise age models.

3.3 Material and methods

3.3.1 Core sampling and sediment composition

The gravity core GeoB15403-4 (39°45.42'N, 17°53.53E'; 170 m water depth) was recovered from the eastern Apulian shelf in the Gulf of Taranto during R.V. Poseidon cruise 411 in April 2011 (Fig 3.1 B). The 5.245 m long core was sampled at 2.5 mm resolution with the present study investigating the uppermost 50 cm at a 1 cm sampling space. Maximum oxygen penetration depth was identified by distinct color changes at 6 cm. This is consistent with maximum oxygen penetration observed in multicores from the same station, suggesting negligible sediment loss during core recovery. Freeze-dried sediment samples were wet sieved and the 63-125 µm fraction was dried at 40°C for tephroanalysis. This fraction has been demonstrated to be the most promising to get analyzable tephra particles from primary eruptive events (e.g. Kutterolf et al., 2008; Schindlbeck et al., 2016).

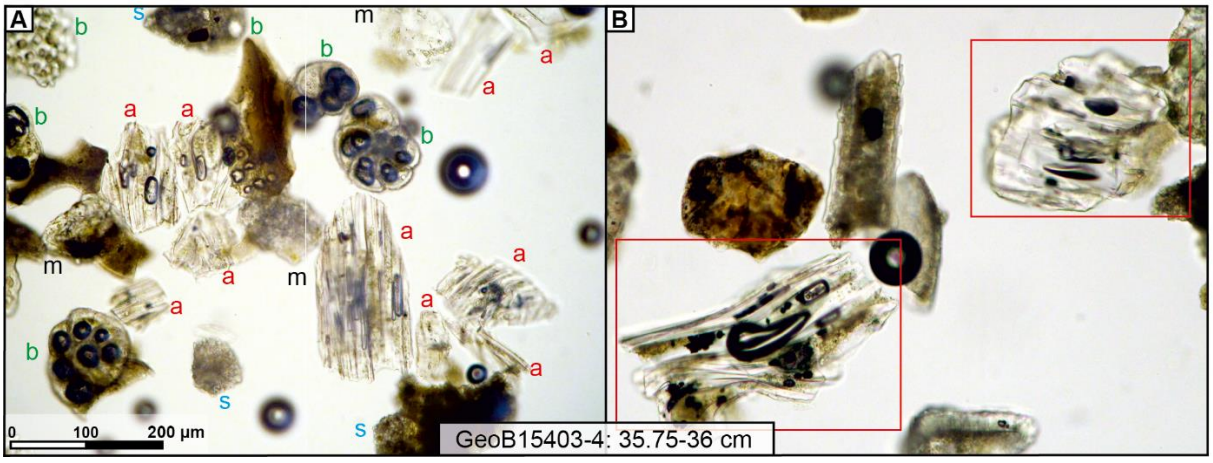

Figure 3.2. Microscopic photographs of the ash horizon at 35.75-36 cm in GeoB15403-4, showing A) the abundance of ash particles (red a) in comparison to biogenic clasts (green b), sedimentary lithics (blue s), and minerals (black m); and B) the appearance of pumiceous, highly vesicular glass shards with tubular bubble structures.

The investigated core interval consists of homogenous, nannofossil-rich grayish to green mud with an undisturbed sediment surface and abundant particles in the fine sand fraction. Sediment in the coarser fraction consists of sedimentary lithic clasts, biogenic particles such as foraminifers, gastropods, pteropods, bivalves and sponge spicules, siliciclastic components

including quartz, feldspar, pyroxene, amphibole, biotite and spinel, and varying amounts of pyroclasts in the form of transparent and brownish and highly vesicular transparent glass shards (Fig. 3.2 A and B).

3.3.2 Analytical techniques

We analyzed glass shards from the grain size fraction 63–125 µmof 50 sediment samples with an electron microprobe (EMP) for major and minor elements following the procedure of Kutterolf et al. (2011) (Table A.2.1). EMP analyses were conducted on epoxy embedded and polished samples with a JEOL JXA 8200 wavelength dispersive electron microprobe at GEOMAR, Kiel, using 15 kV accelerating voltage, a beam defocused to 5 µm, with a beam current of 6 nA and counting times of 30 to 60 s for most major elements and 60 to 100 s for the minor elements. Natural and synthetic glasses and minerals were used as standards for calibration. Accuracy was monitored by standard measurements on Lipari obsidian (rhyolite) (Hunt and Hill, 2001) and Smithsonian basaltic standard VGA (Table A.2.2). When available, 15 glass shards were measured per sample by scanning throughout the entire epoxy embedded sample area. After every sixty individual measurements, two to four standard measurments (always two for Lipari standard and if mafic glass was identified also two for VGA standard) follow to verify the stability of the measuring program. The resulting standard deviation is < 0.5 % for major and < 3 % for most minor elements (Table A.2.3). All analyses were normalized to 100 % to eliminate the effects of variable post-depositional hydration and minor deviations in the electron beam focus. Because variable submarine alteration (Kutterolf et al., 2007) causes elemental exchange at the surface and rims of single glass shards first (e.g. Schacht, 2005), microanalyses aimed at the center of glass shards.

For a semi-quantitative estimation of pyroclast abundance, we point-counted the 63–125 µm fraction of each sample that comprised more than 14 glass shards identified by microprobe analysis (Table A.2.3). We used a regular net on top of the respective BSE pictures of each analyzed sample to create a grid. Particles that intersected the grid were categorized as glass shard or non-glass shard. If the intersection targeted epoxy, no point was counted. At least 400 points were counted to derive a statistical significant estimation (e.g. Van der Plas and Tobi, 1965) of respective volume percentages of the pyroclast and non-pyroclast fraction. Samples including fewer than 10 glass shards were identified during EMP work and were not counted. Based on the point counting results of samples where only 14 glass shards were identified during EMP work, and which account only for 1 to 1.5 vol%, these samples were estimated to contain less than 1 vol% of glass shards.

3.3.3 AMS ^{14}C based age model

For the establishment of an AMS ^{14}C based age model for GeoB15403-4, we selected surface-dwelling planktonic foraminifera from a total of 11 samples along the core (Table 3.1). Dating was performed at Beta Analytic Inc. (Miami, Florida, USA). Radiocarbon dates were converted to calendar years using the MARINE13 database (Reimer and Bard et al., 2013) with a Delta R value of 73 ± 34. Delta R was calculated using the MarineChrono reservoir database through an interpolation of data points close to the core locations.

3.4 Results

3.4.1 Geochemistry

Major element analysis of 503 glass shards, revealed contributions of minor basaltic/andesitic and trachyte-basaltic as well as major rhyolitic magmatic compositions to the sediments (Fig. 3.3 A). In Figure 3.3 the glass shard compositions are plotted with provenance fields of Mediterranean volcanic arcs and in particular with compositional fields of eruptions from the Aeolian Islands for comparison. All analyzed glass shards fall within the potassium-rich High-K calc-alkaline series or the Shoshonitic series (Fig. 3.3 B).

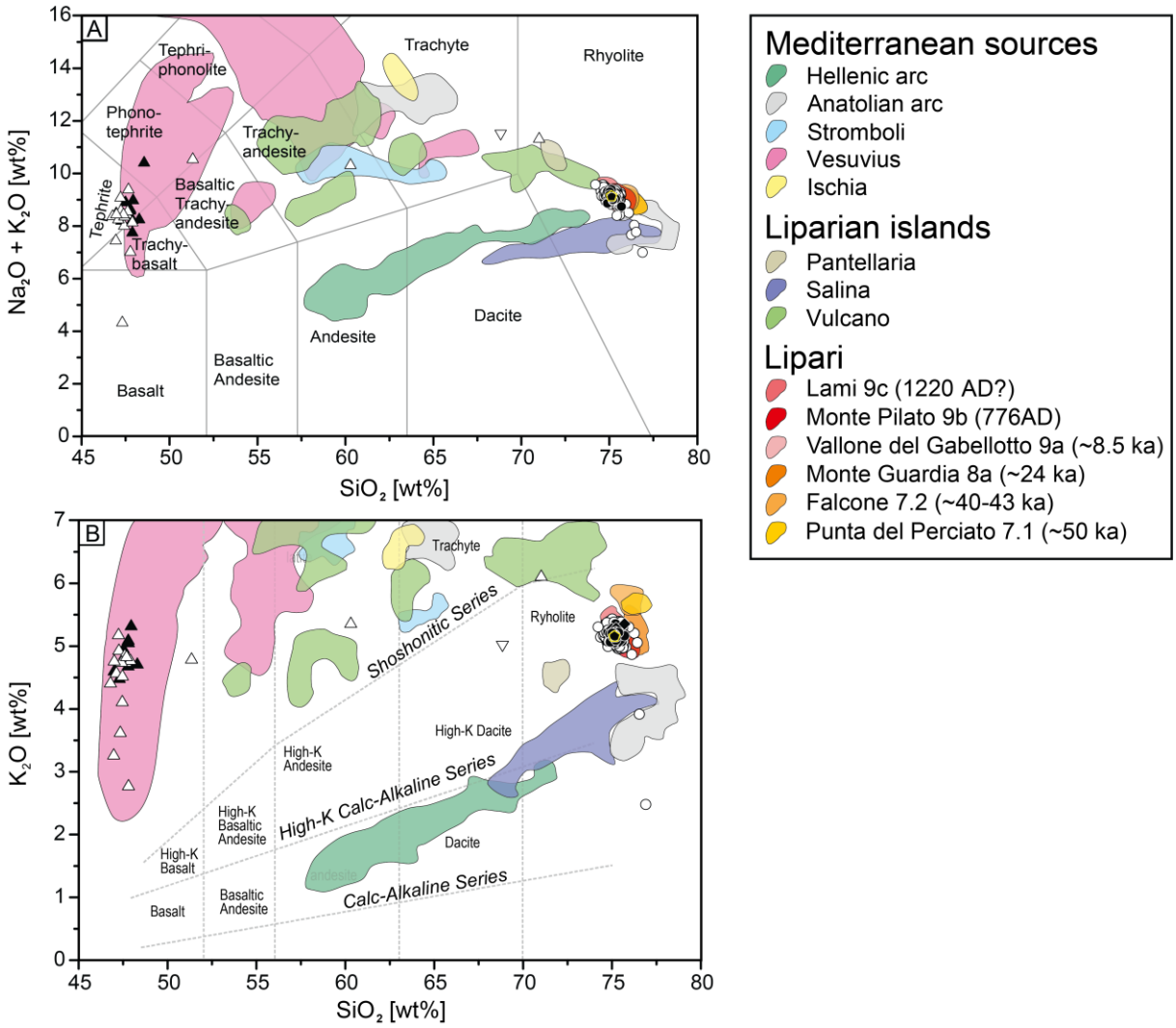

Figure 3.3. A) Total alkalis versus silica diagram after Le Maitre (1989) showing the compositional variability of all analysed samples with circles/diamonds representing felsic compositions in all samples, triangles showing mafic compositions limited to the first 15 cm bsf, black is the inferred primary crypto tephra layer around 36 cm bsf and white is the glass shard composition of all other samples. B) K_2O v. SiO_2 classification diagram (Peccerillo & Taylor 1976) for the volcanic rocks of Lipari modified after Forni et al. (2013). Glass compositions are normalized to anhydrous compositions. Reference field based on data from Forni et al. (2013), Albert et al. (2017), and Tomlinson et al. (2015).

The majority of the investigated glass shards cluster at potassium concentrations > 4 wt% with SiO_2 contents of 47 wt% or 75 wt%, respectively (Figs. 3.3 B, 3.4 A and 3.5 A). Very few exceptions (5 out of 503 glass shards) have potassium concentrations < 4 wt% (Fig. 3.3 B). The majority (~95 %) of the glass shards have a rhyolitic composition and have major element concentrations that cluster around 13 wt% Al_2O_3, 4 wt% Na_2O, 1.5 wt% FeO_t, 0.7 wt% CaO, and 0.1 wt% TiO_2 (Fig. 3.5, Table A.2.1). The tephritic to trachy-basaltic glass shards, concentrated in the first 6 cm of the sediment, contain average compositions of ~17.8 wt% Al_2O_3, ~10.4 wt% CaO, ~9.5 wt% FeO_t, ~4 wt% MgO, ~3.6 wt% Na_2O, and ~1.2 wt% TiO_2 (Fig. 3.4 A; Table A.2.1).

3.4.2 Ash abundance

While the brownish, trachy-basaltic, basaltic and andesitic glass shards are limited to the uppermost 6 cm of the core, the transparent, rhyolithic glass shards occur unequally distributed throughout the entire investigated interval (Fig. 3.4 A).

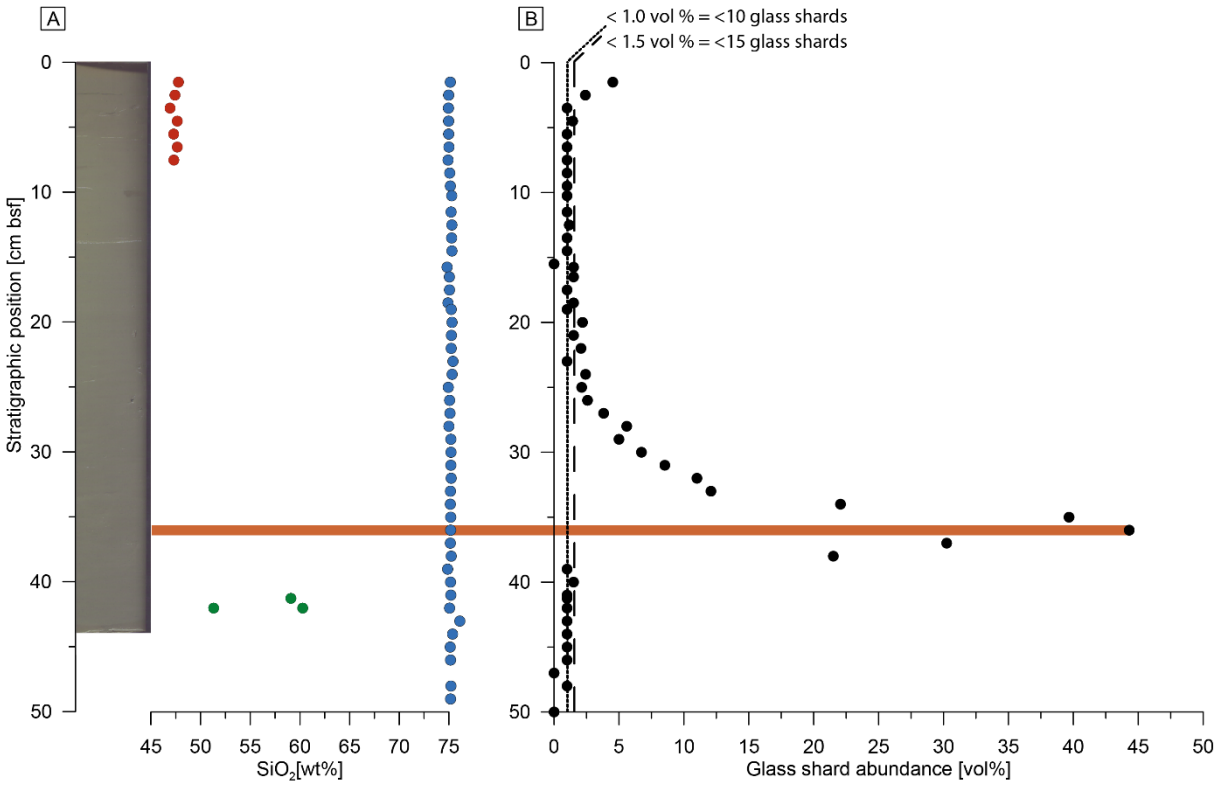

Figure 3.4. A) Left: Core picture showing the undisturbed sediment structure without visible tephra layers. Right: Down-core variation in SiO_2 concentration of average glass shard compositions with red representing trachy-basalt, blue showing rhyolite and green basalt/andesite; B) Relative abundance of glass shards derived by point counting (see methods). Dotted line represents samples with ≤10 (< 1 vol%) and stippled line samples with 10 to 14 (1 to 1.5 vol%) identified glass shards per sample. The horizontal bar (orange) marks the inferred primary cryptotephra layer.

The overall abundance of glass shards within the upper 20 cm of sediment stayed below 1.5 vol%, with the exception of two samples at 1.5 cm bsf (4.5 vol%) and 2.5 cm bsf (2.4 vol%) that contain trachy-basaltic dominated glass shard compositions (Fig. 3.4 B). Between 20 cm bsf and 36 cm bsf there is a continuous increase of glass shard abundance, exclusively of rhyolitic composition, up to 44 vol% (36 cm bsf). Between 36 cm bsf and 38 cm bsf the tephra abundance decreases sharply back to a <1.5 vol % presence of glass shards in the sediments where it remains until the end of the investigated sediment interval (Fig. 3.4 B).

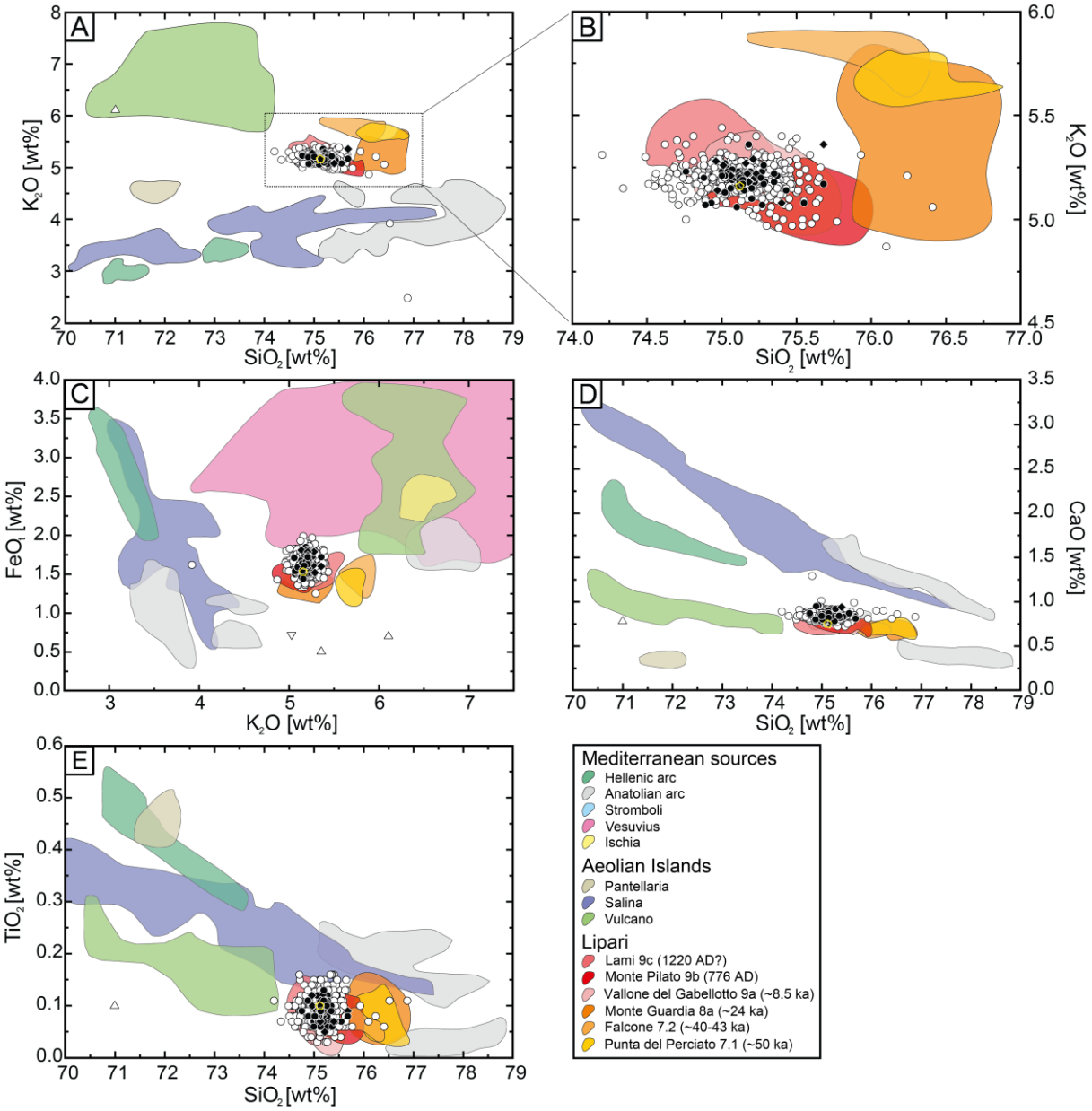

Figure 3.5. A-E: Discrimination diagrams to determine the volcanic provenance of the analyzed glass shards with focus on the Aeolian Islands. Reference fields for Mediterranean sources and eruptions from Lipari are based on the data of Forni et al. (2013), Albert et al. (2017), and Tomlinson et al. (2015). Circles/diamonds represents the felsic compositions in all samples, triangles are mafic compositions limited to the first 15 cm, black is inferred primary cryptotephra layer and white is the glass shard compositions of all other samples. Glass compositions are normalized to anhydrous compositions.

3.4.3 Age model

Results of the AMS ^{14}C dating on plankton foraminifera are given in Table 3.1. The ^{14}C based age model for GeoB15403-4 gives an Age of 55600 yrs BP for the base of the whole core (Fig. 3.6 A). The investigated core interval (0–50 cm) has a basal age of 1305 yrs BP.

Sedimentation rates decrease within this section from 66.5 cm kyr^{-1} in the older part to 23.5 cm kyr^{-1} in the youngest samples (Fig. 3.6 B).

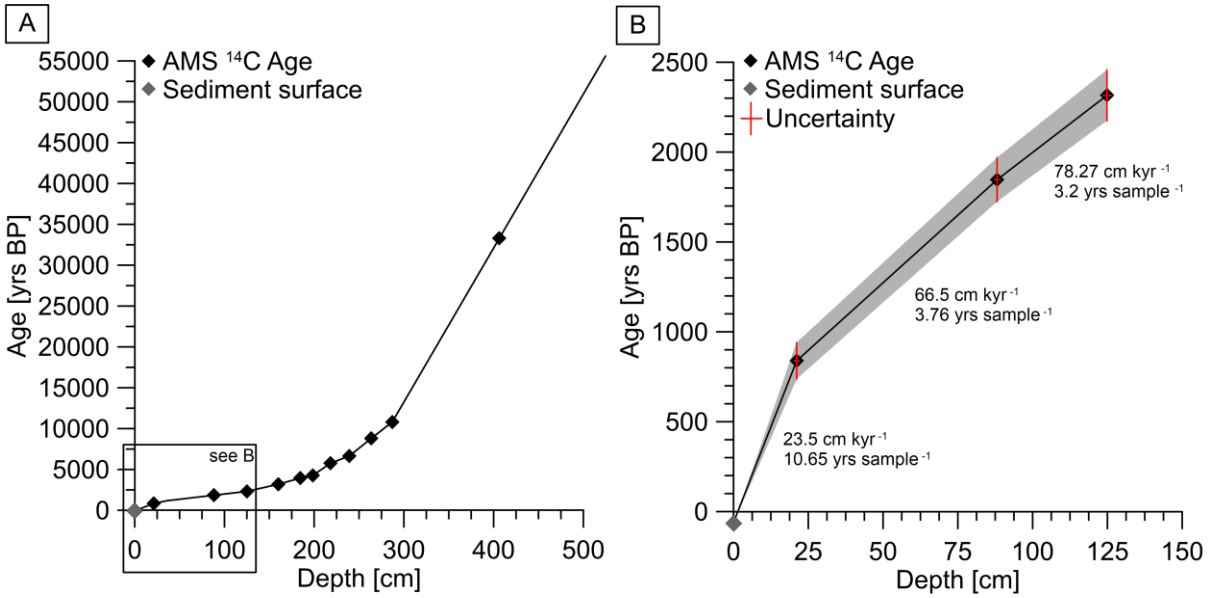

Figure 3.6. A) Results of the AMS ^{14}C based age model for GeoB15403-4. Black diamonds represent AMS ^{14}C dates and gray diamonds show the age of the sediment surface. B) Detailed view of the core interval investigated in this study.

Table 3.1. Results of the AMS ^{14}C dating of planktonic foraminifera in GeoB15403-4.

Depth [mm]	Radiocarbon age [BP]	Calendar years [cal BP]	Calendar years [cal AD]	Data
0.00		-61	2011	Sediment Surface
211.25	1380±30	839±101	1111.0±101	AMS^{14}C dating
881.25	2320±30	1846.5±122.5	103.5±122.5	AMS^{14}C dating
1248.75	2710±30	2316±142	-366.0±142	AMS^{14}C dating
1598.75	3410±30	3191±138	-1241.0±138	AMS^{14}C dating
1845	4020±30	3947±132	-1997.0±132	AMS^{14}C dating
1983.75	4270±30	4277±133	-2327.0±133	AMS^{14}C dating
2181.25	5470±30	5767±116	-3817.0±116	AMS^{14}C dating
2391.25	6290±30	6656.5±124.5	-4706.5±124.5	AMS^{14}C dating
2635.00	8350±40	8807.5±170.5	-6857.5±170.5	AMS^{14}C dating
2868.75	9920±30	10808±169	-8858.0±169	AMS^{14}C dating
4061.25	29550±110	33286.5±356.5	-31336.5±356.5	AMS^{14}C dating

3.5 Discussion

3.5.1 Compositional homogeneity

It is important to assess whether the observed glass shards form homogenous (only from one eruption and source) or heterogeneous (reworked from several eruptions and sources) assemblages. The overall geochemistry of the glass shards indicates very homogenous major elemental concentrations in two clusters (Figs. 3.3, 3.4 and 3.5). Based solely on the compositional homogeneity we can infer that (within the limitations of investigating only one grain size fraction) the interval between 20 and 38 cm contains a primary cryptotephra with a peak in glass shard abundance at 36 cm bsf. Only in four samples within the first 6 cm bsf bimodal compositions can be observed whereas all other samples until 41 cm bsf show very confined homogenous rhyolithic glass shard compositions. The only exceptions are a few single outliers in three samples. These homogenous element concentrations argue for cryptotephras originating from single specific eruptions respectively, which allows for the stratigraphic assignment of historic eruptive events. Below 42 cm the ash abundance significantly decreases, and the glass shard composition is heterogenous.

3.5.2 Provenance of the cryptotephras

So far, the appearance of volcanic material in the Gulf of Taranto has been attributed to volcanic eruptions based on peaks in pyroxene abundances inferred from the density variations within the sediments (e.g. Bonino et al., 1993 Taricco et al. 2009, Vivaldo et al. 2009). The authors argue that the proximity to the Campanian volcanic region as well as the prevailing westerly winds provided a complete and nearly temporally linear record of the eruptive history within the sediments of the Ionian Sea. According to this and the AMS ^{14}C based age model of core GeoB15403-4 (Fig. 3.7), the observed glass shard maximum centered around 36 cm bsf should be associated with the 1301 AD Ischia eruption. The ideal test for the provenance and assignment to a specific eruption is the geochemical fingerprint analysis of volcanic glass shards. Glass shards from Ischia are less silica-rich at higher alkali contents (trachytes) than the high-silica glass shards (rhyolites) in sediments below 6 cm bsf of GeoB15403-4. Comparing the compositional signals with the respective provenance fields (Tomlinson et al., 2015), the assignment of the observed glass shards in the upper 42 cm of core GeoB15403-4 to an Ischia eruption can thus be excluded (Figs. 3.3 and 3.5 C). In the first 6 cm of the sediment core the glass shards reveal a tephritic composition, which is also very different from the Ischia volcanic products.

To confine the possible origin of the glass shards we further compare the geochemical compositions of the analyzed glass shards with provenance data of the Mediterranean volcanic provinces (e.g. Keller et al., 1978; Tomlinson et al., 2015; Albert et al., 2017). Already within

the basic classification diagrams of Figure 3.3 (total alkali versus silica, potassium versus silica) it becomes clear that possible provenance regions are very distinct.

The trachytic composition of the glass shards within the first 6 cm and a peak in 1.5 cm depth bsf only fits to the Somma-Vesuvius eruptions at ages younger than 1000 years B.P. The increase of silica-unsaturated, high-alkali glasses found in Somma-Vesuvius eruptions between 79 AD and 1944 AD is the best fit for the glass compositions of this study (Piochi et al., 2006; Di Renzo et al., 2007 and references therein). Additionally, according to estimated sedimentation rates of 2.5 mm/10 years the AD 1944 eruption bears the highest potential to be the source eruption for the glass shards at 1.5 cm bsf.

The geochemical fingerprint of the glass shard peak at 36 cm bsf unambiguously identifies Lipari as source (Figs. 3.3 and 3.5). Representative compositional data from eruptions from Lipari (Albert et al., 2017) and the very detailed eruptive catalogue of Lucchi et al. (2013) reveal that only the last eruption cycle (9a, b, c) on Lipari (Lami, Monte Pilato, Vallone del Gabellotto eruptions) produced tephra glass compositions that correlate with the analyzed glass shards of core GeoB15403-4. Based on the AMS ^{14}C age model and the derived sedimentation rate of 23.5 cm kyr-1 for the studied core section (Fig. 3.7), the ~8.5 ka Vallone del Gabellotto eruption can be ruled out as responsible source for the tephra peak at 36 cm depth bsf. In addition, the clearly defined glass shard peak and the homogenous geochemical composition contradicts reworking of a potential Vallone del Gabellotto marine ash layer.

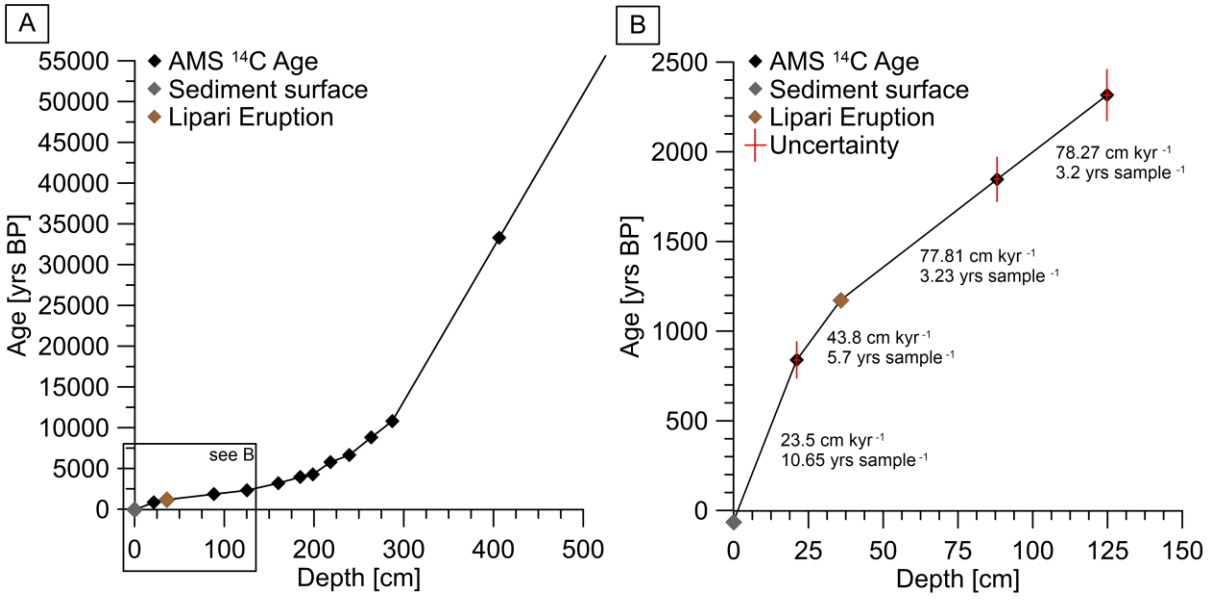

Figure 3.7. Combined age model for GeoB15403-4 A) consisting of AMS ^{14}C and results of the tephroanalysis. Black diamonds represent the AMS ^{14}C dates, gray dots show the age of the sediment surface and light brown shows the Ash layer assigned to the 776 AD eruption of Monte Pilato. B) Detailed view of the core interval investigated in this study.

This leaves two eruptions from Lipari as candidates for the eruptive products in the sediments: the 1220 AD Lami eruption and the 776 AD Monte Pilato eruption. Although both eruptions have very similar geochemical compositions, several arguments favour the 776 AD Monte Pilato eruption as the volcanic event that is responsible for the cryptic tephra layer in 36 cm bsf of core GeoB15403-4. According to our age model an age of 1180 years BP would be assigned to 36 cm bsf, which fits better to the uncorrected ^{14}C age of 1241 ± 31 years BP for the Monte Pilato eruption than an age of 780 years BP recalculated for the 1220 AD Lami eruption. Secondly, the 1220 AD Lami eruption is characterized by slightly lower SiO_2 and higher K_2O contents than the Monte Pilato eruption, which is in accordance with the majority of the measurements from the main part of the cryptotephra layer in 36 cm bsf (Fig. 3.5 B, black filled symbols). Thirdly, whereas the origin and size of the 776 AD Monte Pilato eruption is well constrained (Albert et al. 2017; Albert 2012; Forni et al. 2013), the Lami "eruption" is much more controversial. It has been questioned whether the Lami deposits are assigned to the older Monte Pilato eruption (Davi et al. 2009) or not (Forni et al. 2013). If the glass shards in our sediments would be associated with the Lami eruption, coinciding with the AD 1300 Rocche Rosse coulee, sedimentation rates of >45 cm/ka would be required for the upper part of core GeoB15403-4. Similar or even higher sedimentation rates have been reported from adjacent sediment cores of the Gulf of Taranto (Versteegh et al., 2007; Zonneveld et al., 2016), which leaves some uncertainty in the final assignment of the cryptic tephra at site GeoB15403-4.

The fourth argument concerns the size of the Lami and Monte Pilato eruptions. Compared to the up to 150 m thick pumiceous pyroclastics of the Monte Pilato eruption (Forni et al. 2013), the Lami eruption is only represented by a 10 m thick pyroclastic succession. Aditionally "Lami deposits" are composed of variably sorted tuff-breccias with pumices, lithic clasts, diffused obsidian clasts and bread-crust pumiceous bombs as well as intercalated, variably stratified, medium sorted lapilli layers and massive tuff layers (Forni et al. 2013). These observations suggest that the 776 AD Monte Pilato eruption had at least a subplinian character (Albert et al. 2017; Albert 2012), whereas the Lami succession is associated with a Vulcanian eruption at most (Davi et al. 209; Forni et al. 2013; Albert et al. 2017). The necessary size to inject volcanic matter high into the atmosphere, where it can be transported with the prevailing winds over long distances, is thus only given for the 776 AD Monte Pilato eruption. This interpretation is additionally supported by the occurrence of several cm-thick ash layers of the Monte Pilato eruption at distal outcrops on Vulcano, Stromboli, and Panera, which are located between Lipari and the Gulf of Taranto (Lucchi et al. 2008, 2013; Bertagnini et al. 2011). These data suggest that the 776 AD Monte Pilato eruption is the volcanic event that produced the cryptotephra found at 36 cm bsf in sediment core GeoB15403-4 from the Gulf of Taranto.

3.5.3 Implications for further paleoclimate studies

Paleoclimate studies of Holocene marine sediments on decadal to centennial time scales require accurate age models, which cannot always be provided solely by radiocarbon dating due to uncertainties of local reservoir effects and biological factors (e.g. habitat differences of planktonic foraminifera). In the eastern Mediterranean Sea, tephrochronology provides an additional tool for a reliable age assessment of sediment cores and allows for an optimal correlation of regional paleoclimatic events (e.g. Vinci, 1985). Several efforts have been made to cross-correlate Holocene tephra layers from the central and eastern Mediterranean basin (Zanchetta et al., 2011 and references therein). The widely distributed tephra layers of Y-5 and Y-6 (De Vivo et al., 2001; Margari et al., 2007; Vogel et al., 2010) provide important marker horizons of the late Pleistocene for the central and eastern Mediterranean basin. Volcanic eruptions of the Holocene are numerous and chronically well resolved in the sedimentary record of sites proximal to the eruption centers. However, the existing tephrostratigraphic schemes are currently still disconnected (Zanchetta et al., 2011) and the potential of cryptotephras is not yet fully utilized. We therefore propose to include tephroanalysis as a common method when conducting paleoclimatic studies on high-resolution sediment cores from the central and eastern Mediterranean Sea.

Previous studies on pyroxene grain abundance proved useful in recording late Holocene cryptotephras in the Gulf of Taranto (e.g., CiniCastagnoli et al., 1990). However, the identification of volcanic eruptions solely based on tephra particle abundance remains ambiguous. In this context, our new results highlight the importance of geochemical fingerprinting of volcanic glass shards. The detailed chronologic framework obtained from this study provides an ideal background for further paleoclimate studies conducted on the sediments of GeoB15403-4. It provides new temporal constraints for this area that have previously not been recognized and may therefore provoke revisiting of some marine sediment records of the past. This is particularly relevant for regions such as the Gulf of Taranto located downwind of several highly active volcanic provinces with numerous eruptions during the past 2000 years. The Gulf of Taranto serves as a depositional center for Italian riverine suspension load, which is transported southward along the West Adriatic Current. Thus, Holocene sediments of the Gulf of Taranto provide an excellent archive for the study of regional decadal-scale hydrological changes and climate linkages between the Mediterranean and North Atlantic regions, given that the studied sediment cores can be accurately dated (e.g., Castagnoli et al., 1990; Chen et al., 2011; Versteegh et al., 2007; Taricco et al., 2015).

3.6 Conclusions

Quantitative analysis of pyroclast contents in sediment samples of gravity core GeoB15403-4 from the Gulf of Taranto identified two cryptotephras. Electron microprobe analysis indicates

homogenous element concentrations allowing to disregard potential uncertainties like sediment reworking or multiple possible eruption sources at the time of deposition.

Geochemical fingerprinting of glass shards from the upper 6 cm and the peak at 1.5 cm depth points to Somma- Vesuvius eruptions occurring before 1000 years BP. Based on the increase of silicia under saturated, high alkali glasses of Somma-Vesuvius eruptions between 79 AD and 1944 AD and the timeframe given by our ^{14}C based age model, we argue for the 1944 AD eruption to be the source for this ash layer.

The pronounced peak of rhyolitic glass shards at 36 cm suggests a primary cryptotephra. Elemental composition reveals the volcanoes of the island Lipari as source. Based on the geochemical composition, the eruption type and our ^{14}C age model we argue for the 776 AD Monte Pilato eruption to have emplaced this cryptotephra.

Our study shows, that tephroanalysis provides an important tool for the age assessment of marine sediment cores. Specifically, geochemical fingerprinting proves to be a crucial method ensuring the correct source identification of cryptotephras. Our results will improve the stratigraphic framework for sediments from the high-accumulation areas of the Gulf of Taranto, providing the basis for decadal-scale hydrological and palaeoclimatic reconstructions.

4 Combined North Atlantic and anthropogenic forcing of changes in the marine environments in the Gulf of Taranto (Italy) during the last millennium

Abstract

This study examines the multi-decadal to centennial variability of benthic ecosystems, depositional environments and biogeochemical processes in the Gulf of Taranto (Italy) over the last millennium. Our study is based on sediment cores from two sites in the eastern Gulf of Taranto (Mediterranean Sea), and benthic foraminifera data of 43 surface sediment samples from the western Adriatic Sea reflecting modern conditions. We use the data to unravel relative contributions of natural and anthropogenic forcing to conditions at the sediment-water interface in a marine setting with a long history of human impacts in river catchments. High abundances of infaunal foraminifera in surface sediments trace the nutrient-rich Po river outflow and display an area of high organic matter deposition in the north-eastern Gulf of Taranto. Decreasing Ca/Ti ratios suggest increasing terrigenous fluxes at ~1300 AD driven by wetter conditions during persistent negative phases of the North Atlantic Oscillation (NAO). A strong NAO connection is also evident in high-resolution clay mineral data. The smectite/illite ratio reflects variable Po river runoff, and correlates well with NAO strength for the past 300 years. Benthic ecosystem variability as reflected by foraminifera is closely linked to the Northern Hemisphere temperature evolution during the past millennium. Spectral analysis reveals a quasi-periodicity of 50 to 70 years suggesting an Atlantic Multidecadal Oscillation (AMO) forcing of Italian hydrology. Coeval with increasing anthropogenic activity, the effects of rising temperatures and nutrient discharge during the past 200 years further enhanced nutrient and organic matter fluxes. This is reflected by a substantial rise in the abundance of shallow to intermediate infaunal benthic foraminifera (SIIBF) and a concurrent decrease of *Uvigerina mediterranea* $\delta^{13}C$ since at least 1800 AD. The SIIBF decrease in the youngest samples likely reflects environmental effects of stricter regulations on fertilizer use in Italy and the reduction of sediment transport due to the stabilization of river banks.

This chapter is based on Menke V., Ehrmann W., Milker Y., Brzelinski S., Möbius J., Mikolajewicz U., Zolitschka B., Zonneveld K., Emeis K.C. and Schmiedl S., 2017: Combined North Atlantic and anthropogenic forcing of changes in the marine environments in the Gulf of Taranto (Italy) during the last millennium. Under review in *Climate of the Past*.

4.1 Introduction

In recent years substantial progress has been made to understand large-scale climate trends of the Holocene and their impacts on marine and terrestrial environments based on the integration of proxy data and climate modelling (e.g., Chevalier et al., 2017; Grimm et al., 2015; Donders et al., 2008; Tierney et al., 2011). However, on shorter (i.e. decadal to multi-decadal) time scales, the understanding of regional patterns and their link to climate is still inadequate, partly because high-resolution proxy records are still sparse. The Mediterranean Sea is particularly suitable for investigating short-term and regional responses to climate changes, because it is a semi-enclosed basin with strong influence from land, located at the transition between the temperate mid- to high- latitudes and the subtropical low-pressure belt, and thus responds sensitively to climate variability (Lionello et al., 2006). But the Mediterranean borderlands have also been densely populated and subject to intense land use and agricultural activity during the past millennium (e.g., Holmgren et al., 2016; Lamb, 2013; Luterbacher et al., 2012; Pongratz et al., 2008). Therefore, the Mediterranean region is a highly complex system, and distinguishing between natural and anthropogenic influences on the oceanography and marine ecosystems is complicated but paramount for assessing future impacts of climate change.

The Mediterranean Sea responds to precession-driven changes in African Monsoon strength on orbital time scales (Cramp and O'Sullivan, 1999; Emeis et al., 2000; Rohling et al., 2015 and references therein; Weldeab et al., 2014). On suborbital timescales, Mediterranean climate dynamics are modulated by the North Atlantic climate variability, e.g. during the cooling of the Younger Dryas or the 8.2 ka event (Bar-Matthews et al., 1999; Cacho et al., 2001; Rohling and Pälike, 2005, and references therein). On shorter time scales, Mediterranean climate variability has also been influenced by fluctuations in the North Atlantic Oscillation (NAO) and the Atlantic Multidecadal Oscillation (AMO) in subtle, but nonetheless persistent, ways. While the NAO drives European winter temperatures and precipitation patterns (Beniston et al., 1994; Frisia et al., 2003; Hurrel, 1995, 2001), AMO fluctuations correlate with changes in summer temperature and precipitation (Enfield et al., 2001; Knight et al., 2006; Marullo et al., 2011; Sutton and Hodson, 2005).

Underlying these orbital and suborbital trends are changes in the activity of the sun reconstructed on the basis of atmospheric $\Delta^{14}C$ records (Stuiver, 1994). Solar forcing of Mediterranean climate is documented in various proxy records, e.g., central European lake level and Alpine glacier fluctuations (Holzhauser et al., 2005; Magny et al., 2007). A prominent example for effects of solar forcing is the rapid and short-term cooling of the Little Ice Age (LIA) that terminated the relatively warm and dry conditions of the Medieval Warm Period (MWP) (Despart et al., 2003; Grove, 2001; Guiot and Corona, 2010; Holzhauser et al., 2005; Luterbacher et al., 2001, 2004).

Combined evidence thus suggests that oceanographic and biogeochemical processes of the Mediterranean Sea are intimately linked to global and regional climate dynamics, but the relative influence of anthropogenic processes on late-Holocene marine environments is still a subject of debate. The Gulf of Taranto provides an ideal setting for addressing this question since it is especially susceptible to both climate variability and human-induced changes in land use, eutrophication and pollution on the Italian mainland. High amounts of nutrients and suspended sediments from the Po and other Italian rivers are transported NW-SE along the Adriatic coast and result in unusually high sedimentation rates on the outer shelf of the Gulf of Taranto. Sediment archives from these depocenters provide the basis for climate and environmental reconstructions on decadal to multi-decadal time scales (Grauel et al., 2013a; Taricco et al., 2015; Versteegh et al., 2007; Zonneveld et al., 2012). For example, Versteegh et al. (2007) suggested a centennial solar forcing in alkenone-based sea surface temperature (SST) reconstructions from the Gulf of Taranto, implicating wind-induced mixing to play a crucial role for regional productivity. Goudeau et al. (2013) correlated high rates of detrital matter deposition on the eastern Apulian shelf with negative phases of the NAO and enhanced river discharge. Anthropogenic influences on the trophic state of the Po river discharge plume over the past 200 years is evident in dinoflagellate cyst distributions that responded to industrialization and fertilizer application in Italy (Zonneveld et al., 2012).

Benthic foraminifera are especially suitable for studying climatic and oceanographic processes since their abundance and faunal composition primarily depend on organic matter (OM) fluxes and oxygen availability at the sediment water interface; both factors are linked to atmospheric circulation and anthropogenic activity. Depending on the trophic state at the sea floor, they inhabit stratified microhabitats on and below the sediment surface and are commonly classified as epifaunal (living on top of, or up to 0.5 cm within the sediment), shallow and intermediate infaunal (commonly living between 0.5 and 2 cm in the sediment), and deep infaunal (commonly living below 2 cm in the sediment) (e.g., Corliss, 1985; Linke and Lutze, 1993; Lutze and Thiel, 1989; Mackensen and Douglas, 1989; Murray 2006; Jorissen et al., 1995). Changes in trophic conditions and the oxygenation of bottom waters can therefore be traced in the abundance of certain opportunistic species and shifts in the proportion of epi- and infaunal taxa (e.g.; De Rijk et al., 1999; Jorissen et al., 1992, 1995; Schmiedl et al., 2000). Furthermore, the stable carbon isotope signature of benthic foraminifera is an important tool for assessing deep-water ventilation and for quantifying organic matter fluxes (e.g.; Duplessy et al., 1988; Imbrie et al., 1984; Schmiedl et al., 2004; Shackleton 1987; Theodor et al., 2016 a,b; Zahn et al., 1986). Clay minerals and relative element abundances in sediments represent proxies for weathering on land, river discharge, and dispersal in the ocean that are independent of sea-floor ecology, allowing for a comprehensive reconstruction of past sedimentation processes and changes in climate and ocean circulation. The proportion of individual clay

minerals in marine sediments mainly depends on the climatic conditions in the hinterland and the source rocks, making them ideal proxies for identifying source areas and dispersal pathways (e.g.; Biscaye, 1965; Ehrmann et al., 2007; Petschick et al., 1996; Venkatarathnam and Ryan, 1971).

This study combines high-resolution benthic foraminiferal faunal and clay mineral data from two sediment cores in the Gulf of Taranto. Total organic carbon and nitrogen contents of bulk sediment and X-ray fluorescence elemental ratios provide additional information on organic matter fluxes and sediment origin and dispersal processes. Our multiproxy approach aims at identifying the relative contributions of natural climatic and anthropogenic forcing on benthic ecosystem variability and biogeochemical processes in the Gulf of Taranto over the past 1300 years.

4.2 Environmental setting

The Gulf of Taranto is located at the southern tip of Italy (Fig. 4.1). The oceanography of the Gulf of Taranto is strongly influenced by water masses from the Adriatic Sea to the north and the Ionian Sea to the south. The Po river drains large parts of the southern Alps and northern Apennines and discharges high amounts of sediment- and nutrient-rich freshwater into the northern Adriatic Sea, from where it is transported to the south by the counter clockwise West Adriatic Current (WAC). The WAC (< 37 psu; Lipizer et al., 2014) moves as a narrow coastal band along the western Adriatic margin and is further enriched in nutrients and sediment by smaller river systems of the Apennines before it reaches the Gulf of Taranto. The sediment supply from the southern Apennines is relatively small, but detectable near the coast through elevated smectite concentrations (Degobbis et al., 1986; Tomadin 2000; Milligan and Cattaneo, 2007) (Fig. 4.1 A). The stronger Padane detrital matter flux dominated by illite (from rivers Po, Brenta, Adige, Reno) is seen in a parallel band further in the basin (e.g. Milligan and Cattaneo 2007; Tomadin 1979, 2000) (Fig. 4.1 A). Maximum extension of the WAC plume along the coast and into the Gulf of Taranto occurs in late spring due to snow melt in the Alps and the northern Apennines, and in fall when enhanced precipitation in the catchment areas leads to increased runoff. In the Gulf of Taranto, the WAC mixes with the warmer, oligotrophic and more saline Ionian Surface Water (ISW) (38.8–38.9 psu, 17–19 °C; Budillon et al., 2010) flowing into the gulf from the central Ionian Sea (Poulain, 2001; Turchetto et al., 2007) (Fig. 4.1 B). Annual mean SST in the Gulf of Taranto are ~18.7 °C. The cold (13.5 C; Artegiani et al., 1997), highly saline (>38.7 psu; Turchetto et al., 2007) and relatively nutrient-rich Levantine Intermediate Water (LIW) flows into the Gulf of Taranto from the Levantine basin at a depth of 200–600 m (Fig. 4.1 B). Below the LIW, Adriatic Deep Water (ADW) consists of Northern Adriatic Dense Water (NadDW) formed by downwelling as a result of wintertime NE

Bora wind outbreaks, and of Southern Adriatic Dense Water (SAdDW) formed by deep-water convection in late winter to early spring (Grbec et al., 2007; Turchetto et al., 2007).

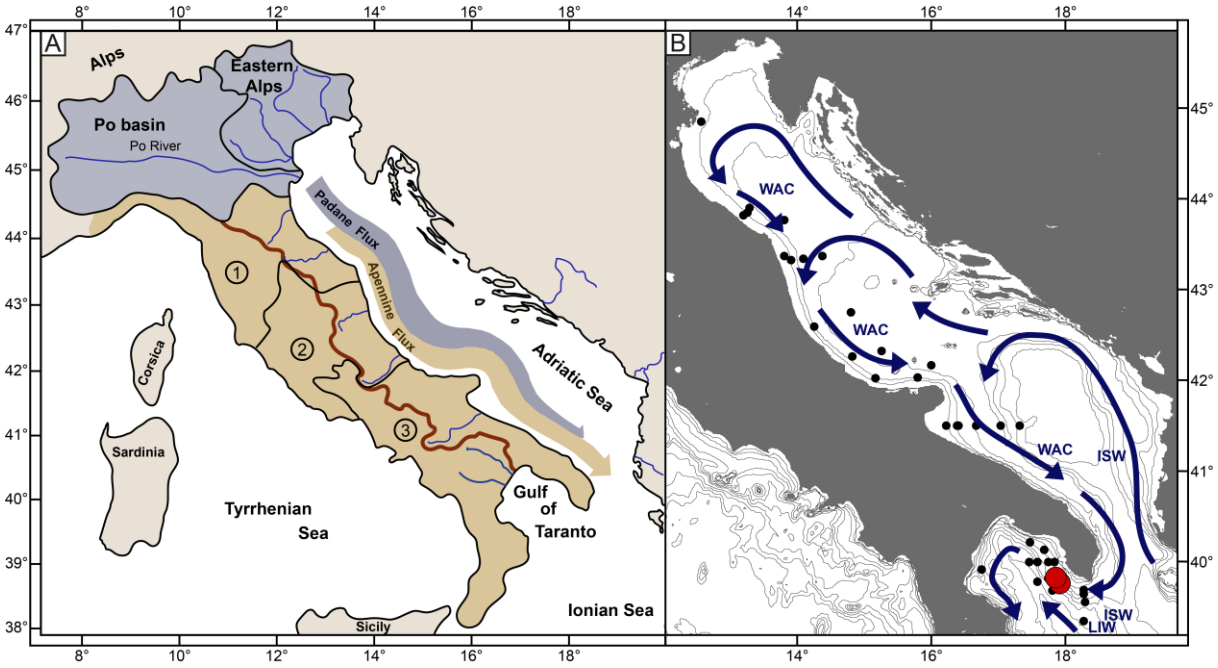

Figure 4.1. A) Large scale overview of Italian catchment areas and dispersal pathways of the different freshwater sources. The coastal Apennine flux (brown) is fed by several smaller Apennine rivers and flows parallel to the Padane flux (grey) which carries material from the Po valley and the eastern Alps. Numbers denote Apennine areas including the northern (1), middle (2), and southern (3) Apennines. Red bold line displays the border of the Apennine river catchments. B) Location of the sediment cores investigated in this study. Black dots display the position of surface sediment samples. The red dot on the lower right shows the locations of core sites GeoB15403-4 and -6 (site 03) and upper left red dot shows the location of GeoB15406-4 (site 06) in the Gulf of Taranto. Blue arrows show the flow directions of the West Adriatic Current (WAC), the Adriatic Surface Water (ASW), the Ionian Surface Water (ISW) and the Levantine Intermediate Water (LIW). Bathymetric map was generated with Ocean Data View (Schlitzer, 2017).

Nutrient transport into the Adriatic Sea and the Gulf of Taranto is influenced by climate and precipitation with marked seasonal variations in river discharge. In summer, when the Inter Tropical Convergence Zone (ITCZ) migrates north, the Mediterranean is under the influence of the Hadley cell that creates hot and dry conditions (Alpert et al., 2006). In winter, the Hadley cell shifts south, and the westerlies become the dominant driver of temperature and precipitation in the Mediterranean Sea region. Changes in the position of the moisture-rich westerlies during winter are closely linked to the NAO. The NAO index reflects an atmospheric pressure gradient between the subtropical high-pressure cell over the Azores and the low-pressure cell over Iceland (Hurrel et al., 2001). A positive mode of the NAO index is connected to warm and wet winters over northern Europe, whereas a negative mode is connected to wet and relatively warm winters in southern Europe including the Mediterranean region (Ferrarese

et al., 2008). The Atlantic Multidecadal Oscillation (AMO), expressed by SST anomalies over the North Atlantic, is a mode of western European summer temperature and precipitation patterns with a quasi periodic variability of about 70 years (Enfield et al., 2001; Knight et al., 2006; Sutton and Hodson, 2005). The origin of the AMO is either linked to internal variability of the oceanic thermohaline circulation only, or to a free oscillation of the coupled ocean-atmosphere system (e.g. Delworth and Mann, 2000; Jungclaus et al., 2005).

Cold and dry Bora winds blow in strong pulses over the Adriatic Sea in winter (Orlic et al., 1994; Rachev and Purini, 2001) and enhanced wind-induced mixing of the oligotrophic ISW and the nutrient-rich LIW results in locally enhanced phytoplankton productivity. Northward winds called Siroccos bring warm and humid air from the Sahara to the Adriatic region year-round, but most commonly in spring (Sivall, 1957). Although Bora and Sirroco winds are short in duration, they can have substantial impact on sea level and circulation of the Adriatic Sea (Ferrarese et al., 2008; Jeromel et al., 2009; Orlic et al., 1994). An aeolian sediment flux related to Bora or Sirroco winds is quantitatively negligible compared to the extensive sediment supply from local rivers (Chester et al., 1997).

4.3 Methods

Sediments from two sites on the eastern Apulian shelf were sampled during RV Poseidon cruise 411 in April 2011. Gravity core GeoB15403-4 and multicore GeoB15403-6 were recovered from site 03 (39°45.42 'N, 17°53.53' E; 170 m water depth); multicore GeoB15406-4 was recovered from site 06 (39°49.49' N, 17°50.02 'E; 214 m water depth) (Fig. 4.1 B). The 524.5 cm long gravity core from site 03 was sampled at 2.5 mm resolution for this study focusing on the uppermost 34 cm. GeoB15403-6 was sampled at 5 mm resolution over the length of 19 cm. The 34 cm long multicore from site 06 was sampled at 5 mm resolution. At both sites, sediments consisted of homogenous, nannofossil-rich greyish to olive green muds. The core tops contain basically undisturbed surface sediments as indicated by the presence of an oxidized sediment layer. The oxygen penetration depth can be identified by distinct color changes at ca. 6 cm for GeoB15403-4, and at 8 cm for GeoB15403-6. This suggests negligible sediment loss during core recovery. Oxygen penetration was down to 4 cm in GeoB15406-4. The difference between the stations is in good agreement with the eutrophic contrast between both sites. We further analysed the distribution patterns of Recent benthic foraminifera in the upper 1-2 cm of multicores from 43 stations along the western coastline of the Adriatic Sea and the Gulf of Taranto to identify gradients in modern environmental conditions. All surface samples were stained with rose Bengal after core retrieval to distinguish living from dead benthic foraminifera.

For faunal investigations, freeze-dried samples of GeoB15403-4 and GeoB15406-4, as well as the stained surface samples were weighed and washed over a 63 µm sieve. The sub-

fractions were dried at 40 °C. The coarse fraction was weighed and dry sieved over a 125 µm sieve before being split into subsamples containing on average 300 individuals. The identification of benthic foraminifera, preferentially on species level, was mainly based on the studies of Cimerman and Langer (1991), Jones and Brady (1994), Milker and Schmiedl (2012), Rasmussen and Thomson (2005) and Sgarella and Moncharmont Zei (1993).

Stable isotope ($\delta^{13}C$, $\delta^{18}O$) analyses of *Uvigerina mediterranea* (1–3 tests) *Cibicidoides pachyderma* (1–5 tests) from GeoB15406-4 were carried out at the Institute of Geophysics and Geology at the University of Leipzig. Carbonate powders were reacted with 105% phosphoric acid at 70°C using a Kiel IV online carbonate preparation line connected to a MAT 253 mass spectrometer. All carbonate values are reported in per mil relative to the Vienna PDB standard. Reproducibility was ensured by replicate analysis of the NBS19 standard and was better than ± 0.029 ‰ for carbon and better than ±0.063 ‰ for oxygen isotopes.

The clay mineral analyses followed standard procedures (Ehrmann et al., 2007) and used bulk sediment samples from GeoB15406-4 and GeoB15403-6. Each sample was oxidized and disaggregated in a 5 % H_2O_2 solution. Then, carbonate was removed using 10 % acetic acid. The fine fraction was separated from the sand fraction by dry sieving through a 63 µm sieve. Settling tubes were used to separate the clay fraction (<2 µm) from the silt fraction. The clay fraction was then analysed for its clay mineral composition using X-ray diffraction (XRF). We mounted the samples as texturally oriented aggregates and solvated them with ethylene-glycol vapour. A Rigaku Miniflex system with CoKα radiation (30 kV, 15 mA) was used for all analyses. Using a step size of 0.02°2θ and a measuring time of 2 s/step, the samples were X-rayed in the range 3–40°2θ. To better resolve the (002) peak of kaolinite and the (004) peak of chlorite, the range 27.5–30.6°2θ was analysed with a step size of 0.001°2θ and a measuring time of 4 s/step. The respective clay minerals were identified through their basal reflections. A semi-quantitative evaluation of the clay mineral assemblages was conducted by the use of empirically estimated weighting factors on integrated peak areas of the individual clay mineral reflections (Biscaye, 1964, 1965; Brown and Bindley, 1980). The respective clay mineral proportions of smectite, illite, chlorite and kaolinite are given in percent of the total clay mineral assemblage.

Total carbon and nitrogen were quantified in samples from GeoB15403-4 by a Carlo Erba Nitrogen Analyser 1500 (Milan, Italy). Particulate organic carbon was determined in weighed powdered bulk samples after acid treatments that removes carbonate. Precision is 0.05 % for total and organic carbon and 0.005 % for nitrogen.

GeoB15403-4 was scanned for the detection of major and trace elements with an ITRAX XRF-core scanner, COX analytical systems (Croudace et al., 2006), of GEOPOLAR at the University of Bremen. Sections were scanned applying a Mo-tube with a step size of 2 mm and a count

rate of 10 s/per step. Tube settings were kept constant using a voltage of 30 kV and a current of 20 mA.

The age model for GeoB15403-4 is based on 11 analyses of surface-dwelling planktonic foraminifera by the AMS ^{14}C method (Table 4.1). Dating was performed at Beta Analytic Inc. (Miami, Florida, USA). Radiocarbon dates were converted to calendar years using the MARINE13 database (Reimer et al., 2013) with a Delta R value of 73 ± 34. Delta R was calculated using the MarineChrono reservoir database through an interpolation of data points close to the core locations. The ^{14}C based age model was complemented by tephroanalysis of the upper 45 cm of the core (Menke et al., 2017 a, under review). Each sample was analysed for its glass shards content in Vol% to identify primary tephra layers. Glass shards from the 63–125 µm fraction were analysed for major and minor elements following the procedure of Kutterolf et al. (2011) using a JEOL JXA 8200 wavelength dispersive electron microscope at GEOMAR, Kiel. The age model for GeoB15406-4 was calculated based on one AMS ^{14}C date and a Delta R value of 73 ± 34 (Table 4.1).

Table 4.1. Age tie points used for generating the age models for sediment cores GeoB15403-4 (site 03) and GeoB15406-4 (site 06).

Site	Depth [mm]	Radiocarbon age [BP]	Calendar years [cal BP]	Data
03	0.00		-61	Sediment Surface
	211.25	1380±30	839±101	AMS^{14}C dating
	358.00		1174	Lipari X tephra (a)
	881.25	2320±30	1846.5±122.5	AMS^{14}C dating
	1248.75	2710±30	2316±142	AMS^{14}C dating
	1598.75	3410±30	3191±138	AMS^{14}C dating
	1845	4020±30	3947±132	AMS^{14}C dating
	1983.75	4270±30	4277±133	AMS^{14}C dating
	2181.25	5470±30	5767±116	AMS^{14}C dating
	2391.25	6290±30	6656.5±124.5	AMS^{14}C dating
	2635.00	8350±40	8807.5±170.5	AMS^{14}C dating
	2868.75	9920±30	10808±169	AMS^{14}C dating
	4061.25	29550±110	33286.5±356.5	AMS^{14}C dating
06	0.00		-61	Sediment Surface
	307.50	670±30	208±126	AMS^{14}C dating

References: (a) Keller, 2002, Albert et al., 2012, Menke et al., 2017 a, under review.

Blackman-Tukey spectral analysis was performed on the original and detrended foraminiferal epifaunal and infaunal datasets of site 03. Both time series have been smoothed by subtraction of a 21-point running average to remove trends reoccurring on greater timescales. After resampling with Δt = 9.03 yrs, spectral analysis was performed using the software AnalySeries 2.0.8 (Paillard et al., 1996).

4.4 Results

4.4.1 Age model

Results of AMS ^{14}C dating are listed in Table 4.1 and are shown in Figure 4.2. Accordingly, core GeoB15403-4 has a basal age of ca. 55,600 yrs BP. Sedimentation rates increase from the older to the younger part of the core from 5.3 cm/kyr to 28.3 cm/kyr. Within the upper 38 cm, the sedimentation rates decrease to 23.47 cm/kyr. Due to the similar oxygen penetration depths in GeoB15403-4 and GeoB15403-6, we applied the age model of the gravity core also to the multicore. GeoB15406-4 has a basal age of ca. 236 yrs BP with a sedimentation rate of 114 cm/kyr.

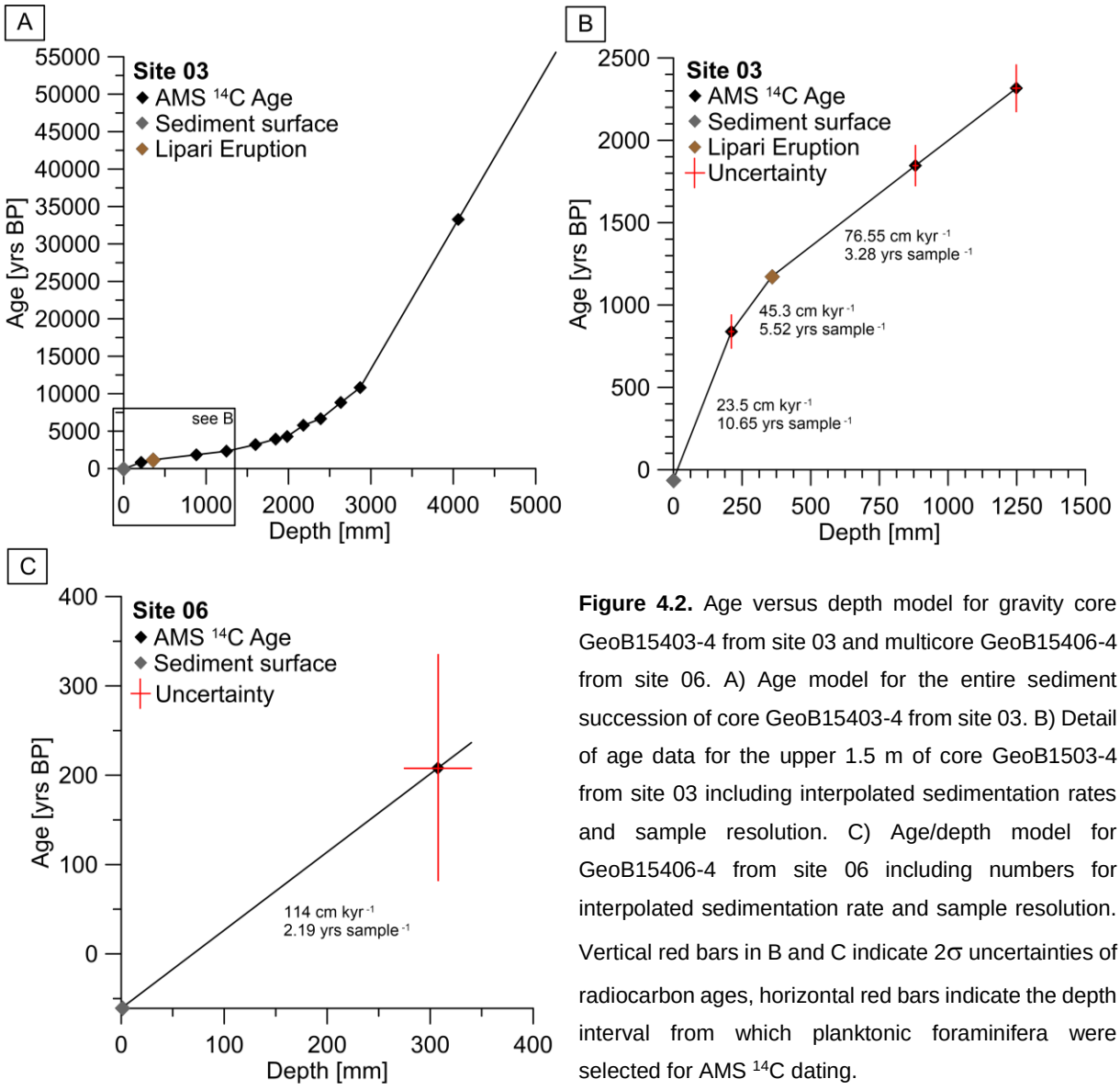

Figure 4.2. Age versus depth model for gravity core GeoB15403-4 from site 03 and multicore GeoB15406-4 from site 06. A) Age model for the entire sediment succession of core GeoB15403-4 from site 03. B) Detail of age data for the upper 1.5 m of core GeoB1503-4 from site 03 including interpolated sedimentation rates and sample resolution. C) Age/depth model for GeoB15406-4 from site 06 including numbers for interpolated sedimentation rate and sample resolution. Vertical red bars in B and C indicate 2σ uncertainties of radiocarbon ages, horizontal red bars indicate the depth interval from which planktonic foraminifera were selected for AMS ^{14}C dating.

4.4.2 Benthic foraminifera

At site 03 and site 06, a total of 247 different foraminifera species were identified (Tables A.2.4 and A.2.5). The diversity at site 03 is generally higher and ranges from 52 to 95 taxa per sample compared to site 06 with 27 to 85 taxa. The most abundant species at site 03 are *Cassidulina laevigata s.l.*, *Melonis barleeanus*, *Gavelinopsis praegeri*, *Bulimina aculeata*, *Cassidulina crassa*, *Textularia pseudogramen*, *Miliolinella subrotunda*, *Globocassidulina subglobosa*, *Brizalina spathulata* and *Bulimina marginata* (Table A.2.4). The most abundant species at site 06 are *Cassidulina laevigata s.l.*, *Melonis barleeanus*, *Uvigerina mediterranea*, *Bulimina marginata*, *Brizalina spathulata*, *Cassidulina crassa*, *Gavelinopsis praegeri*, *Gyroidina umbonata*, *Bulimina costata* and *Quinqueloculina viennensis* (Table A.2.5). In order to characterize changes in food and oxygen supply over time, benthic foraminifera were grouped according to their environmental preferences. Species preferring epifaunal and very shallow infaunal microhabitats and are known to be well adapted to oligotrophic to mesotrophic conditions with relatively low food supply and high oxygen availability (e.g., *Miliolida* spp.) are referred to as Epifaunal Benthic Foraminifera (EBF) (see Table A.1 for classification). Foraminifera preferring mesotrophic environments with elevated food supply and tolerance to moderate oxygen levels are referred to as Shallow to Intermediate Infaunal Benthic Foraminifera (SIIBF) (i.e. *Bulimina* spp., *Bolivina* spp., *Uvigerina* spp; Table A.1). Species tolerant to eutrophic conditions and very low oxygen availability in the sediment pore water are classified as “Deep Infaunal Benthic Foraminifera (DIBF)” due to their ability to live deeper below the sediment surface (i.e. *Chilostomella oolina* and *Globobulimina pseudospinescens*; Table A.1).

SIIBF are dominant at both sites with higher values at site 06 (41.6-67.4 %) after a steady and steep rise up to the most recent samples (Fig. 4.3 A and B). SIIBF at site 03 vary between 40.4 % and 56.3 % peaking at 1830 AD. Thereafter, values decrease and fluctuate around 50 %. EBF at site 03 vary between 9.9 % and 21 % without a clear long-term trend, while EBF at site 06 (5.3–23.9 %) begin at a similar concentration as at site 03 (Fig. 4.3 A), but steadily decrease to 5.3 % in the second to youngest sample. DIBF show the low concentrations at both sites and vary between 0 % and 3.4 % at site 03, and between 0 % and 2.9 % at site 06. Although site 03 shows a slightly higher maximum than site 06, the overall abundance of DIBF over the course of the core is slightly higher at site 06. The $\delta^{13}C$ of *U. mediterranea* at site 06 ranges between -1.07 ‰ and 0.36 ‰ and steadily decreases at the same rate in step with the decrease in EBF (Fig. 4.3 B, Table A.2.6). *Cibicidoides pachyderma* $\delta^{13}C$ varies from -0.3 to 1.05 ‰ and follows the trend of *U. mediterranea*, but because individuals of *C. pachyderma* were not abundant in every sample, the temporal resolution is smaller (Fig. 4.3 B; Table A.2.6). A closer look at the dominant species at site 03 reveals that much of the high abundance after 1600 AD and the sharp peak at 1840 AD are based on rising relative abundances of *Bulimina*

species, as well as *U. mediterranea* and *U. peregrina* (Fig. 4.4). Other dominant species, such as *M. barleeanus,* remain nearly constant, except during a sharp peak at 1787 AD and rising relative abundance in the most recent samples.

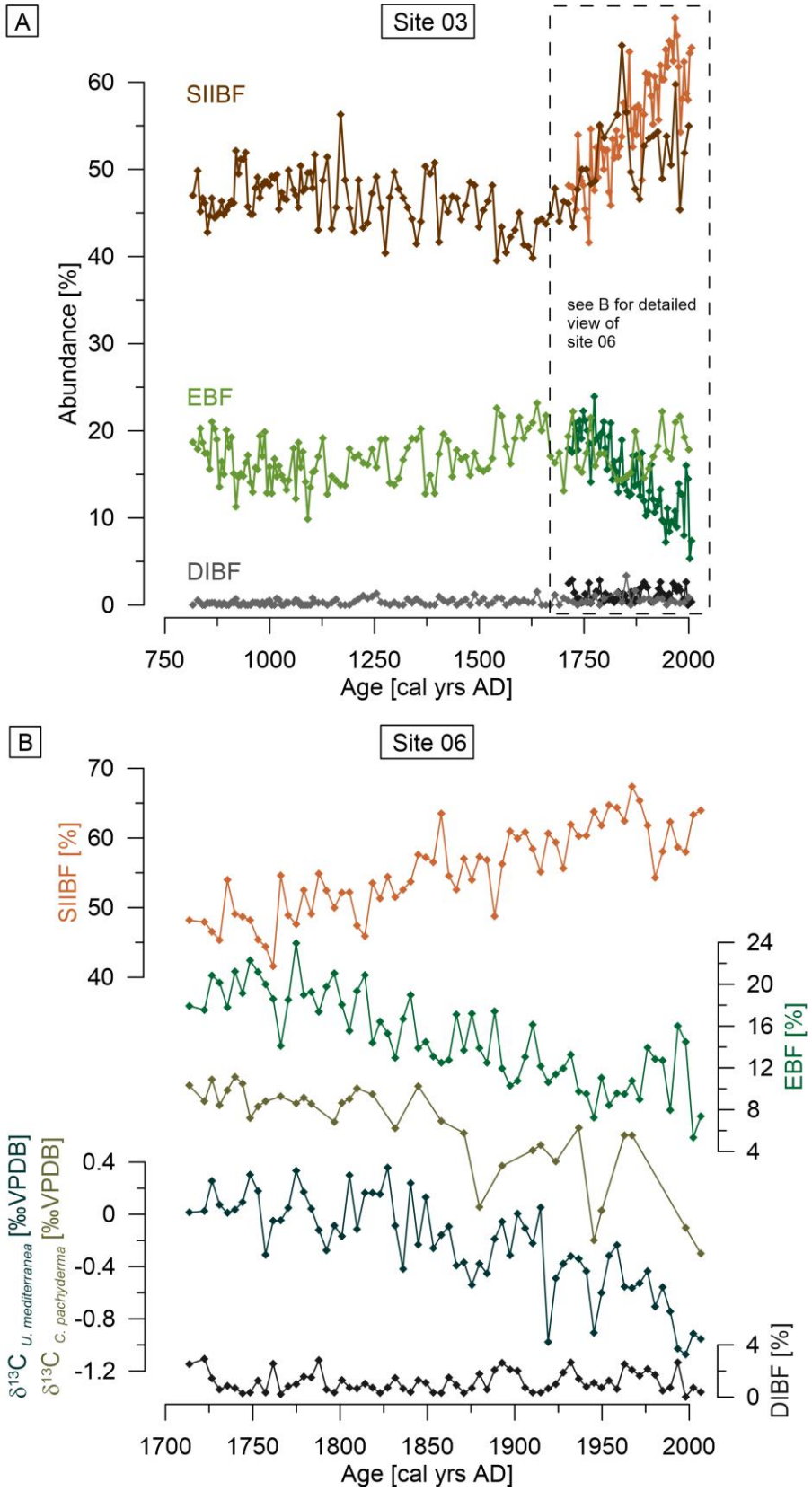

Figure 4.3. A: Relative abundance of benthic foraminiferal microhabitat groups versus time including EBF: Epifaunal Benthic Foraminifera (bright green for site 03, dark green for site 06), SIIBF: shallow to intermediate infaunal benthic foraminifera (brown for site 03, orange for site 06), and DIBF: Deep Infaunal Benthic Foraminifera (grey for site 03, black for site 06). B: Detailed view of microhabitat groups at site 06 (colors as in A) and $\delta^{13}C$ of *C. pachyderma* (olive green) and *Uvigerina mediterranea* (dark green) versus time.

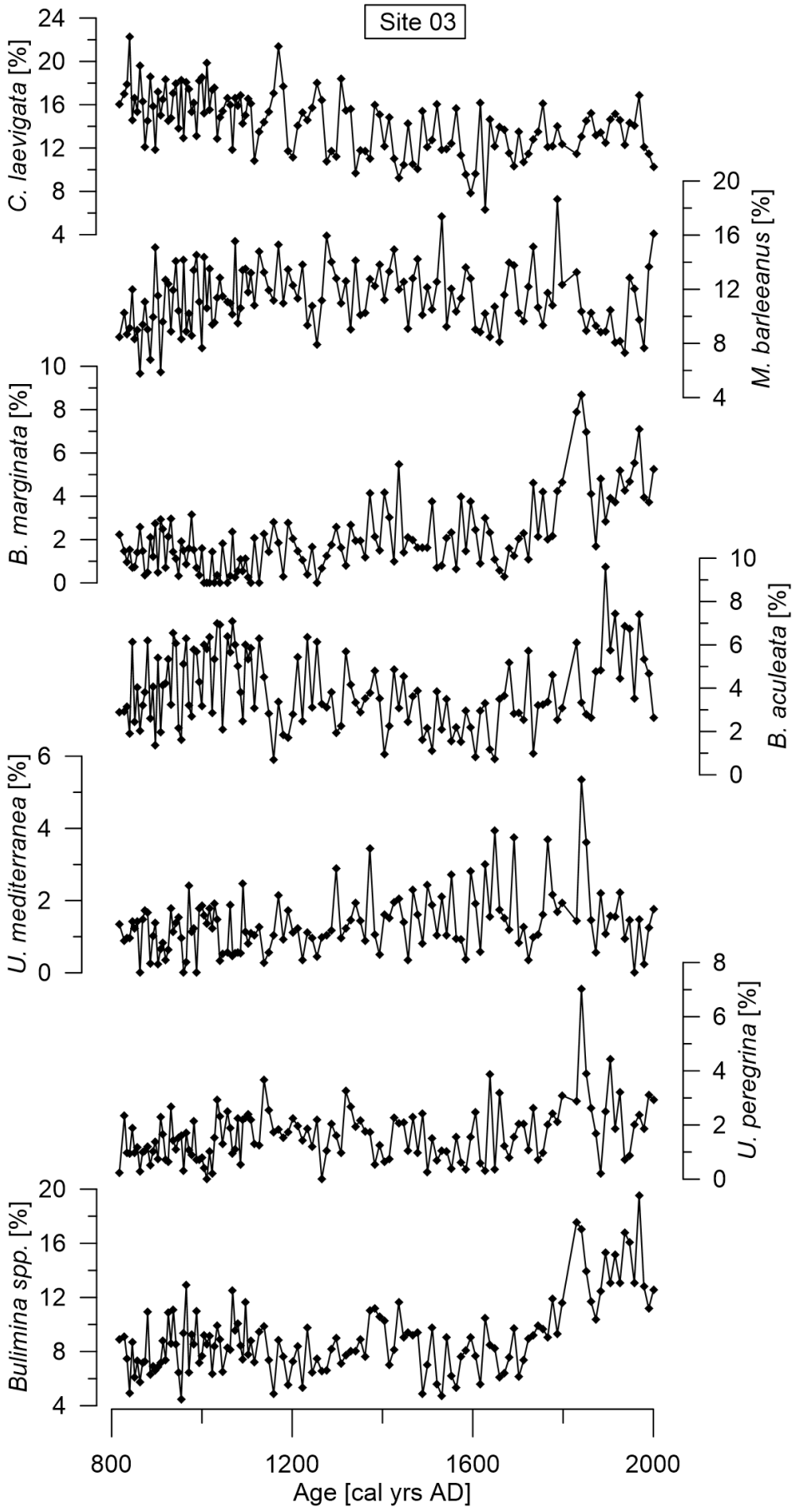

Figure 4.4. Relative abundance of dominant benthic foraminifera taxa versus time at site 03.

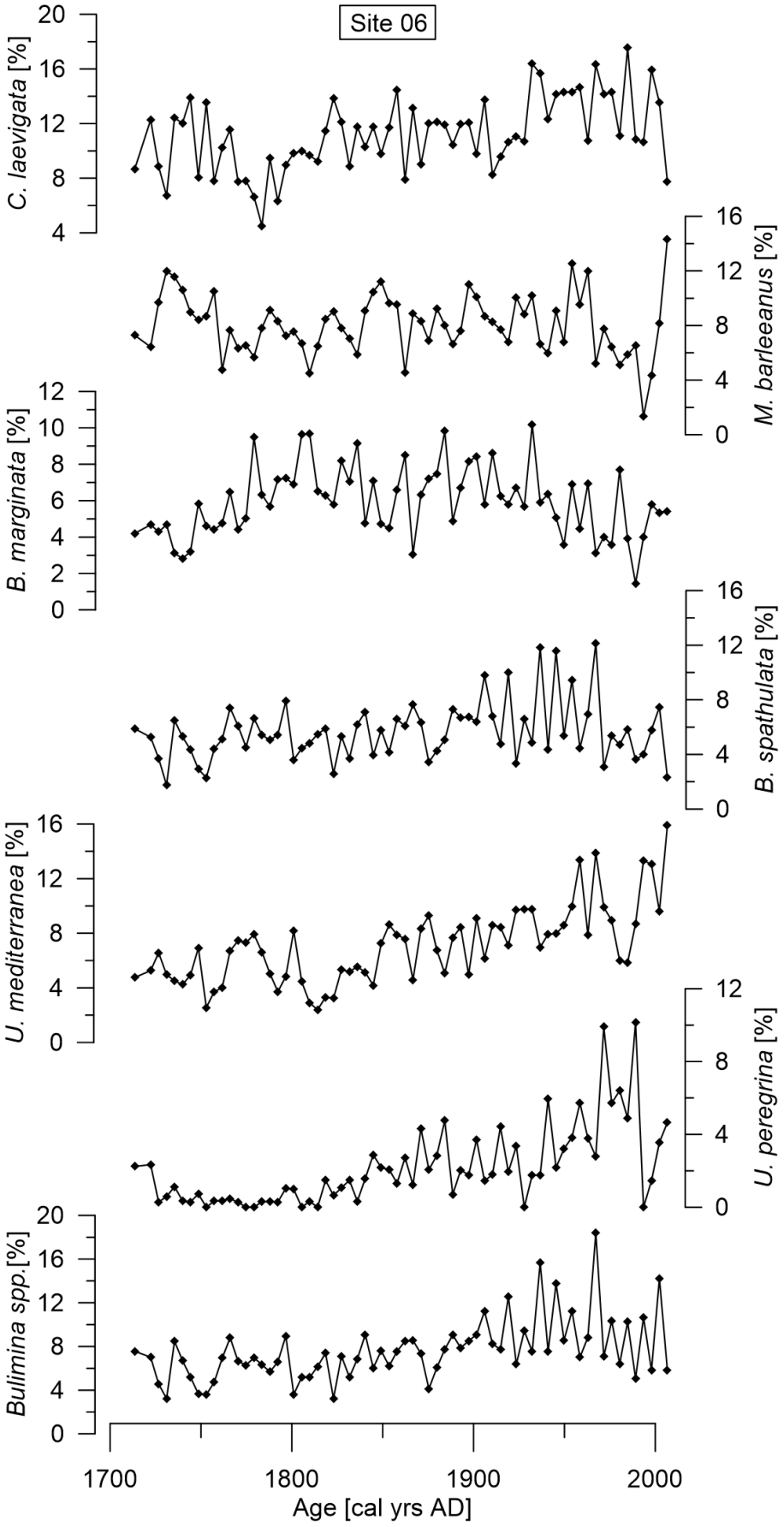

Figure 4.5. Relative abundance of dominant benthic foraminifera taxa versus time at site 06.

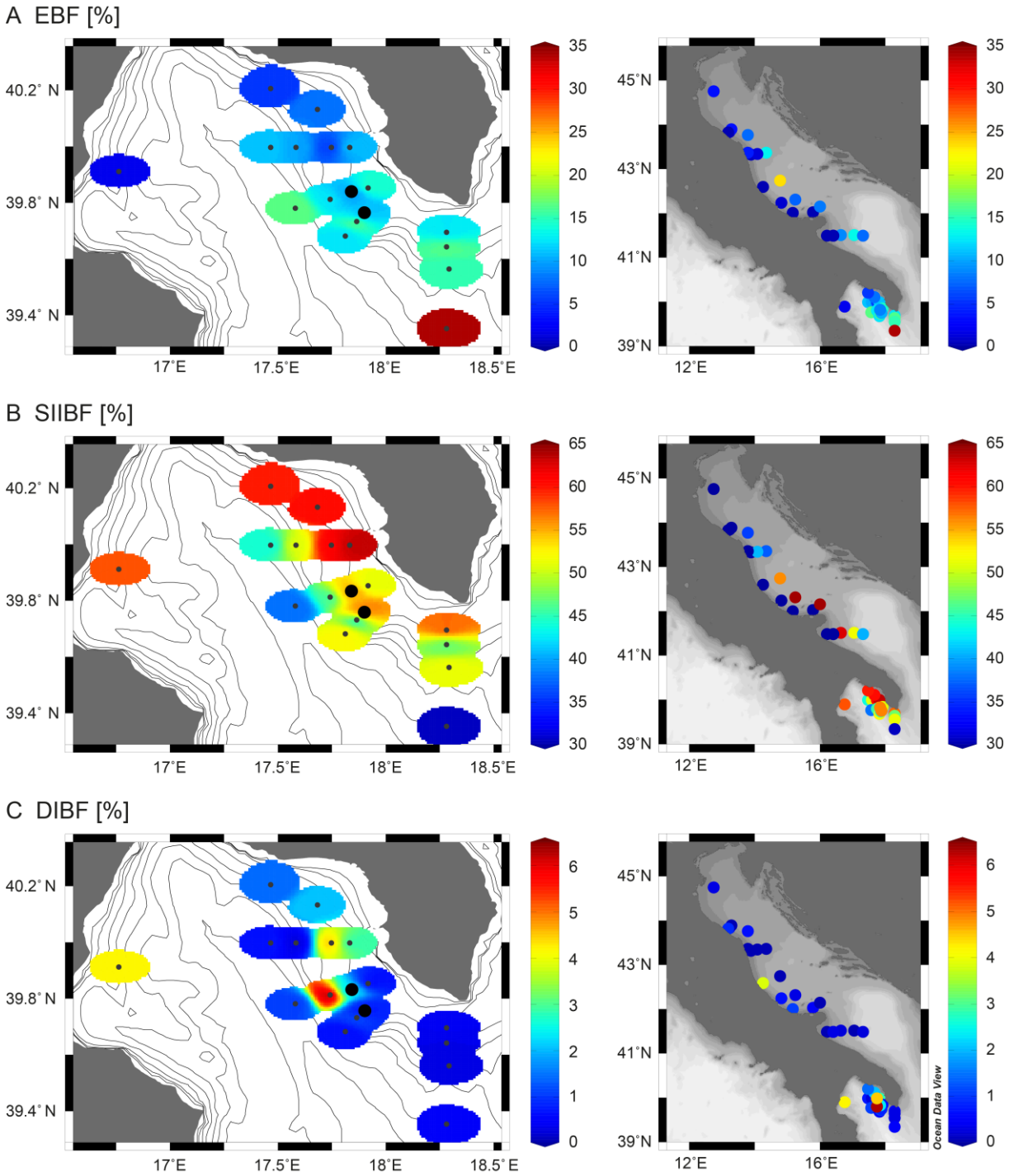

Figure 4.6. Relative abundance of the main foraminiferal microhabitat groups (A-C) in surface sediment samples from the Gulf of Taranto and the western Adriatic Sea. Grey dots display the surface sediment samples, black bold dots show site 03 (lower right) and site 06 (upper left). EBF = epifaunal benthic foraminifera, SIIBF = shallow to intermediate infaunal benthic foraminifera, DIBF = deep infaunal benthic foraminifera. Maps were created with Ocean Data View (Schlitzer, 2017).

Some species, such as *C. laevigata* s.l. even decrease in relative abundance (Fig. 4.4). The latter species ranges between 6.3 % and 22.3 % and shows a general decrease towards the youngest samples, after a maximum abundance between ~800 and 1170 AD (Fig. 4.4). Site

06, covering ~230 yrs BP, shows different patterns in species abundance, even though most dominant species are the same (Fig. 4.5). *Cassidulina laevigata* s.l. (4.5-18 %) shows an overall trend to higher values in the younger samples, while *M. barleeanus* fluctuates around a relatively constant background value and increases sharply (to 14 %) in the youngest sample. Similar to their patterns at site 03, *Bulimina* species and in particular *U. peregrina* and *U. mediterranea* are responsible for much of the rise in IIBF abundance at site 06. *Uvigerina peregrina* rises steadily from values around zero before 1800 AD to around 10 % in 1991 AD, following a steady rise of *U. mediterranea* relative abundances that peaks in the youngest sample at ~16 %.

Differences in species abundance between site 03 and site 06 are in good agreement with faunal distribution patterns in the surface sediments of the Gulf of Taranto (Fig. 4.6, Table A.2.7). Site 06 is located close to a region with a high abundance of intermediate and deep infaunal species. The main SIIBF species in both sediment cores (*Bulimina spp*., *U. mediterranea* and *U. peregrina*) exhibit elevated abundances in surface sediments around the station at which the DIBF percentage is highest in the core record. The modern SIIBF abundance is more variable but high values also concentrate in this area. Site 03 is located just at the southern border of this "infaunal hot spot", well represented by lower overall abundances of SIIBF including *Bulimina* spp., *U. mediterranea* and *U. peregrina.* The relative abundance of *C. laevigata* is higher around site 03 and matches the higher overall abundance of this species in the down-core sediment record of this site when compared to site 06. *Melonis barleeanus* shows slightly higher abundances around site 03 but a more patchy distribution pattern with an exceptional high value at the north-easternmost surface station of the easternmost transect. For most surface stations, DIBF abundance is anti-correlated to EBF abundance, which shows the highest value at the deepest station in the southeast. Elevated abundances of SIIBF can be traced along the western Adriatic Sea into the Gulf of Taranto where SIIBF values are generally high and also DIBF are most abundant (Fig. 4.6 B).

4.4.3 Clay minerals

The kaolinite concentration at site 03 fluctuates between 16 % and 20 %, while chlorite fluctuates between 8 % and 12 % (Table A.2.8). Kaol/Chl ratios vary from 1.6 to 2.4 with a general increase from bottom to top (Fig. 4.7 A). A marked shift from lower values of approximately 1.8 to higher values of approximately 2.2 occurs at ~1600 AD. Kaolinite concentration at site 06 varies between 18 % and 24 %, while chlorite varies between 8 % and 10 % (Table A.2.8). Kaol/Chl ratios fluctuate between 2.0 and 2.8, are constant at 2.4 before 1775 AD, reach a short maximum at around 1800 AD and then generally decrease in younger times (Fig. 4.7 A). Kaol/Chl ratios decrease from older to the younger samples with exception of a strong rise in the youngest sample and a pronounced peak at ~1800 AD (Fig. 4.7 B).

Smectite concentrations at site 03 vary between 32 % and 41 %, and illite concentrations fluctuate between 31 % and 42 % (Table A.2.8). Sm/Ill ratios range between 0.8 and 1.3. The lowest values occur before 1300 AD. Sm/Ill is relatively high between 1300 and 1700 AD. In the younger part of the core the values generally decrease and show a strong variability. Smectite at site 06 varies from 31 % to 38 %, and illite varies from 32 % to 40 % (Table A.2.8). Sm/Ill ratios fluctuate between 0.9 and 1.3 (Fig. 4.7 B) showing a similar but overall lower range of values than Sm/Ill in the same time interval of site 3 (Fig. 4.7 A).

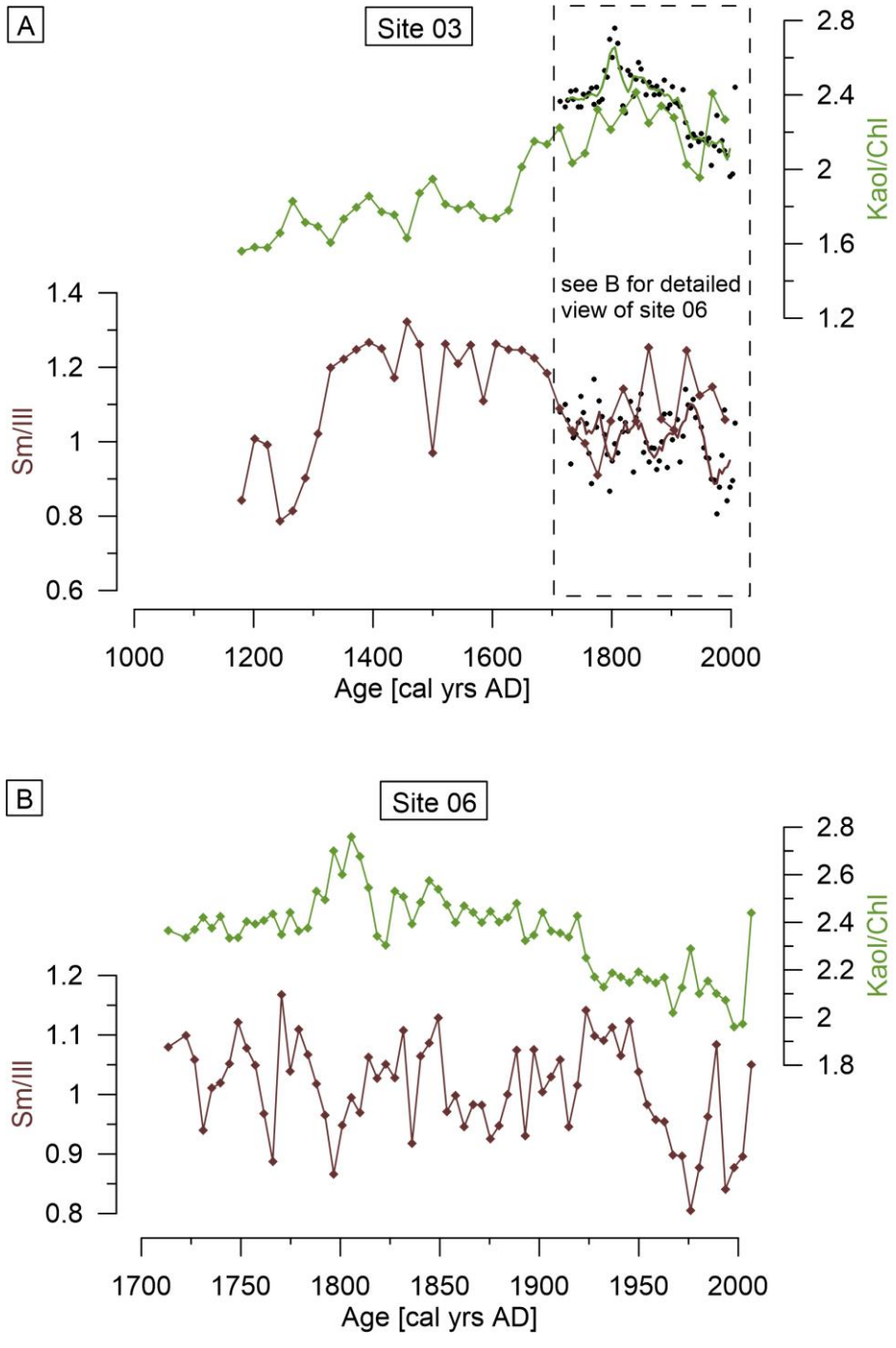

Figure 4.7. A) Clay mineral data of site 03 and site 06 with a detailed view of 06 in B) versus time. The

kaolinite/chlorite ratio is shown in green, the smectite/illite ratio is shown in brown. Single black dots in A) depict data points from site 06, with the associated line presenting a five-point running average.

4.4.4 Organic carbon and nitrogen

Organic carbon at site 03 ranges between 0.5 and 0.8 % with one outlier of 0.9 % at 142.5 mm, which was excluded from our interpretation (Table A.2.9, Fig. 4.8). Values decrease relatively steadily from ~0.6 % to ~0.5 % between 900 AD and 1600 AD. After 1600 AD the organic carbon content rises continuously and exhibits highest values in the youngest samples. C/N ratios at site 03 range between 6.85 and 10.08 with the outlier of 12.5 at 142.5 mm (Fig. 4.8). The trend in the C/N ratios is similar to that in organic carbon content, with generally high values after 1600 AD and a maximum value in the youngest sample.

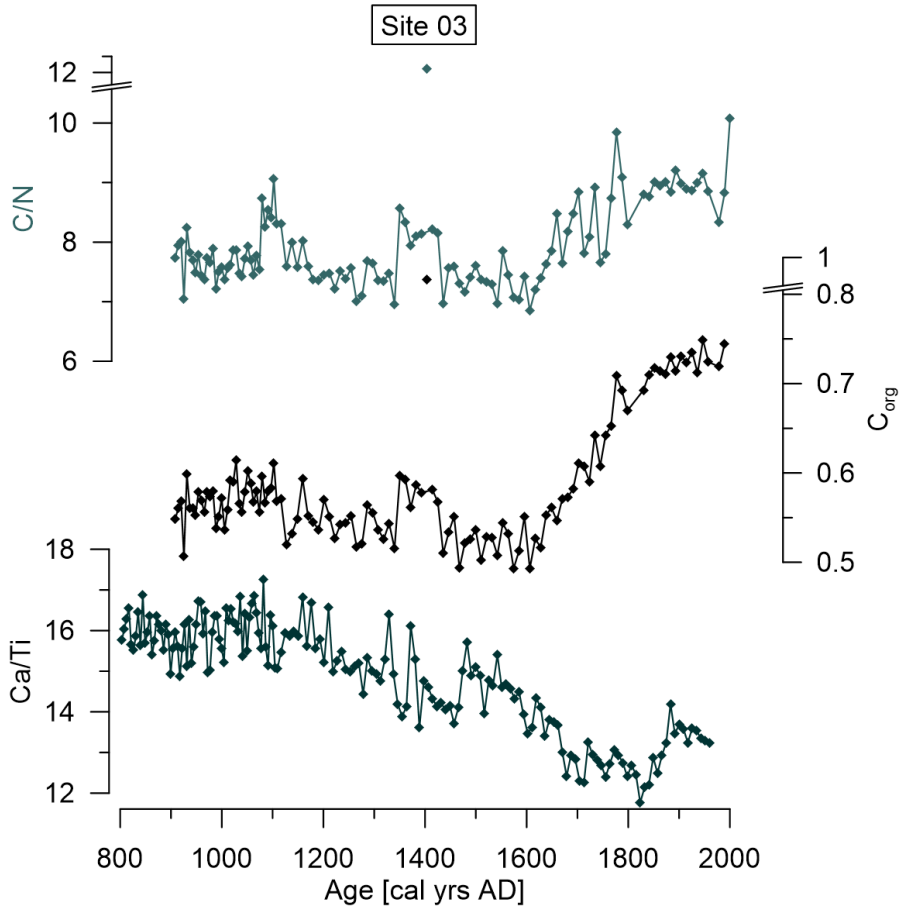

Figure 4.8. C/N ratio, organic carbon content and Ca/Ti ratio of site 03 versus time.

4.4.5 XRF scanning for element composition

Ca/Ti ratios vary between 11.8 and 17.3 with a steady decline from values around 16 in the older part of the core to the lowest value at 1820 AD (Table A.2.10, Fig. 4.8). After that, Ca/Ti ratios increase again until 1880 AD and level of around 13.5 in the youngest samples.

4.5 Discussion

4.5.1 Hydrological forcing of terrigenous matter fluxes to the Gulf of Taranto

The clay mineral composition documents the source areas and dispersal pathways of suspended terrigenous material from the Po and the Apennine rivers through the Adriatic Sea into the Gulf of Taranto. The offshore Po (Padane) flux is rich in illite (> 50 %); in contrast, the coastal Apennine flux is characterized by a generally high smectite concentration (> 30 %) with the southern Apennines providing kaolinite-rich suspensions (Tomadin, 1979, 2000). Low Sm/Ill ratios therefore document a strong influence of the Padane flux. Minima occur around 1750 AD, 1470 AD and 1250 AD (Fig. 4.9 D). They coincide with high abundance of SIIBF (Fig. 4.9 B), which implies that more nutrients and suspended matter at times of enhanced Po river outflow lead to more eutrophic conditions in the Gulf of Taranto and foster the development of shallow and intermediate infaunal microhabitats. The drop of Po-derived suspension at 1300 AD roughly coincides with the onset of the LIA and glacier advances in the Alps (Holzhauser et al., 2005; Le Roy et al., 2015). The cool climate possibly led to increased accumulation of ice and snow in the Alps and to overall low Po river runoff and sediment discharge. While Sm/Ill ratios forced by the Po runoff appear to have been limited by the cool climate, the Kaol/Chl ratios rise steadily since 1300 AD and follow the general trend towards a more negative NAO after 1300 AD (Fig. 4.9 H and I). This can be explained by the fact that the southern Italian borderlands and Apennine mountains are less susceptible to a colder climate due to their lower elevation and location further south (Drever and Zobrist, 1992; Matsuoka, 2008; Cyr et al., 2010). A negative NAO index corresponds to warmer and wetter winters across southern Europe and the Mediterranean Sea (Hurrel, 1995; Tomasino and Dalla Valle, 2000; Trouet et al., 2009), which explains the observed increase in discharge and sediment transport from the southern Apennines and the borderlands of the Gulf of Taranto. The abundance of the shallow infaunal *U. mediterranea* slightly rises simultaneously arguing for a steady increase in organic matter fluxes since ~1300 AD and a relatively high OM quality (Fig. 4.4) (Fontanier et al., 2002; Koho et al., 2008). A close relation between NAO strength and precipitation in the Po river catchment has been confirmed based on direct measurements of the NAO index and Po discharge since 1921 (Tomasino and Dalla Valle, 2000). It is also evident by the correlation of high proportions of illite (low Sm/Ill ratios) with a negative NAO index, as illustrated in the high-resolution record for the past 300 years at site 06 (Fig. 4.10 A and B). Although at site 06 the Sm/Ill ratios trace fluctuations in the NAO index well within the accuracy of the age model, the reliability of different NAO reconstructions has to be questioned because of significant discrepancies between reconstructed and measured NAO indices of the past ~200 years (Fig. 4.10 A black and red lines, e.g. Jones and Mann, 2004). We therefore argue that a comparison of the NAO index and proxy data can provide useful insights into

North Atlantic climate links for the past 200 years, while applications predating this period are less confident.

The longer Sm/Ill record at site 03 is most likely overprinted by the strong temperature influence on large areas of the Po river catchment during the LIA. The steady decline in southern Apennine suspension load since ~1800 AD, evident through lower Kaol/Chl ratios at site 06, is likely attributed to a growing dominance of Po-derived material since the end of the LIA (Fig. 4.10 E). This interpretation appears reasonable, because the Po catchment area is much larger when compared to that of the Apennine rivers. Accordingly, Po suspension loads increased proportionally to precipitation at times of a persistent negative NAO mode and generally increasing temperatures.

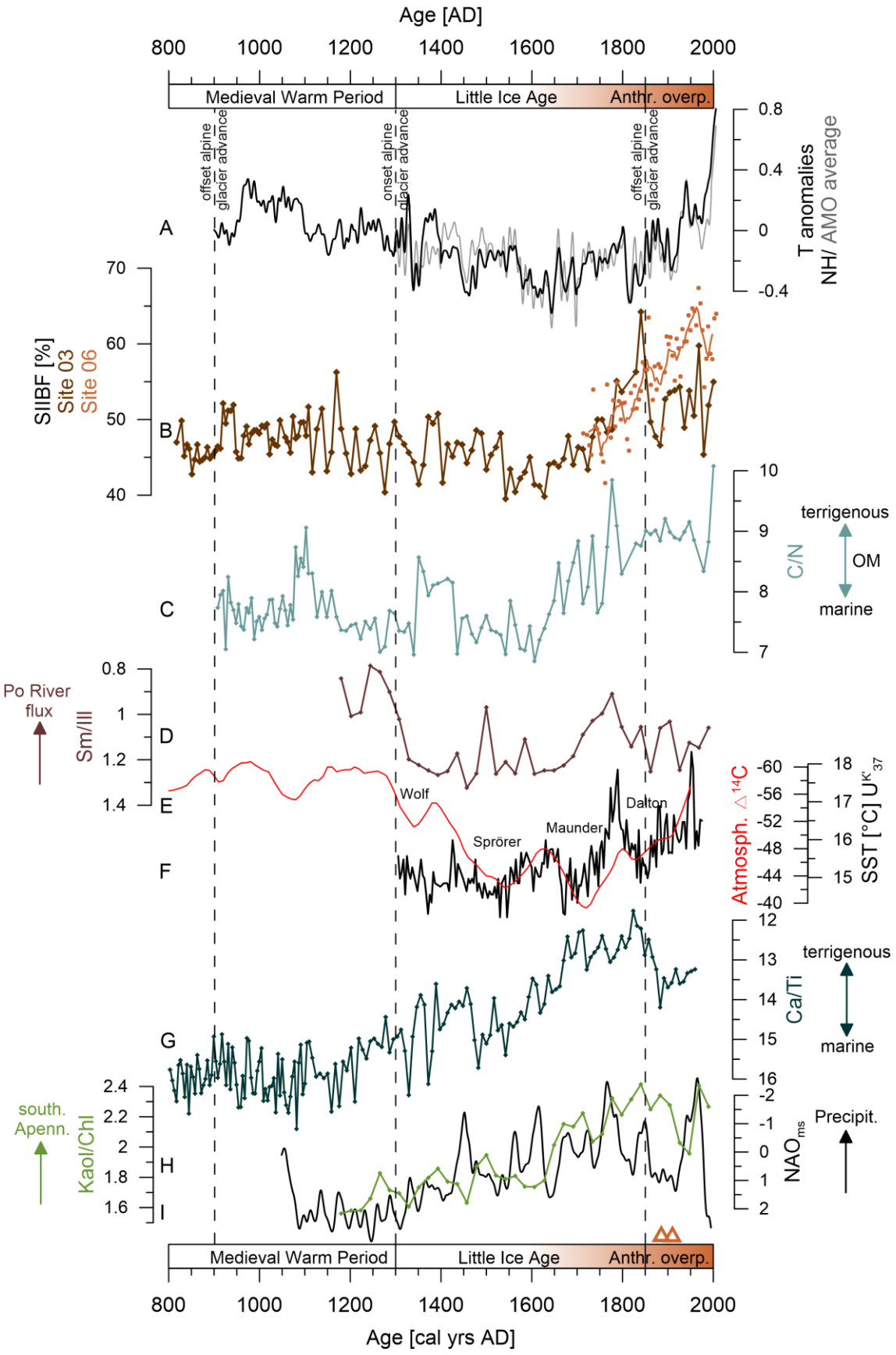

Figure 4.9. Records for North Atlantic climate and solar activity compared to Italian environments for the last millennium. A) Northern Hemisphere temperature anomaly (black) and strength of the Atlantic Multidecadal Oscillation (AMO) (gray) derived from average North Atlantic temperature anomalies (after Mann et al., 2009).

B) Relative abundance of shallow to intermediate infaunal benthic foraminifera (SIIBF) at site 03 (brown) and site 06 (orange dots; orange line displays the five point running average). C) C/N ratio of site 03 as indicator for the origin of organic matter. D) Smectite/ illite ratio of site 03 as indicator for Po river suspension load, with lower values suggesting higher Po River fluxes (dark brown). E) Atmospheric $\Delta^{14}C$ as a measure for solar activity (red; after Reimer et al., 2004). F) Alkenone-based sea surface temperature (SST) record for the Gulf of Taranto (Versteegh et al., 2007). G) Ca/Ti ratio of site 03. H) Kaolinite/chlorite ratio of site 03 as an indicator for sediment input from the Apennines shown in light green. I) Reconstructed North Atlantic Oscillation (NAO) index (after Trouet et al., 2009). Orange triangles on the lower time axis mark the onset of the industrial revolution in Italy at around 1890 AD and the introduction of ammonia as fertilizer at 1913 AD. Dashed black lines show the onset and termination of alpine glacier advances (Holzhauser et al., 2005). The Medieval Warm Period and Little Ice Age are also indicated (Lebreiro et al., 2006; Guiot and Corona et al., 2010; Abrantes et al., 2005; Frisia et al., 2005).

A strong increase in terrigenous sediment input around 1300 AD, simultaneous to rising Kaol/Chl ratios, is also documented by the Ca/Ti ratios obtained from site 03 (Fig. 4.9 G). Previous studies in the Gulf of Taranto based on XRF core scanning showed that changes in Ca/Ti primarily reflect the relative dominance of terrigenous minerogenic versus marine biogenic input (Goudaeu et al., 2014; Richter et al., 2006; Rothwell and Rack, 2006). These studies further demonstrated a positive correlation between low Ca/Ti values, high terrestrial matter input and a negative NAO index for the past 16 kyrs. They also documented the same steep rise in terrestrial matter input during the past 1000 years that is also found in our data.
To summarize, the combination of clay mineral and XRF data concordantly suggests an increase in terrigenous fluxes to the Gulf of Taranto at ~1300 AD. This change in sedimentation can be attributed to generally wetter conditions and enhanced runoff from the borderlands of the Gulf of Taranto and is correlated to persistent negative NAO phases. The Po river runoff shows a strong correlation to NAO strength for the past 300 years. However, runoff declined at the onset of the LIA during which only strong runoff events had an impact on the benthic foraminifera record.

4.5.2 Northern hemisphere climate forcing of marine ecosystems of the Gulf of Taranto

The pronounced mobilization of terrestrial material and its deposition in the Gulf of Taranto around 1300 AD is not reflected in the abundance and species composition of the benthic foraminiferal fauna (Fig. 4.9 B and G). Obviously, the fauna did either not respond to the associated changes in substrate or these changes were negligible. Instead, the trend in the relative abundance of SIIBF taxa generally follows the Northern Hemisphere temperature curve reconstructed from tree ring, ice core, coral and sediment records of the past 1500 years (Mann et al., 2009) (Fig. 4.9 A). Numerous previous studies demonstrated that the abundance of shallow and intermediate infaunal foraminifera is closely related to the availability of food (e.g., De Rijk et al., 2000; Jorissen et al., 1995; Schmiedl et al., 2000), which in the Gulf of Taranto is controlled by riverine nutrient sources and related surface water productivity (e.g.

Focardi et al., 2009; Zonneveld et al., 2009;). This suggests that positive northern hemisphere temperature anomalies resulted in enhanced precipitation in the catchment areas of the Italian rivers in the borderlands of the Adriatic Sea and the Gulf of Taranto. The positive correlation between temperature anomalies and Po river discharge during the instrumental period since 1920 AD (Tomasino and Dalla Valle, 2000) corroborates this interpretation. The C/N ratios in our cores increase simultaneously with the abundance of the SIIBF at around 1600 AD (Fig. 4.9 B and C). The two curves also show similarities during other time intervals, for example a rise around 1350 AD and minimum values between 1500 and 1600 AD, followed by a steep increase. Increased C/N ratios at 1600 AD suggest enhanced input of terrestrial organic matter (Meyers, 1994) and Kaol/Chl and Sm/Ill ratios show a concurrent steep rise of suspended terrigenous material. These observations support our conclusion of elevated precipitation and associated runoff at times of enhanced Northern Hemisphere temperatures (Fig. 4.9 D and H).

Other proxy data from this region documented a similarly strong temperature component in their records. Frisia et al. (2003) argue that their stalagmite record is not predominantly reflecting variations in precipitation but also temperature. Low winter temperatures limited stalagmite growth and pronounced lamina growth started at about 1850 AD, when Northern Hemisphere temperatures began to rise steeply after the LIA. Alkenone-derived sea surface temperatures (SST) from the Gulf of Taranto show a similar temperature trend (Fig. 4.9 F; Versteegh et al., 2007). The SST record corresponds to changes in atmospheric $\Delta^{14}C$ for the period between 1420 AD and 1920 AD, the time before human interferences have likely substantially overprinted the natural climate signal (Fig. 4.9 E and F). Some short-term fluctuations in the SST and benthic foraminiferal records, however, do not correspond to changes in the Northern Hemisphere temperature record. The most prominent example is a SST and infauna maximum between 1650 AD and 1850 AD. Since the change in solar forcing is too small to directly influence regional SST, Versteegh et al. (2007) imposed wind stress to be a key factor, because it influences sensible and latent heat exchange at the water-air interface and strongly modulates the surface-water productivity via turbulence. Turbulence causes deeper convection (Grbec and Morovic, 1997), which in turn cools the surface water and introduces nutrients into the photic zone (Boldrin et al., 2002). This process could expand the season of alkenone production from late autumn to early spring when overall temperatures

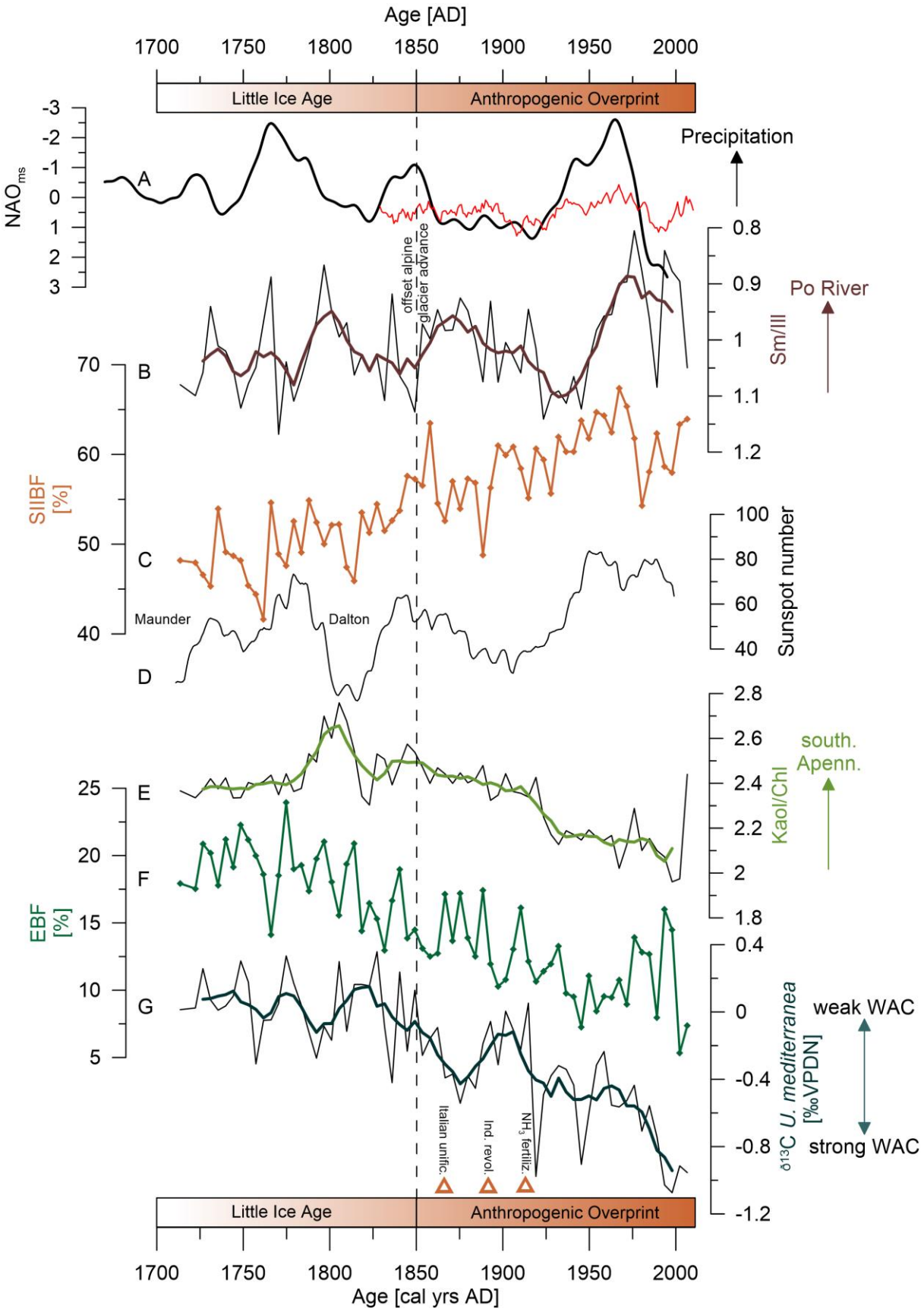

Figure 4.10. Comparison of records for North Atlantic climate, sunspot number, and Italian environments for the last three hundred years. A) Reconstructed North Atlantic Oscillation (NAO) index after Trouet et al. (2009, black line) and measured NAO index from NOAA (https://www.esrl.noaa.gov/psd/gcos_wgsp/Timeseries/NAO/) (red line).

B) Smectite/ illite ratio of site 06 as indicator for Po river suspension load, with lower values suggesting higher Po river fluxes. Bold brown line represents a five point running average. C) Relative abundance of shallow to intermediate infaunal benthic foraminifera (SIIBF) at site 06 and thin line representing a five point running average. D) 21 point running average of the sunspot number from NOAA (https://www.ngdc.noaa.gov/stp/solar/ssndata.html). E) Kaolinite/ chlorite ratio of site 06 as indicator for sediment input from the Apennines. Bold light green line represents a five point running average. F) Relative abundance of epifaunal benthic foraminifera (EFB) of site 06. G) $\delta^{13}C$ of *U.mediterranea* of site 06 as indicator for organic matter fluxes, with lower values suggesting higher organic matter fluxes. Bold dark green line represents a five point running average. Orange triangles on the lower time axis mark the unification of Italy at 1870 AD, the onset of the industrial revolution at around 1890 AD and the introduction of ammonia as fertilizer at 1913 AD. Dashed vertical line represents the termination of alpine glacier growth recorded by Holzhauser et al. (2005).

are higher and could also cause the peak in alkenone temperatures between 1650 AD and 1850 AD. Enhanced primary production and related organic matter fluxes to the sea-floor is a plausible explanation for the peaks in the SIIBF abundance in both sediment cores (Fig. 4.9 B and Fig. 4.10 C) indicating a temporal shift to more eutrophic conditions. The higher temporal resolution at site 06 allows to identify smaller peaks within the overall rise in SIIBF abundance that coincide with high sunspot numbers supporting the hypothesis of sunspot variations influencing seafloor ecosystems through surface productivity (Fig. 4.10 D). However, at the time of SST, SIIBF and C/N maxima, the Sm/Ill ratios indicate elevated Po river input. This implies that the eutrophic conditions were caused by enhanced Po river outflow, possibly due to the combined effects of a negative NAO index and rising temperature.

Power spectra of the detrended time series of the different benthic foraminiferal microhabitat groups at site 03 reveal a significant quasi- periodic variability on multi-decadal time scales, centered at ~54 yrs and ~72 yrs (Fig. 4.11). According to Knudsen et al. (2011) a 55- to 70-year persistent AMO existed through most of the Holocene and was forced by internal ocean-atmosphere variability. The AMO coupling to regional climate appears to have been modulated by insolation-driven shifts in atmospheric circulation patterns and sea-ice cover. Sutton and Hodson (2005) proposed that warm phases of the AMO led to elevated summer temperatures and precipitation over Western Europe during the 20th century. A study on multi-decadal variability of Mediterranean SST's (Marullo et al., 2011) revealed a 70 yr periodicity suggesting a stimulation by the AMO. Our benthic foraminiferal record reveals striking similarities with the AMO reconstruction (Mann et al., 2009) and supports the hypothesis that the AMO influenced the central Mediterranean hydrology and marine environments during the past 1100 years.

Although the fluctuations of the different mineralogical (Ca/Ti, clay mineral ratios), biogeochemical (C/N ratio) and foraminiferal proxy records can be generally reconciled with regional precipitation changes and hemispheric climate modes, a detailed comparison reveals a decoupling of the terrigenous fluxes and faunal development for most species (Figs. 4.9 and 4.10). One explanation could be that changes in terrestrial input due to elevated precipitation

at times of a negative NAO were too subtle to influence substrate composition, organic matter availability and biogeochemical gradients in the sediment. This seems likely when comparing the relatively low-amplitude changes in clay mineral ratios at site 03 to the pronounced shifts observed in sediment cores from the Aegean Sea across major transitions such as the last glacial termination (Ehrmann et al., 2007). We argue that while the NAO signal seems to modulate the overall hydrological regime, the AMO paces rainfall and related impacts on marine environments on multidecadal time scales.

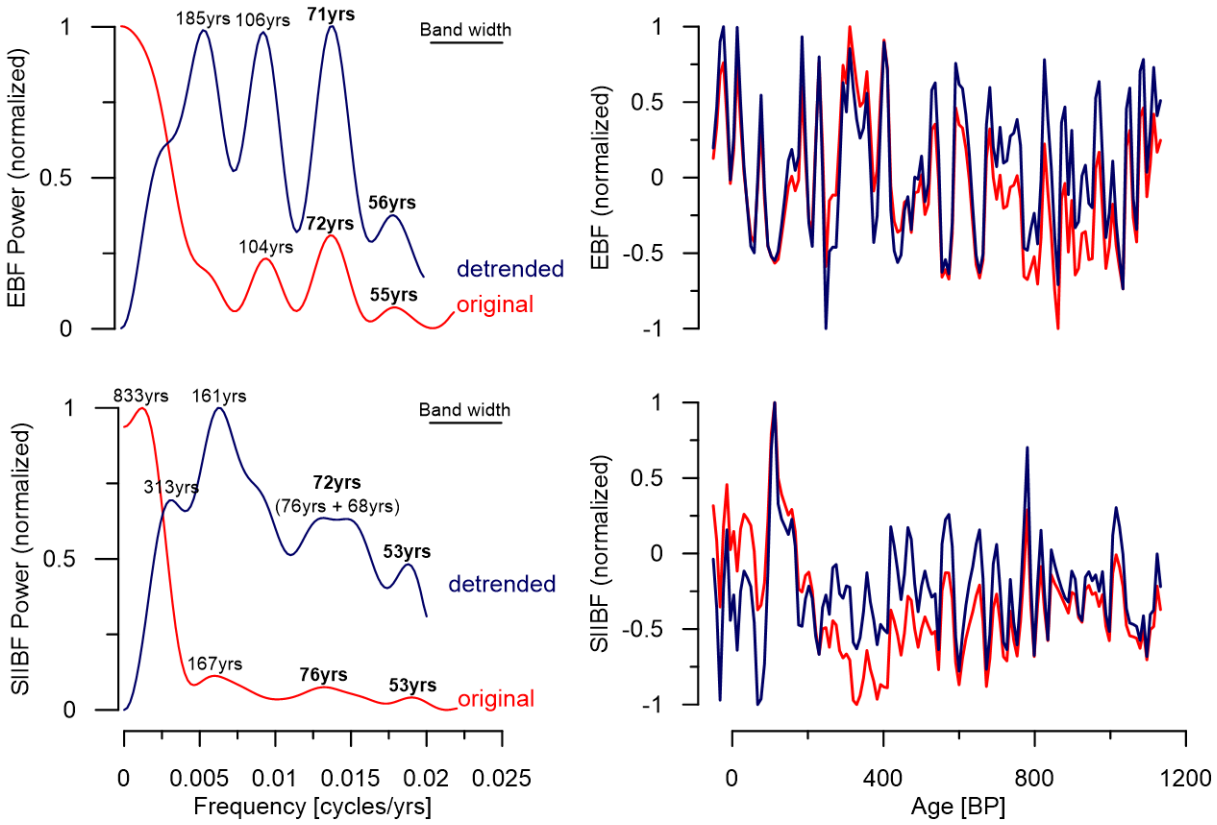

Figure 4.11. Blackman-Tukey power spectra of the original (red) and detrended and normalized (blue) records of epifaunal and shallow infaunal benthic foraminifera of site 03. The foraminiferal data reveal periodic multi-decadal to centennial environmental variations.

4.5.3 Anthropogenic impact on marine environments of the Gulf of Taranto

At least since the time of the Roman Classical Period anthropogenic activity had a significant impact on the depositional dynamics of the Po River and on the western Adriatic Sea. At that time erosion and sediment input increased due to deforestation, agriculture and river embankment (Stefani and Vincenzi, 2005). The demise of the Roman infrastructure after the fall of the Roman Empire resulted in the re-establishment of near-natural conditions over large areas of Italy. This was around 450–650 AD, a time when climate was cooling (Luterbacher et al., 2012). Between 1465 AD and the end of the 1500s, large hydraulic construction projects

were completed in order to protect the local agriculture. Negligence of these constructions combined with strong storm surge events and disastrous flooding, which characterized the LIA, resulted in a loss of reclaimed territories and a transfer back to marshland between the 17th and the first half of the 19th century (Simeoni and Corbau, 2009, and references therein). Increasing population and anthropogenic activity in the Po Valley since at least the 1600s (Lahmeyer, 2006; Lotze et al., 2011; McEverdy and Jones, 1978) most likely resulted in enhanced discharge of suspended matter, nutrients and trace elements into the northern Adriatic Sea. This eutrophication caused intense and recurrent local plankton blooms and anoxia (e.g., Degobbis et al., 2000; Giordani and Angiolini, 1983; Justic, 1987; Marchetti et al., 1989). The quality of the plume waters has also an impact on the composition of dinoflagellate cyst associations (Zonneveld et al., 2012), and the accumulation rate and abundance of different dinoflagellate species registering distinct historical events and inventions, such as the beginning of the industrial revolution in Italy, the introduction of ammonia as fertilizer, and the recent restriction of fertilizer use within the Po Valley (Figs. 4.9 and 4.10, orange triangles).

Persistent dominance of shallow to intermediate infaunal benthic foraminifera in the Gulf of Taranto since ~1800 AD also expresses eutrophication by Po riverine nutrients, but the faunas at the two study sites differ in the proportions of shallow infaunal and epifaunal foraminifera. The relative abundance of SIIBF at site 03 declines after a peak at ~1800 AD, whereas the SIIBF at site 06 continues to rise until about 1970 AD (Figs. 4.3 and 4.9). Also, the proportion of the epifauna at site 03 shows only minor variations, while it continuously declines at site 06. Sedimentation rate at site 06 is about three times higher than at site 03. Varying sedimentation rates between different stations in the Gulf of Taranto have also been reported by Goudeau et al. (2014) supporting earlier evidence for regionally heterogeneous sediment accumulation in this region (Rossi et al., 1983). The difference in the depositional environment between the two sites is today reflected in the distribution pattern of modern benthic foraminifera in surface sediments of the Gulf of Taranto when compared to the Adriatic Sea (Fig. 4.6). Elevated abundances of SIIBF taxa and the development of deep infaunal niches (Jorissen et al., 1995) around site 06 suggest the presence of high organic matter availability at the sea floor. This eutrophic hotspot spreads across isobaths (Fig. 4.6; Zonneveld et al., 2008) and thus is not directly linked to water depths, but to more or less stationary small-scale eddies in the surface water causing zones of nutrient injection and enhanced primary productivity in the surface ocean (Pinardi et al., 2016) and related organic matter fluxes to the sea-floor. Small-scale variability and local patchiness of high-productivity zones in the Gulf of Taranto are also indicated by satellite images of chlorophyll-a concentration in the upper ocean (Zonneveld et al., 2009). The associated regional slow-down of current velocities induces deposition of suspended matter and leads to enhanced accumulation of organic matter at the sea-floor. Accordingly, the fauna comprises both less opportunistic taxa, such as *U. mediterranea,* and

more opportunistic taxa, such as *U. peregrina* (Fontanier et al., 2002; Koho et al., 2008). The latter species benefits from seasonal pulses of freshly deposited phytodetritus and its abundance mimics the seasonal dynamics of surface water productivity as well as the total amount of riverine nutrient fluxes. This makes *U. peregrina* a suitable indicator species for the human-induced eutrophication in the Gulf of Taranto that started around 1800 AD or even earlier. The abundances of *Bulimina* species (Figs. 4.4 and 4.5) resemble the trends seen in *U. peregrina* and argue for similar controls by organic matter fluxes.

Independent micropaleontological and biogeochemical data corroborate the inference of enhanced nutrient input into near-coastal Italian surface waters and associated higher organic matter fluxes in the Gulf of Taranto during the past two centuries. The decrease in the $\delta^{13}C$ record of the shallow infaunal *U. mediterranea* corresponds to a similar trend in the $\delta^{13}C$ record of the epifaunal *C. pachyderma.* Therefore, we assume that *U. mediterranea* is suitable to display the general source of the bottom water mass for a first approximation, although it is a shallow infaunal species whose isotopic signature is commonly influenced by the pore water isotopic gradient (Linke and Lutze, 1993; Schmiedl et al., 2004) (Fig. 4.3 B). Accordingly, $\delta^{13}C$ values of *U. mediterranea* can be used to trace the influence of the nutrient-rich WAC (Grauel et al. 2013b). The $\delta^{13}C$ values of *U. mediterranea* decrease around 1770 AD towards the younger part at site 06 and suggest increased organic matter fluxes and associated remineralisation rates (Theodor et al., 2016a, b) (Fig. 4.10). The inferred elevated nutrient input is consistent with increasing concentrations of plant waxes suggesting an enhanced supply of terrestrial plant material into the Gulf of Taranto starting around 1800 AD (Grauel et al., 2013 b). Concurrent with the pronounced maxima in the SIIBF at ~1850 AD in both of our sediment cores, epiphytic benthic foraminifera diminished around the Po delta as response to higher nutrient loads between 1840 and 1870 AD (Barmawidjaja et al., 1995). The dinoflagellate abundance started to increase in the 1830s and specific species, which prefer eutrophic conditions, increased again around 1930 AD (Sangiorgi and Dongers, 2004). In a more recent study, Zonneveld et al. (2012) used the abundances of dinoflagellate cysts to document changes in the nutrient status of surface waters in the Golf of Taranto that responded to the industrial revolution and the introduction of ammonia as fertilizer in Italy in 1890 and 1920, respectively. In addition, the abundance of coccolithophores started to increase from the late 1800s, followed by the increase of diatoms and other siliceous plankton in the 20th century (Puskaric et al., 1990). We conclude that combined evidence from our own and other biogeochemical and micropaleontological studies document a pronounced human-induced eutrophication of marine environments along the Italian coast of the Adriatic Sea and the Gulf of Taranto since approximately 1800 AD. Our new data demonstrate that the impacts of changes in Italian land-use are not restricted to near-coastal surface water ecosystems, but

can be traced even in outer shelf benthic ecosystems, a case of strong regional land-ocean linkages and tight bentho-pelagic coupling.

The decline of the shallow infauna in the youngest sediments of both cores (Figs. 4.9 and 4.10) reflects decreasing surface water productivity that may be the result of strict environmental regulations and the decline in fertilizer use in Italy since the 1970s (Zonneveld et al., 2012). But it is unclear whether the observed decrease in chlorophyll-a concentrations over the last decades is due to environmental legislation, changing population dynamics or to natural causes such as changes in the precipitation patterns in the river catchments (Mozetic et al., 2010). Over the same time span there is evidence for a reduction of sediment transport due to reforestation and stabilization of lower order channels, and the construction of embankments and dams along the course of the Po River (Galay, 1983; Herget 2000; Marchetti et al., 2002 and references therein; Rodolfi, 1988). The input of sediment particles from the Po river to coastal environments in the Adriatic has almost completely ceased since the mid-20th century because of dam construction, measures against soil erosion, and massive legal and illegal river bed excavation (Stefani and Vincenzi, 2005).

4.6 Conclusions

Benthic ecosystem variability in the Gulf of Taranto is driven by nutrients from the Po and to a lower extent from Apennine rivers that are transported along the Italian east coast with the WAC. A high-accumulation depocenter is developed at the distal end of the WAC in the northeastern Gulf of Taranto. Enhanced sedimentation rates in this area are accompanied by eutrophic conditions reflected by regionally high abundances of shallow and deep infaunal benthic foraminifera at the sea floor.

Clay mineral and XRF data provide evidence for an increase in terrigenous fluxes to the Gulf of Taranto at ~1300 AD driven by generally wetter conditions and enhanced river runoff from the borderlands of the gulf at times of persistent negative NAO phases. Elevated Po River runoff correlates to NAO strength for the past 300 years. However, during the LIA overall river runoff declined and only strong runoff events had an impact on the trophic state of benthic ecosystems in the Gulf of Taranto.

Benthic ecosystem variability on the outer shelf of the Gulf of Taranto is closely linked to the Northern Hemisphere temperature record. Positive temperature anomalies most likely resulted in enhanced precipitation delivering nutrients and organic matter to the gulf. Spectral analyses of benthic microhabitat groups reveal a quasi-periodic variability of ~50 to 70 years suggesting an AMO forcing of benthic ecosystems through elevated summer temperatures and precipitation in the river catchment. Our results suggest, that the NAO determines the overall hydrological regime but the AMO paces rainfall and marine ecological and biogeochemical responses on multi-decadal timescales.

The effect of rising temperatures and nutrient transport during the past 200 years is amplified by increasing anthropogenic activity since the 1600s. Enhanced nutrient input and higher organic matter fluxes transported by a strong WAC resulted in increasing SIIBF abundance (especially the opportunistic *U. peregrina*), and since ~1800 AD led to a decrease of $\delta^{13}C$ values of the shallow infaunal *U. mediterranea*. The decline of the SIIBF abundance during the past few decades is likely the result of stricter regulations on fertilizer use in Italy and the reduction of riverine suspension load due to the stabilization of river bank

5 Centennial-scale climate modulation of the 8.2 ka and 4.2 ka events in the central Mediterranean Sea

Abstract

We present a high-resolution study on multi-decadal to centennial variability of the hydrological regime and the trophic state of the Gulf of Taranto during the 8.2 ka event and the 4.2 ka event, both periods of pronounced cooling and drought in the Mediterranean region. Our study is based on a marine sediment core from the Gulf of Taranto (central Mediterranean Sea) and 44 surface sediment samples from the Gulf of Taranto and the western Adriatic Sea. In the Gulf of Taranto, marine processes are closely linked to large-scale and regional climate patterns because precipitation changes in the Po River catchment and related fluctuation in riverine runoff drive changes in nutrient and suspended sediment load, local phytoplankton blooms and organic matter availability at the sea floor. High levels of shallow to intermediate infaunal benthic foraminifera (SIIBF) in the intervals before 8.5 ka BP and after 8.0 ka BP record meso- to eutrophic boundary conditions. These are punctuated by an approximately 500-year long period of more oligotrophic conditions evident in elevated abundance of epifaunal benthic foraminifera (EBF). The persistence of more oligotrophic conditions across this time interval is most likely due to an overall colder and drier climate and reduced riverine input. Centennial-scale SIIBF and EBF variability responds to variations of the Atlantic Multidecadal Oscillation (AMO) influencing Mediterranean temperature and precipitation patterns. The amplitude of epifaunal *C. pachyderma* $\delta^{13}C$ and $\delta^{18}O$ is much more variable around the 8.2 ka event compared to the 4.2 ka event. The high correlation between $\delta^{13}C$ and $\delta^{18}O$ as well as the comparison with the modern foraminiferal isotope pattern suggest recurrent hydrological shifts at the deeper shelf of the Gulf of Taranto. The observed changes between a highly saline and nutrient-poor water mass (high $\delta^{18}O$ and $\delta^{13}C$) and a relatively fresh and nutrient-rich water mass (low $\delta^{18}O$ and $\delta^{13}C$) most likely mirror different source areas, comprising the more oligotrophic Ionian Sea waters and the more eutrophic river-influenced Adriatic Sea waters. The cold and dry 4.2 ka event is not associated with a general shift in the hydrological and trophic conditions, which appear much more stable when compared to the 8.2 ka event. Comparison of the pre-8.2 ka trophic levels with modern data from the Gulf of Taranto suggests, that human-induced eutrophication since ~1800 AD reaches magnitudes similar to those prevailed during sapropel formation in the early Holocene.

This chapter is based on Menke V., Ehrmann W., Winkelbauer H.A., Theodor M., Mackensen A., Andersen N. and Schmiedl G.: Centennial-scale climate modulation of the 8.2 ka and 4.2 ka events in the Central Mediterranean Sea. In preparation for submission.

5.1 Introduction

Against the background of orbital-driven climate changes and the millennial-scale climate variability of the last glacial period, the Holocene is characterized by a comparatively stable climate (Dansgaard et al., 1993; Grootes and Stuiver, 1997). However, closer inspection of high-resolution proxy records demonstrates that the Holocene is punctuated by a series of millennial to centennial climate variations, which appear particularly strong at high latitudes but also impacted the temperate and subtropical regions leading to climate perturbations such as around 8.2 and 4.2 ka BP (e.g. Bond et al., 1997; Gupta et al., 2003). Various processes have been invoked to explain the origin and propagation of these abrupt climate changes, including variations in solar output (Bond et al., 2001; Schulz and Paul, 2002; Soon et al., 2014) and polar ice sheet discharges and related freshwater perturbations (Alley et al., 1997; Bakker et al., 2017; Barber et al., 1999).

The most prominent climate perturbation is centred around 8.2 ka B.P., when northern hemisphere winter temperatures dropped by 0.5 to 1°C on average. In various regions winter temperatures decreased by as much as 2–4°C, including the Arctic (Renssen et al., 2002) and the northeastern Mediterranean (Pross et al., 2009). This prominent cooling has been attributed to a catastrophic drainage of Lake Agassiz (Barber et al., 1999; Lajeunesse, 2012) and associated reduction of North Atlantic Deep Water formation (Kleiven et al., 2008). In the Mediterranean region this cold event was accompanied by reduced precipitation leading to a widespread drought (Staubwasser and Weiss, 2006; Weiss and Bradley, 2001). It has been hypothesized that these dry conditions caused a fundamental socio-cultural reorganization, the expansion of farming into southern Europe, rapid population movements as well as the transient abandonment of settlements in central Anatolia that ultimately propagated the Neolithization in southeastern Europe (Turney and Brown, 2007; Weninger et al., 2006).

The 8.2 ka event did not only affect human population patterns but also led to a resumption of deep-water formation in the eastern Mediterranean Sea (EMS), evident in a 200-year interruption of the Holocene sapropel S1 (De Rijk et al., 1999; Myers and Rohling, 2000; Rohling et al., 1997). Even though causes and mechanisms leading to the deposition of this organic-rich sediment layer are still subject of debate, the relatively wet and warm climatic boundary conditions of the early Holocene played a significant role for the basin-wide anoxia (Rohling and Hilgen, 2007). Various observations suggest that the sharp 8.2 ka event punctuates a multi-century climate deterioration occurring between approximately 8.5 and 8.0 ka BP. This multi-centennial cold anomaly is evident in summer-dominated records that started well before the S1 interruption and the 8.47 ± 0.3 ka BP meltwater flood from lake Agassiz and Ojibway (Rohling and Pälike, 2005 and references therein).

The 4.2 ka event is less well expressed in the ice core record and in other North Atlantic climate records (Grootes and Stuiver, 1997; Schulz and Paul, 2002). In the Mediterranean region and

the Near East, it resulted in a marked drought event, which is cited as one of the main reasons for the collapses of the Old Egyptian Kingdom and the Akkadian Empire in Mesopotamia (Arz et al., 2006; Drysdale et al., 2006; Weiss et al., 1993). During this drought Nile river fluxes dropped drastically (Schmiedl et al., 2010) and large amounts of dust were mobilized and emitted from arid and semiarid regions of the Near East and the Arabian Peninsula (Cullen et al., 2000). The 4.2 ka event is particularly prominent in the northern sector of the African monsoon domain but its occurrence on northern European latitudes is still uncertain (Zanchetta et al., 2016).

The Gulf of Taranto (southern Italy) in the central Mediterranean is particularly suitable for high-resolution studies of short-term climate change. Here, the link between climate and marine environments is especially strong because precipitation-driven riverine input has significant impacts on hydrology, sediment supply and nutrient availability (Goudeau et al., 2014; Versteegh et al., 2007; Zonneveld et al., 2012). Changes in organic matter availability and bottom water oxygenation can be recorded in the abundance of individual benthic foraminifera species and their stable isotope signals as well as the proportion of certain foraminifera groups that inhabit stratified microhabitats on and within the sediment, hence reflecting different nutrient levels and oxygen availability (Corliss, 1985; Jorissen et al., 1995; Lutze and Thiel, 1989; Mackensen and Douglas, 1989; Murray, 2006). On the other hand, clay minerals represent an independent proxy for terrestrial weathering, sediment mobilization and river discharge allowing for a reconstruction of climatic conditions and sediment dispersal pathways independent from sea floor ecology (e.g. (Biscaye, 1965; Ehrmann et al., 2007; Petschick et al., 1996).

Despite recent progress in accumulating proxy information, the spatial and temporal expressions of the 4.2 ka and 8.2 ka events in the Mediterranean region are not yet well constrained. Specifically, little is known on the links of these intervals to multi-decadal to centennial climate changes of the North Atlantic region, including the Atlantic Multidecadal Oscillation (AMO). Here we use information from benthic foraminiferal faunas and stable isotopes as well as clay mineral data from an exceptional high-resolution sediment archive of the Gulf of Taranto to evaluate the internal variability of Italian hydrology, river-runoff and marine ecosystems during the 4.2 ka and 8.2 ka intervals.

5.2 Environmental setting

The Gulf of Taranto (Fig. 5.1) is located in the central Mediterranean Sea at the transition of the subtropical high-pressure belt and the temperate mid-latitude westerlies. In summer, when the Hadley cell is located in the north, the northward shift of the Intertropical Convergence Zone (ITCZ) results in a warm and relatively dry climate (Alpert et al., 2006). In winter, when the Hadley cell shifts south, the region is influenced by moist westerlies being the main driver

of precipitation. Fluctuations in the strength and direction of the westerlies are controlled by the North Atlantic Oscillation (NAO). The NAO index discribes the dipole-like gradient between the high-pressure system over the subtropical Azores and the subpolar low- pressure system over Iceland (e.g., Hurrell, 1995). A negative NAO mode corresponds to a more southerly location of the westerlies leading to humid winter conditions in the Mediterranean region. In contrast, during a positive NAO mode, the westerlies are deflected further north leaving the Mediterranean warm and dry (Hurrell, 1995).

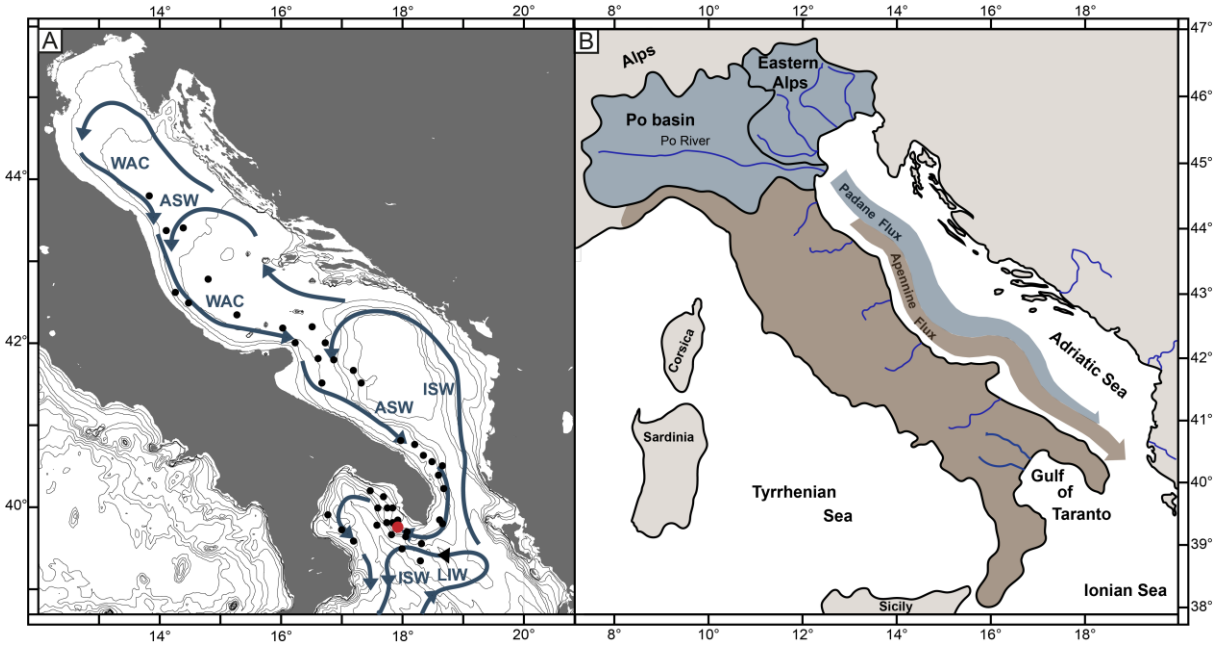

Figure 5.1. A) Bathymetric map of the Adriatic Sea and the Gulf of Taranto (generated with Ocean Data View, Schlitzer (2017)). Blue arrows show the general surface water circulation, the West Adriatic Current (WAC) and the Northern Ionian Cyclonic Gyre south of the Gulf of Taranto. Dominant water masses are the Ionian Surface Water (ISW, Levantine Intermediate Water (LIW) and Adriatic Surface Water (ASW). Surface sediment stations for isotope analysis are marked with black dots while the location of gravity core GeoB15403-4 is marked in red. B) Large scale overview of the Adriatic Sea and the Gulf of Taranto with the dominant Italian river catchments and pathways of clay mineral distribution.

Mediterranean summer temperature and precipitation is linked to the Atlantic Multidecadal Oscillation (AMO) with a periodicity of 50 to 70 years (Marullo et al., 2011; Sutton and Hodson, 2005). Although the origin of the AMO is complex and not yet fully understood, it is either linked to internal variability of the thermohaline circulation or to a free oscillation motion of the ocean atmosphere coupled system (e.g., Delworth and Mann, 2000; Jungclaus et al., 2005).

Year round but most commonly in spring, Scirocco winds bring warm and humid air from the Sahara into the Adriatic Sea. The Sirocco winds potentially impact local sea level and circulation but only transport minor amounts of aeolian sediment into the Gulf of Taranto (Jeromel et al., 2009; Sivall, 1957).

The location of the Gulf of Taranto at the southern tip of the Adriatic Sea and transition to the Ionian Sea leads to a complex circulation pattern involving various water masses entering the gulf from different directions and at different water depths (Fig. 5.1 A). Surface water masses comprise the Adriatic Surface Water (ASW) and the Ionian Sea Water (ISW). The ASW originates from the northern Adriatic Sea and is characterized by comparatively low salinities (< 37 psu) (Lipizer et al., 2014) and high nutrient concentrations. It is transported with the West Adriatic Current (WAC) in a narrow coastal band along the coastline of Italy before it enters the gulf. The relatively warmer, saltier (38.8-39.9 psu) (Budillon et al., 2010), and more oligotrophic ISW enters the gulf from the Ionian Sea (Fig. 5.1 A). In the Gulf of Taranto both surface water masses generally follow a cyclonic circulation with various small-scale gyres. The WAC nutrient and suspension load is strongly driven by seasonal pulses of nutrient-rich freshwaters from the Po river, draining large parts of the western and central Alps and northern Apennines, and smaller rivers draining the eastern Alps (Turchetto et al., 2007). The clay mineral fraction of the suspension load is characterized by high illite concentrations, allowing for tracing the so-called Padane flux along the western border of the Adriatic Sea. The Padane flux reaches maximum extension during late spring and autumn when enhanced precipitation over Italy and Alpine snow melt lead to peaks in river discharge, respectively (Fig. 5.1 B) (Milligan and Cattaneo, 2007; Poulain, 2001; Tomadin, 2000; Tomadin 1979; Zonneveld et al., 2012). While flowing southwards, the WAC gets further enriched with sediment and nutrients by fluvial contributions from several smaller river systems draining the middle and southern Apennines. Southern Apennine derived suspension is enriched in smectite forming a weaker signal, which can be detected in sediments closer to the Italian coast (Fig. 5.1 B) (Degobbis et al., 1986; Milligan and Cattaneo, 2007; Tomadin, 2000). The nutrients of the ASW are the main driver of primary production in the western Adriatic Sea leading to strong phytoplankton blooms in autumn and spring (e.g., Boldrin et al., 2002). At a depth of 200–600 m, the colder (13.5°C) (Artegiani et al., 1997), saline Levantine Intermediate Water (LIW; >38.7 psu) enters the Gulf of Taranto from the Levantine and Ionian basins. Northern Adriatic Dense Water (NAdDW) is formed in the northern Adriatic during winter, when cold and dry Bora winds blow in strong pulses south-eastward (Orlić et al., 1994; Rachev and Purini, 2001; Turchetto et al., 2007). Southern Adriatic Dense Water (SAdDW) forms in late winter and early spring as a result of deep-water convection. Both water masses form the dense Adriatic Deep Water (ADW), which enters the Gulf of Taranto from the Adriatic Sea and bathes the deep basins of the Ionian and Levantine seas (Turchetto et al., 2007).

5.3 Methods

Gravity core GeoB15403-4 (39°45.42'N, 17°53.53E'; 170m water depth) was recovered from the southwestern Apulian shelf in the eastern Gulf of Taranto during RV Poseidon cruise 411

in April 2011. The maximum depth of oxygen penetration into the surface sediment was identified by distinct color changes at 6 cm, well in accordance with multicores from the same station suggesting negligible sediment loss during core recovery. The 5.25 m long sediment core was sampled at a 2.5 mm resolution. This study focuses on two intervals comprising the "4.2 ka interval" from 1877.5-2002.5 mm core depth (52 samples) and the "8.2 ka interval" from 2500-2625 mm core depth (52 samples). Sediments in both intervals consist of faintly laminated grayish to green foraminifera-bearing nannofossil mud.

All freeze-dried samples were weighted, washed over a 63 µm sieve and the residue dried at 40°C. The coarse fraction was dry sieved over a 125 µm sieve. For benthic foraminiferal faunal analyses, sediment samples of the 8.2 ka interval were divided into sub samples containing on average 300 individuals. The identification of benthic foraminifera, preferentially on the species level, is mainly based on the studies of Cimerman and Langer (1991), Sgarrella and Moncharmont Zei (1993), Jones (1994), Rasmussen (2005), and Milker and Schmiedl (2012). The dominance D and Shannon Wiener Diversity H were calculated using the PAST (PAleontological STatistics) software applying the equations $D=\Sigma (n_i/n)^2$ and $H= -\Sigma n_i/n*\ln(n_i/n)$, with "$n_i$" representing the number of taxa and "n" the number of individuals (Hammer et al., 2001; Hammer et al., 2008).

For stable oxygen and carbon isotope analyses of benthic foraminifera, adult specimens were selected from the >125 µm size fraction of the 4.2 ka and 8.2 ka intervals, including the epifaunal species *Planulina ariminensis* (1–5 tests) and *Cibicidoides pachyderma* (2–5 tests), the shallow infaunal *Uvigerina mediterranea* (1–3 tests), and the deep infaunal *Globobulimina pseudospinescens* (1–3 tests). Isotope measurements of both core intervals were carried out at the Alfred Wegener Institute, Helmholtz Centre for Polar and Marine Research at Bremerhaven with a Finnigan MAT 253 stable isotope ratio mass spectrometer coupled to an automatic carbonate preparation device (Kiel IV). The mass spectrometer was calibrated to the PDB scale using the international standard NBS 19. All results are given in δ notation vs. VPDB. Based on an internal laboratory standard (Solnhofen limestone) measured over a 1-year period together with samples, the precision of stable isotope measurements was better than ± 0.06 and ± 0.08 ‰ for carbon and oxygen, respectively.

The clay mineral analyses followed standard procedures (Ehrmann et al., 2007) and used bulk sediment samples from GeoB15406-4 and GeoB15403-6. Each sample was oxidized and disaggregated in a 5 % H_2O_2 solution. Then, carbonate was removed using 10 % acetic acid. The fine fraction was separated from the sand fraction by dry sieving through a 63 µm sieve. Settling tubes were used to separate the clay fraction (<2 µm) from the silt fraction. The clay fraction was then analysed for its clay mineral composition using X-ray diffraction (XRF). We mounted the samples as texturally oriented aggregates and solvated them with ethylene-glycol vapour. A Rigaku Miniflex system with CoKα radiation (30 kV, 15 mA) was used for all

analyses. Using a step size of 0.02°2θ and a measuring time of 2 s/step, the samples were X-rayed in the range 3–40°2θ. To better resolve the (002) peak of kaolinite and the (004) peak of chlorite, the range 27.5–30.6°2θ was analysed with a step size of 0.001°2θ and a measuring time of 4 s/step. The respective clay minerals were identified through their basal reflections. A semi-quantitative evaluation of the clay mineral assemblages was conducted by the use of empirically estimated weighting factors on integrated peak areas of the individual clay mineral reflections (Biscaye, 1964, 1965; Brown and Bindley, 1980). The respective clay mineral proportions of smectite, illite, chlorite and kaolinite are given in percent of the total clay mineral assemblage.

The age mod

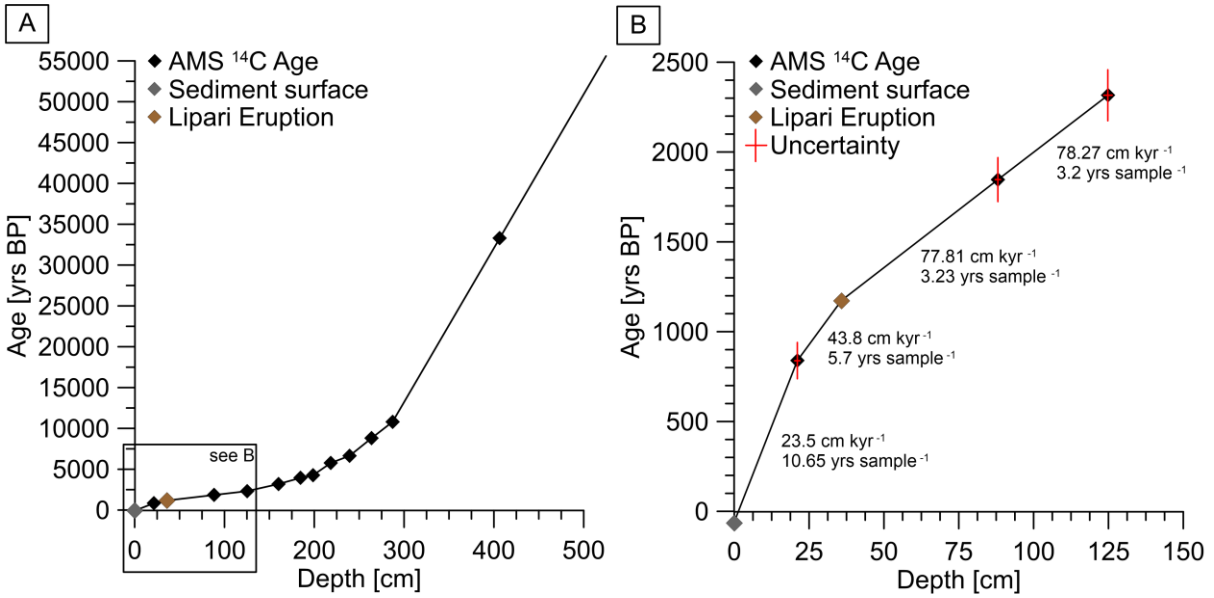

el of GeoB15403-4 consists of 11 AMS ^{14}C dates on surface-dwelling planktonic foraminifera complemented by tephroanalysis of the upper 45 cm of the core (Menke et al., 2017 a, under review) (Table 5.1). Dating was performed at Beta Analytic Inc. (Miami, Florida, USA). Radiocarbon dates were converted to calendar years using the MARINE13 database (Reimer et al., 2013) with a Delta R value of 73 ± 34. Delta R was calculated using the MarineChrono reservoir database through an interpolation of data points close to the location of GeoB15403-4.

Surface sediments were sampled at 44 stations from the Gulf of Taranto and the western Adriatic Sea with a multicorer. All samples were subsequently stained with a Rose Bengal solution (1.5 g Rose Bengal per litre 96% ethanol). Samples from the upper 3 cm (25 samples) and upper 5 cm (19 samples) were washed through a 63µm sieve and the coarse fraction was dried at 40°C. For stable oxygen and carbon isotope analyses of benthic foraminifera, adult live (Rose Bengal stained) specimens of the epifaunal species *Cibicidoides pachyderma* (1–5 tests), and the shallow infaunal *Uvigerina mediterranea* (1-4 tests) were selected from the >125 µm size fraction of each station. Isotope measurements were performed at the Leibniz-

Laboratory for Radiometric Dating and Stable Isotope Research in Kiel on a Finnigan MAT 251 stable isotope ratio mass spectrometer coupled to an automatic carbonate preparation device (Kiel IV). The data are given in δ -notation, standardized to the Vienna Pee Dee Belemnite (VPDB). The external precision is better than ±0.05 and better than ± 0.07 ‰ for $\delta^{13}C$ and $\delta^{18}O$, respectively.

5.4 Results

5.4.1 Age model

Results of the AMS ^{14}C age dating and tephrochronology are shown in Table 5.1 and Figure 5.2. Gravity core GeoB15403-4 has a basal age of 55600 yrs BP. Sedimentation rates increase from the older to the younger parts of the core from 5.31 cm ka^{-1} to 28.27 cm ka^{-1}. Sedimentation rates in the 4.2 ka interval increase from 13.3 cm ka^{-1} to 42.1 cm $ka^{-1}$from the older to the younger part. Sedimentation rates in the 8.2 ka interval remain more or less constant at 11.3 cm ka^{-1}.

Table 5.1. Age tie points used for generating the age model for GeoB15403-4. For radiocarbon ages 2σ dating uncertainties are given. The age and identification of the Lipari X tephra is based on Keller (2002), Albert et al. (2012) and Menke et al. (2017 a, under review).

Depth [mm]	Radiocarbon age [BP]	Calendar years [cal BP]	Data
0.00		-61	Sediment Surface
211.25	1380±30	839±101	AMS^{14}C dating
358.00		1174	Lipari X tephra
881.25	2320±30	1846.5±122.5	AMS^{14}C dating
1248.75	2710±30	2316±142	AMS^{14}C dating
1598.75	3410±30	3191±138	AMS^{14}C dating
1845	4020±30	3947±132	AMS^{14}C dating
1983.75	4270±30	4277±133	AMS^{14}C dating
2181.25	5470±30	5767±116	AMS^{14}C dating
2391.25	6290±30	6656.5±124.5	AMS^{14}C dating
2635.00	8350±40	8807.5±170.5	AMS^{14}C dating
2868.75	9920±30	10808±169	AMS^{14}C dating
4061.25	29550±110	33286.5±356.5	AMS^{14}C dating

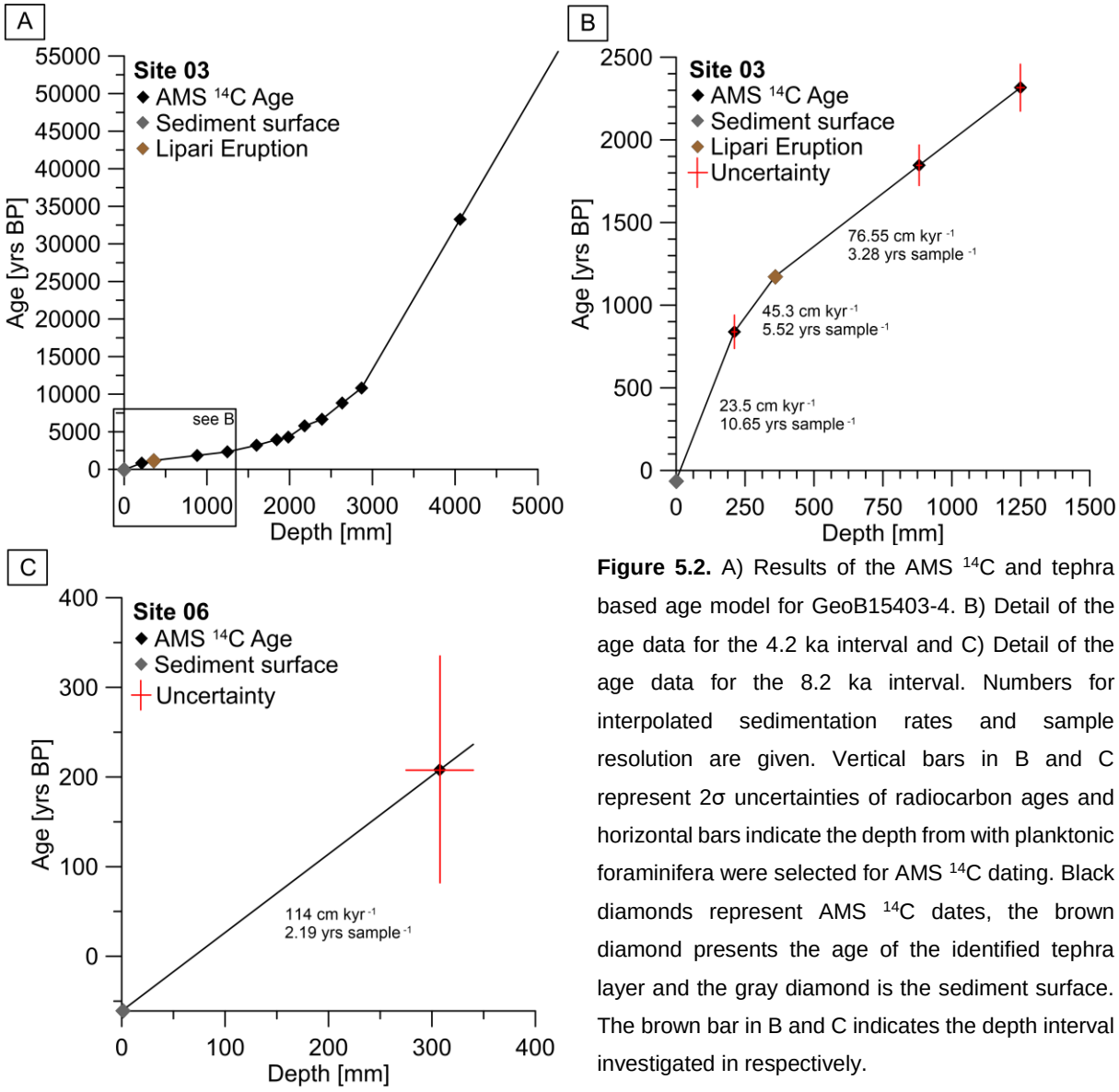

Figure 5.2. A) Results of the AMS ^{14}C and tephra based age model for GeoB15403-4. B) Detail of the age data for the 4.2 ka interval and C) Detail of the age data for the 8.2 ka interval. Numbers for interpolated sedimentation rates and sample resolution are given. Vertical bars in B and C represent 2σ uncertainties of radiocarbon ages and horizontal bars indicate the depth from with planktonic foraminifera were selected for AMS ^{14}C dating. Black diamonds represent AMS ^{14}C dates, the brown diamond presents the age of the identified tephra layer and the gray diamond is the sediment surface. The brown bar in B and C indicates the depth interval investigated in respectively.

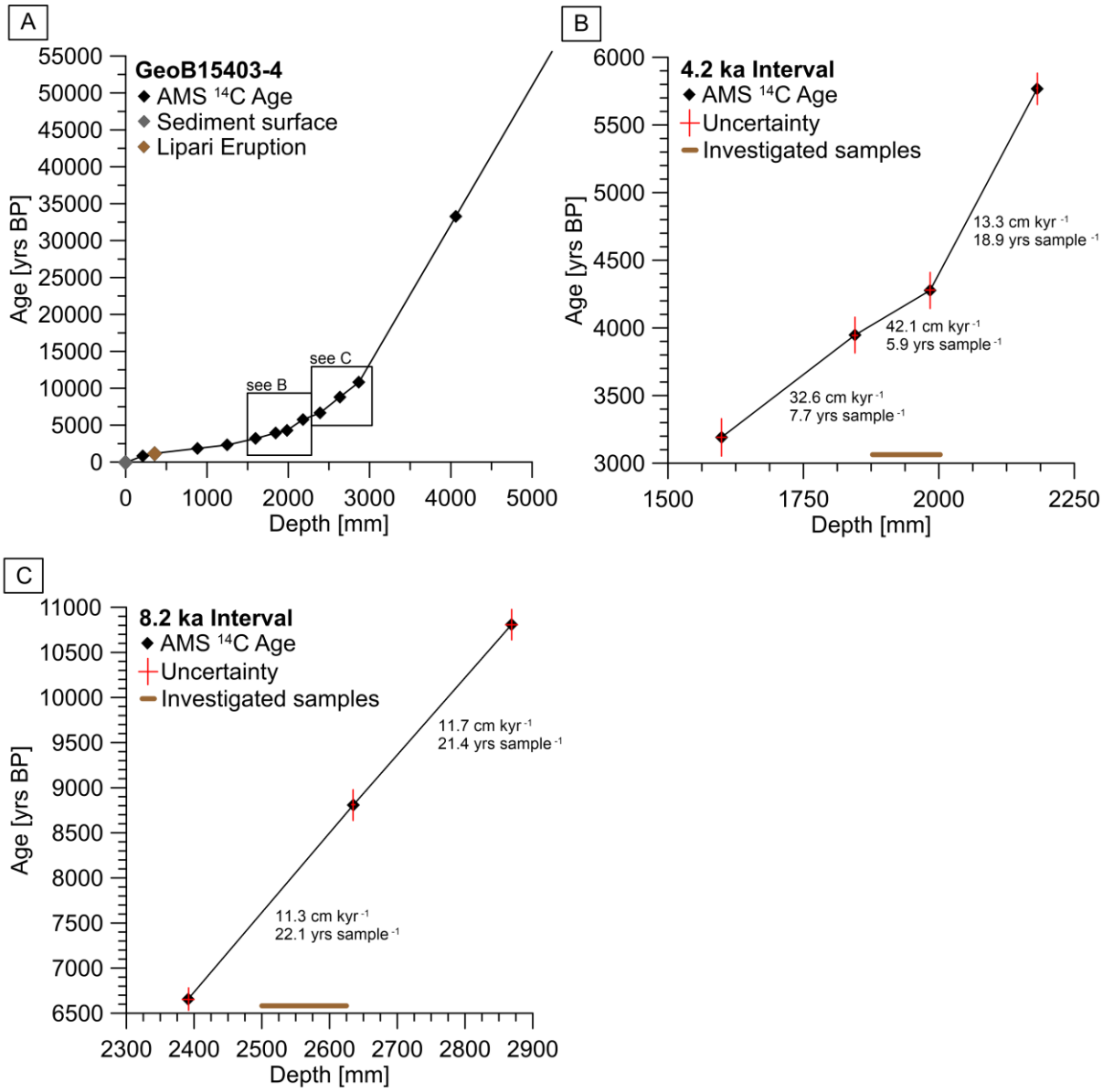

5.4.2 Benthic foraminifera fauna

In the 8.2 ka interval of GeoB15403-4, a total of 142 different foraminiferal taxa were identified (Table A.2.11). The number of taxa ranges between 46 in the oldest sample and 75 with a general trend towards higher numbers of taxa in the younger samples (Fig. 5.3). The dominance decreases from the older to the younger parts of the interval and ranges between 0.3 and 0.6. The Shannon diversity H varies between 3.2 and 3.9 and generally increases from the older to the younger part and exhibits relatively high variability in the middle part of the interval (Table A.2.12).

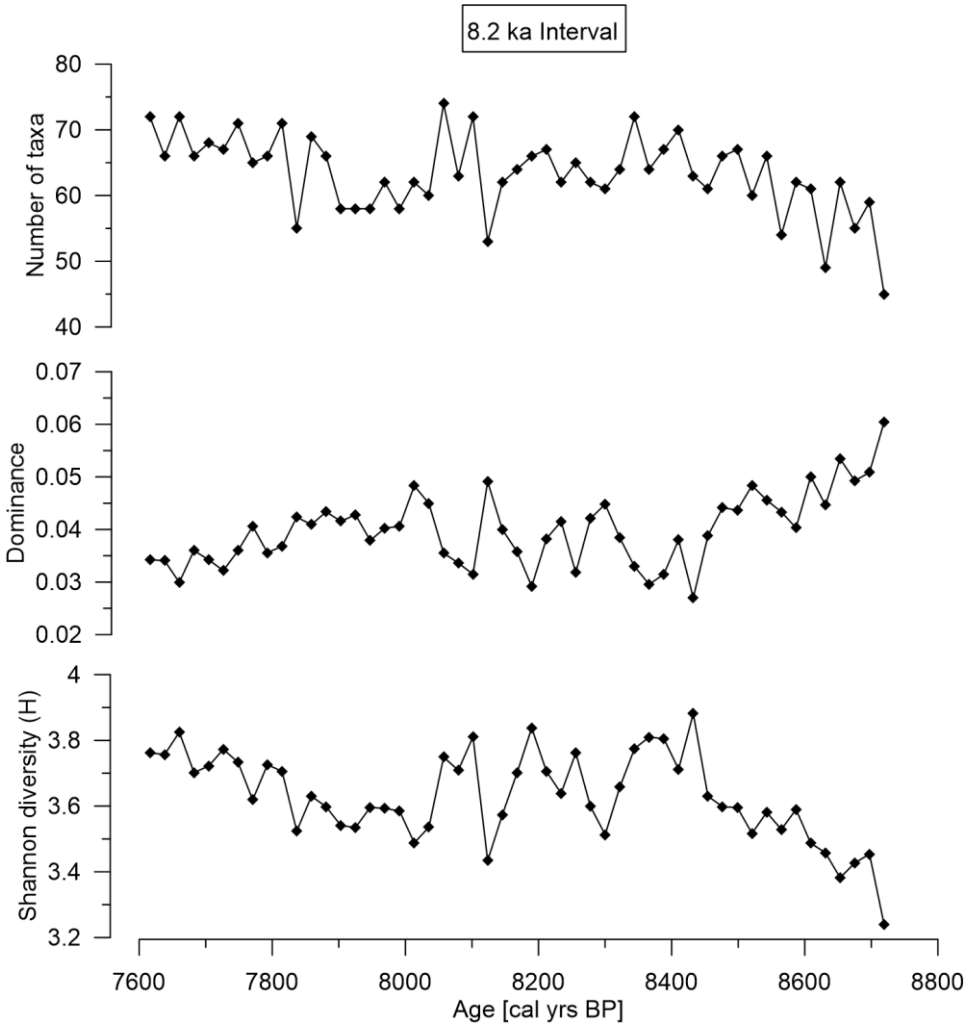

Figure 5.3. Number of individual benthic foraminiferal taxa, dominance and Shannon diversity (H) versus age for the 8.2 ka interval of core GeoB15403-4.

The most abundant species are *Brizalina spathulata*, *Cassidulina laevigata* s.l., *Bulimina striata*, *Gavelinopsis praegeri*, *Uvigerina peregrina*, *Uvigerina mediterranea*, *Textularia pseudogramen*, *Discorbinella bertheloti*, *Lobatula lobatula* and *Globocassidulina subglobosa* (Table A.2.11). In order to characterize temporal changes in food and oxygen supply, benthic foraminifera were grouped according to their environmental preferences. Species preferring epifaunal and shallow infaunal environments and known to be well adapted to oligotrophic to mesotrophic conditions with relatively low food supply and high oxygen availability (e.g. miliolids) are referred to as “Epifaunal Benthic Foraminifera (EBF)” (see Table A.1 for classification). Shallow to intermediate infaunal foraminifera preferring mesotrophic environments with elevated food supply and high to moderate bottom water oxygenation are referred to as “Shallow to Intermediate Infaunal Benthic Foraminifera (SIIBF)” (i.e. *Bulimina* spp., *Bolivina* spp., *Uvigerina* spp; Table A.1). Species tolerant to eutrophic conditions with low oxygen availability in the sediment pore water and adaptation to high food availability are

classified as “Deep Infaunal Benthic Foraminifera (DIBF)” due to their ability to live deeper below the sediment surface (i.e. *Chilostomella oolina, Globobulimina pseudospinescens* and *Fursenkoina acuta*; Table A.1).

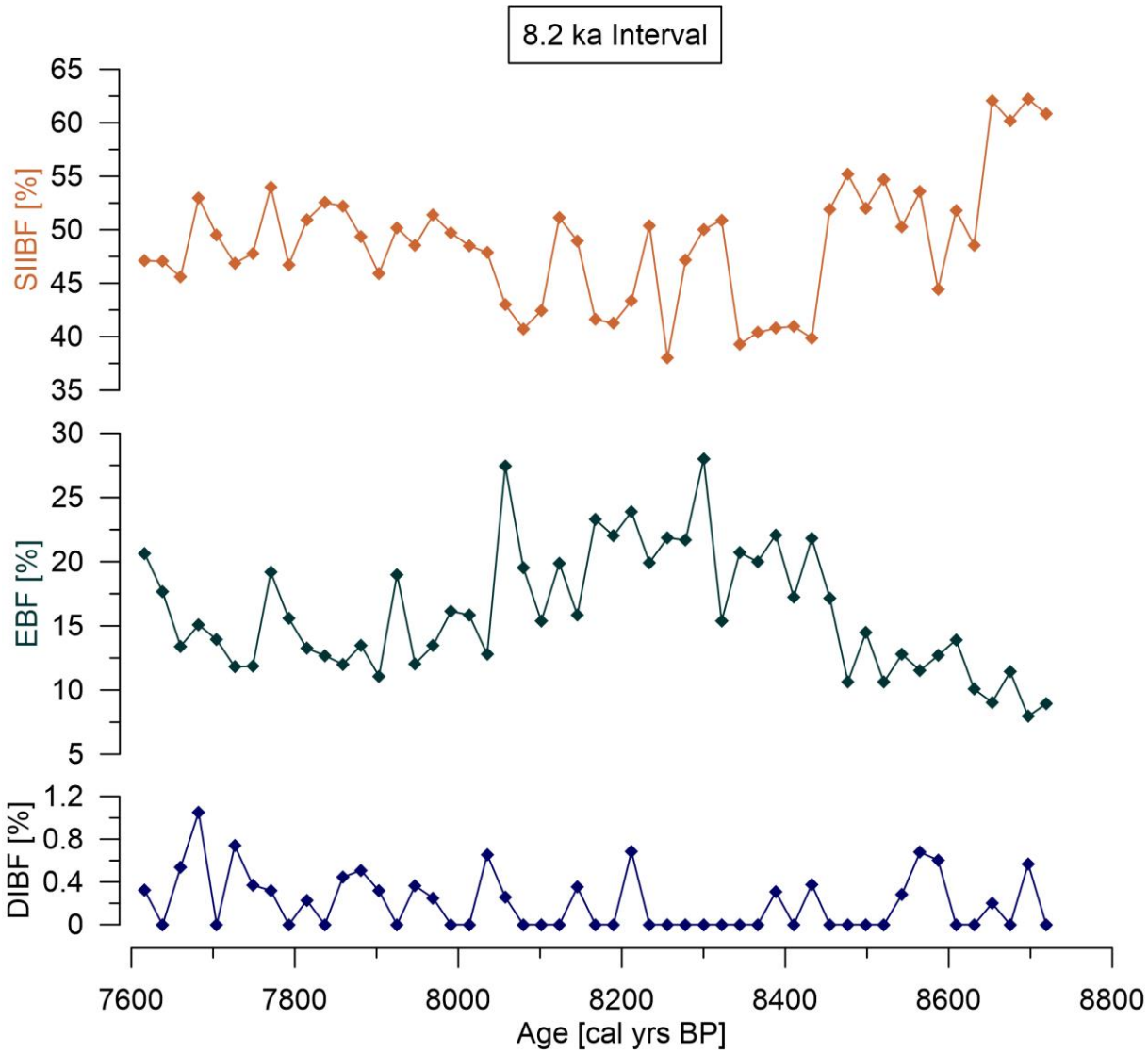

Figure 5.4. Relative abundance of benthic foraminiferal microhabitat groups versus age for the 8.2 ka interval of core GeoB15403-4. SIIBF: Shallow and intermediate infaunal benthic foraminifera (orange), EBF: Epifaunal benthic foraminifera (dark green), DIBF: Deep infaunal benthic foraminifera (blue).

SIIBF are dominant in the 8.2 ka interval ranging from 38 % to ~62 % (Fig. 5.4). SIIBF abundance is highest in the oldest samples, declining first to values of ~52 % around 8.5 ka BP and then to a period of relatively constant values around 49 % at ~8.5 ka BP. Between 8.4 ka BP and 8 ka BP SIIBF abundance shows large variations and levels off around 50 % starting at ~8 ka BP. EBF show a steady rise from lower values in the oldest samples (8% in the second to oldest sample) to the highest value of 28 % at 8.3 ka BP (Fig. 5.4). After this peak, the proportion of EBF decreases towards the youngest samples but remains higher than in the

older part. DIBF abundance is generally low varying from 0 to 1.1 % with a slight trend to higher values in the oldest and youngest parts of the core. The interval between 8240 and 8370 yrs BP is marked by a persistent DIBF absence (Fig. 5.4). Among the dominant taxa, *U. peregrina* declines steadily from high values around 8.9 % in the older part to the lowest values of 0.7 % at 8260 yrs BP (Fig. 5.5). Its abundance increases up to the highest values of 10.5 % at 7840 yrs BP and levels of around 6 % in the youngest part. In contrast, the *U. mediterranea* abundance ranges between 1.7 % and 8.4 % without a clear trend (Fig. 5.5). *Bulimina* species grouped as *Bulimina* spp. also show no clear trend across the 8.2 ka interval and vary between 8.6 % and 16.9 % (Fig. 5.5). The relative abundances of the genera *Bolivina* and *Brizalina* slightly decrease from the older to the younger part of the 8.2 ka interval with values ranging between 4.7 % and 16.8 % (Fig. 5.5).

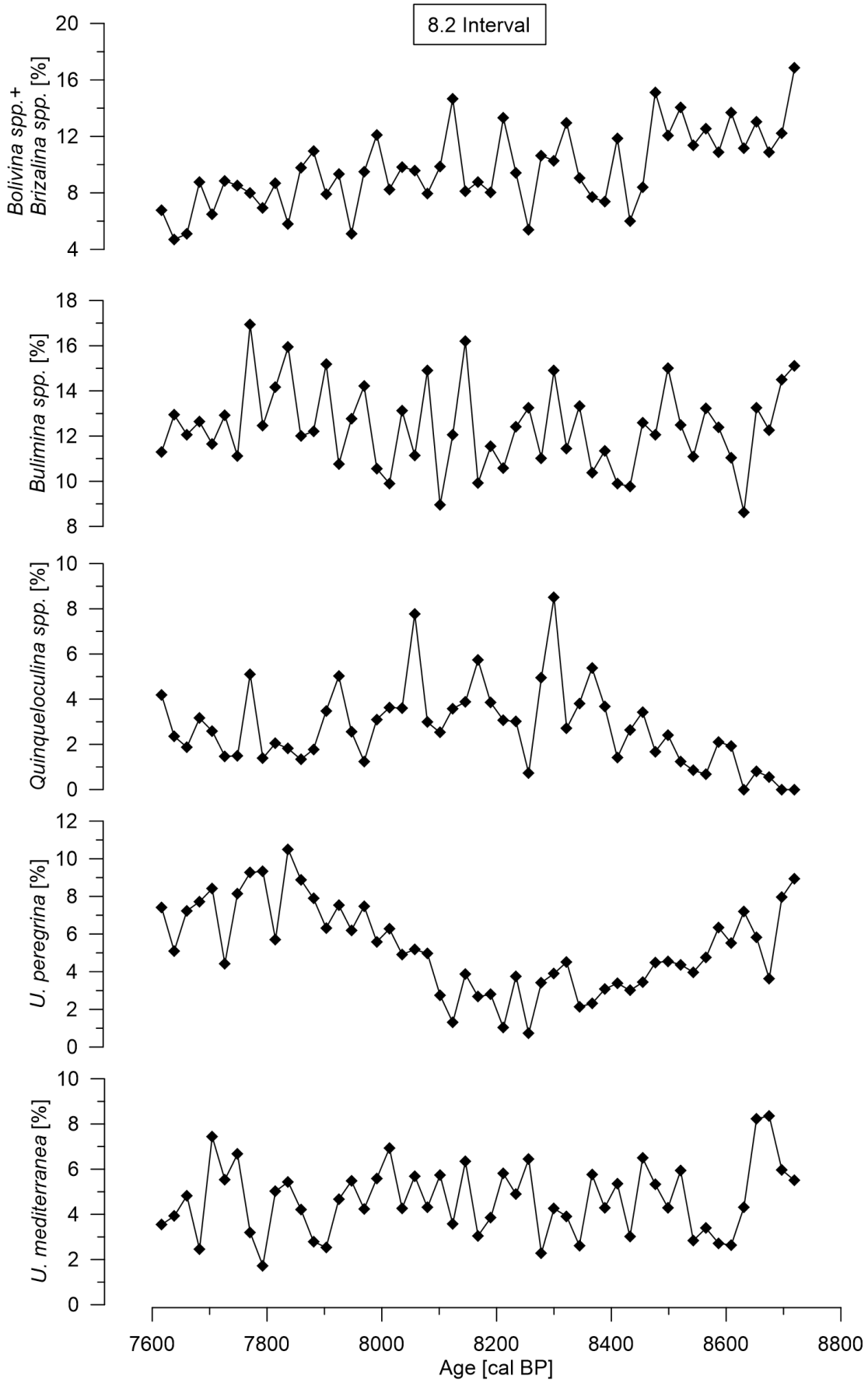

Figure 5.5. Relative abundance of dominant benthic foraminiferal taxa versus age for the 8.2 ka interval of core GeoB15403-4.

5.4.3 Stable isotopes

Stable isotope data for living (stained) *C. pachyderma* are available from 32 stations of the south-western Adriatic Sea and the Gulf of Taranto (Fig. 5.1; Table A.2.13). The $\delta^{13}C$ values of *C. pachyderma* vary between -0.29 ‰ and 1.69 ‰, and the corresponding $\delta^{18}O$ values range between 1.45 ‰ and 3.58 ‰ VPDB (Fig. 5.6). Stable isotope data for living (stained) *U. mediterranea* are available from 37 stations (Fig. 5.1; Table A.2.13). The measured values range from -1.91 ‰ to 0.79 ‰ for $\delta^{13}C$ and from 1.99 ‰ to 2.97 for $\delta^{18}O$ (Fig. 5.6).

Epifaunal (*P. ariminensis* and *C. pachyderma*) stable isotope ratios reveal a wider range of values in the 8.2 ka interval when compared to the 4.2 ka interval. In contrast, the amplitude of stable isotope variations of *U. mediterranea* is higher in the 4.2 ka interval compared to the 8.2 ka interval (Figs. 5.7 and 5.8; Tables A.2.14 and A.2.15). Epifaunal species of both intervals show higher overall $\delta^{13}C$ values compared to infaunal *U. mediterranea*. There are no values of *P. ariminensis* for the 4.2 interval because sufficient tests of this species were only present in the 8.2 interval.

In the 8.2 ka interval, the $\delta^{13}C$ values of *P. ariminensis* range between 0.53 ‰ and 1.51 ‰ with one measurement excluded from interpretation due to a very low amount of sample material and thus low confidence level of the measurement (Fig. 5.8; Table A.2.15). There is one period of lower values around 0.7 ‰ between ~7.7 ka and ~8.1 ka. However, it has to be noted, that in this period the sampling space is higher because individuals of *P. ariminensis* were not present in every sample. The $\delta^{13}C$ of *C. pachyderma* ranges between 0.65 ‰ and 1.62 ‰ and the $\delta^{13}C$ of *U. mediterranea* varies between -0.36 ‰ and 0.22 ‰. The $\delta^{13}C$ records of both species lack long-term trends (Fig. 5.8). The $\delta^{18}O$ of *P. ariminensis* varies between 1.32 ‰ and 3.11 ‰ with a similar period of lower values (~1.6 ‰) between ~7.7 ka BP and 8.1 ka BP as in the $\delta^{13}C$ record. The $\delta^{18}O$ of *C. pachyderma* varies between 1.2 ‰ and 3.4 ‰ and the $\delta^{18}O$ of *U. mediterranea* varies between 1.7 ‰ and 2.43 ‰, both lacking long-term trends (Fig. 5.8).

In the 4.2 ka interval, the $\delta^{13}C$ values of *C. pachyderma* range between 0.84 ‰ and 1.33 ‰ and those of *U. mediterranea* vary between -0.18 ‰ and 0.64 ‰ (Fig. 5.8; Table A.2.14). The $\delta^{18}O$ values of *C. pachyderma* vary between 1.29 ‰ and 1.71 ‰ and those of *U. mediterranea* vary between 1.75 ‰ and 2.37 ‰. Both records lack clear long-term trends (Fig. 5.8).

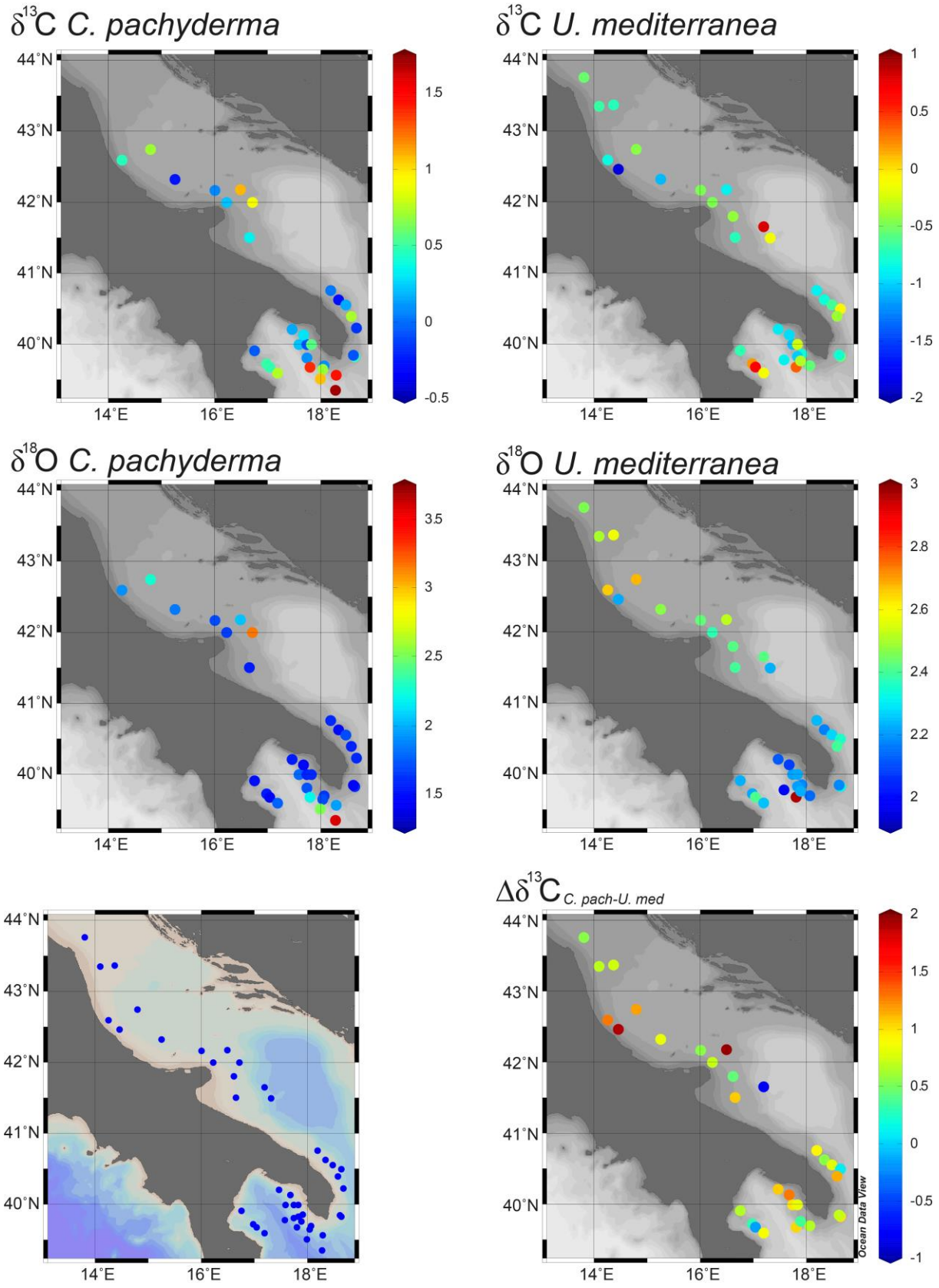

Figure 5.6. Stable carbon and oxygen isotope compositon of live (Rose Bengal stained) specimens of the epifaunal *Cibicidoides pachyderma* (left) and the shallow infaunal *Uvigerina mediterranea* (right) from surface sediment samples along the western Adriatic coast and the Gulf of Taranto. The $\delta^{13}C$ difference between *C. pachyderma* and

U. mediterranea is displayed at the bottom right. All stable isotope results are reported in ‰VPDB. Map was created with Ocean data view (Schlitzer, 2017)

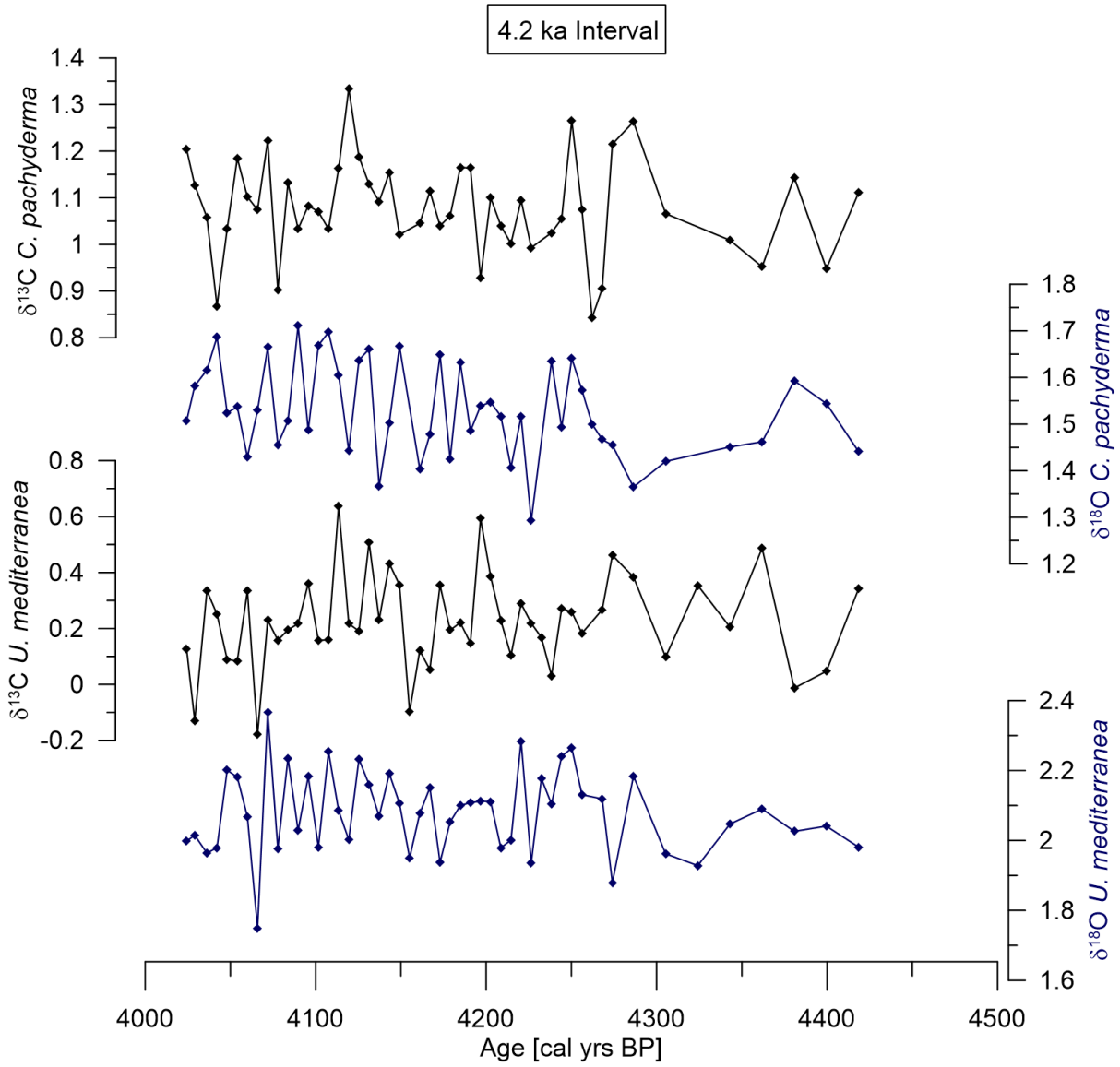

Figure 5.7. Stable carbon (black) and oxygen (blue) isotope records of *C. pachyderma* and *U. mediterranea* versus age for the 4.2 ka interval of GeoB15403-4. Stable isotope values are reported in ‰VPDB.

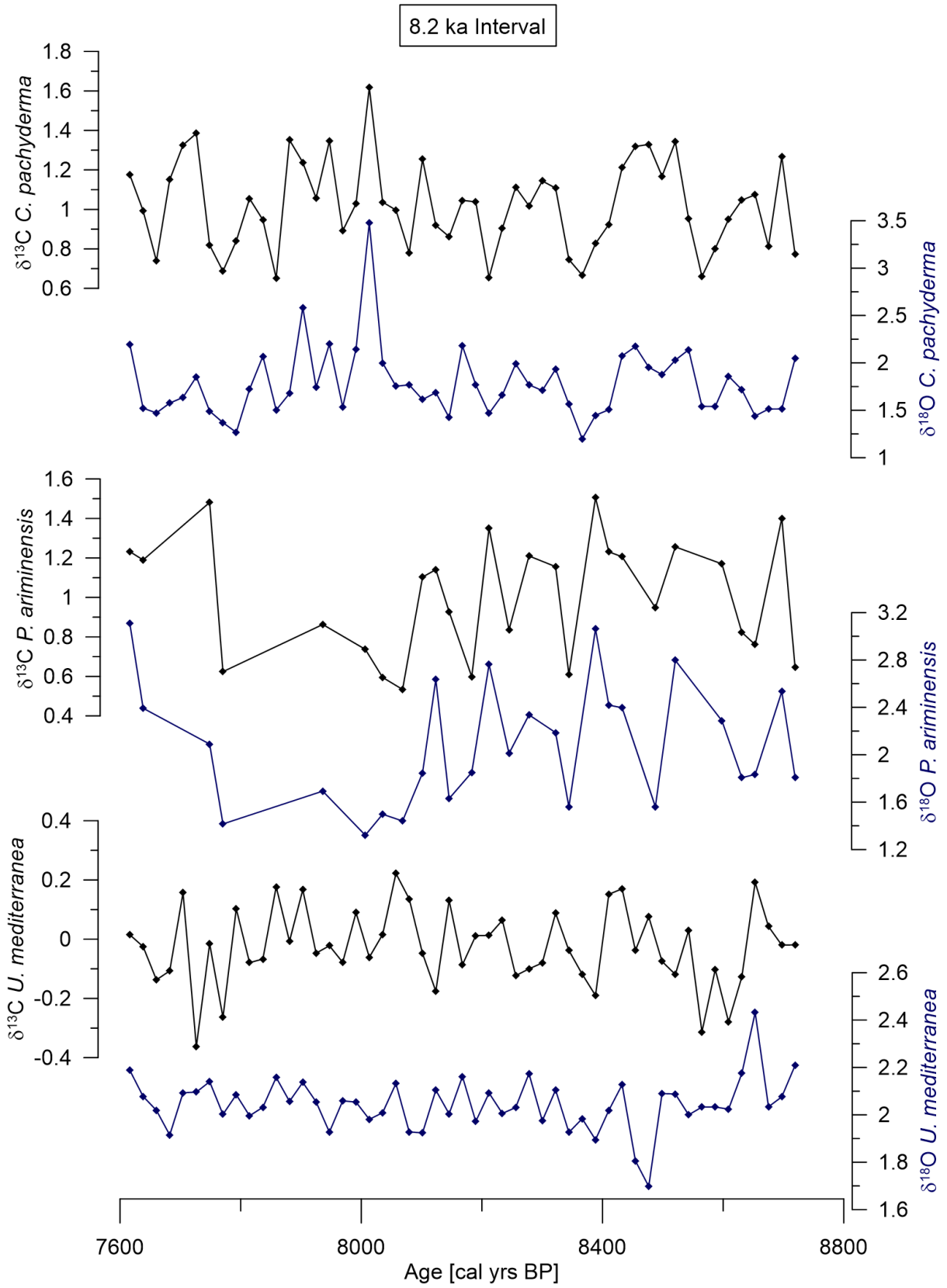

Figure 5.8. Stable carbon (black) and oxygen (blue) isotope records of *C. pachyderma*, *U. mediterranea* and P. ariminensis versus age for the 8.2 ka interval of core GeoB15403-4. Stable isotope values are reported in ‰VPDB.

5.4.4 Clay minerals

In the 8.2 ka interval, the chlorite concentration varies between 8 % and 11 %, while kaolinite fluctuates between 16 % and 20 % (Table A.2.16). The kaolinite/ chlorite (Kaol/Chl) ratios vary from 1.6 to 2.2 with a slight trend to higher values in the younger part of the core (Fig. 5.9). Highest overall values are reached in 6 samples cantered around 8.2 ka BP. Smectite concentrations vary between 34 % and 41 % while illite fluctuates between 32 % and 37 % (Table A.2.16). Smectite/ illite (Sm/Ill) ratios range from 1 to 1.3, overall declining from ~1.1 in the older to ~1 in the younger part of the core. The record is interrupted by two intervals with higher Sm/Ill ratios, one between 8.4 and 8.5 ka BP and the other around 8 ka BP, both reaching values as high as 1.3 (Fig. 5.9).

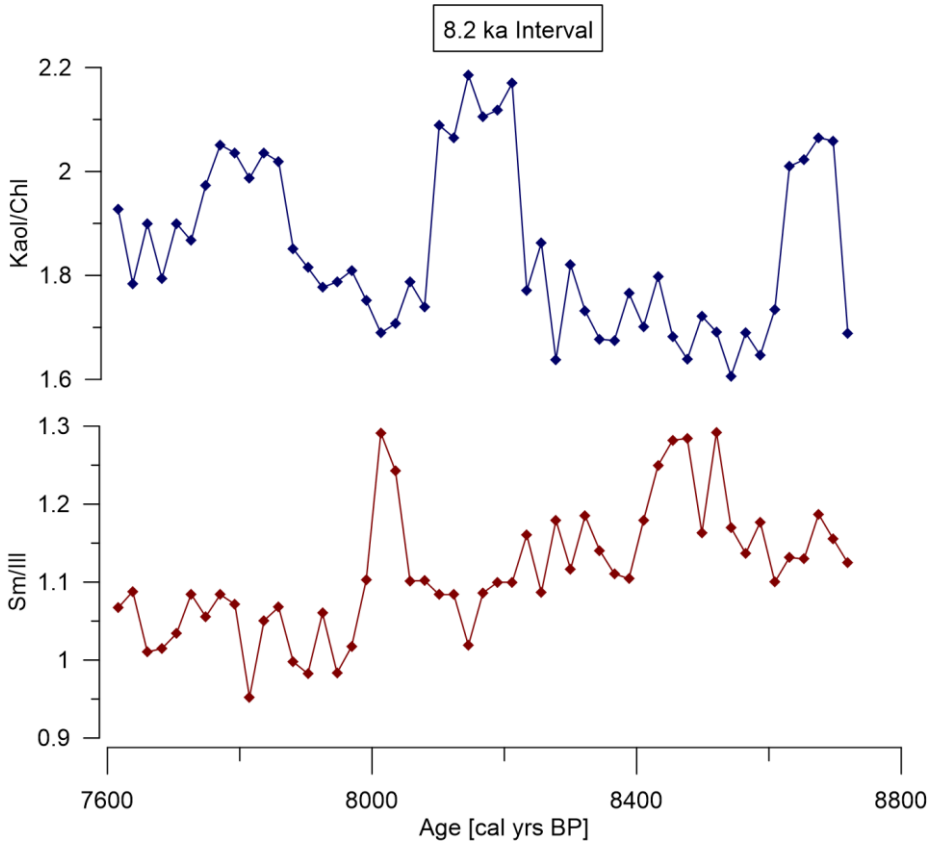

Figure 5.9. Kaolinite/chlorite (blue) and smectite/illite (red) ratios versus age for the 8.2 ka interval of core GeoB15403-4.

5.5 Discussion

5.5.1 Climatic boundary conditions and marine ecosystem response in the central Mediterranean during the 8.2 ka interval

Our EBF record traces a 500-year long period of reduced organic matter supply between approximately 8.5 and 8.0 ka BP corresponding to the cooling and drying of the 8.2 ka event (Fig 5.10 J) (Rohling and Pälike, 2005). This period of higher EBF abundance interrupts a period of relatively eutrophic conditions evident by high abundance of SIIBF and low abundance of EBF. This eutrophic period corresponds to the relatively humid and warm boundary conditions of the interval of sapropel S1 formation in the eastern Mediterranean basin between ~10.2 and 6.4 ka BP (Mercone et al., 2000; Schmiedl et al., 2010). In eastern Mediterranean deep-sea records the 8.2 ka event is commonly marked by a sharp, 200-yearlong interruption of sapropel S1 (e.g., Myers and Rohling, 2000; Rohling et al., 1997). In contrast, the time interval of reduced organic matter fluxes in the Gulf of Taranto lasted for approximately 500 years and is characterized by relatively gradual onset and termination. The timing of the gradual EBF increase matches the onset of cool and arid summer conditions over central Europe evident in compiled tree ring width data from Germany displaying a distinct growth minimum between 8.4 and 8.0 ka BP (Fig. 5.10 H) (compiled by Rohling and Pälike, 2005; Spurk et al., 2002). Since the Po River is an important source for nutrients and suspended sediments in the Gulf of Taranto, both local phytoplankton production and trophic state of benthic ecosystems are closely linked to precipitation over the Italian mainland and ultimately to Northern Hemisphere temperature (Menke et al., 2017 b, under review, Zonneveld et al., 2012). EBF are most competitive in oligotrophic environments with seasonal food fluxes and high bottom water oxygenation (Jorissen et al., 1995; Lutze and Thiel, 1989; Murray, 2003). The overall dominance of SIIBF as well as especially high numbers of *Bolivina* and *Brizalina* species before 8.4 ka BP indicate eutrophic conditions with high organic matter availability in the Gulf of Taranto at the time of sapropel S1 formation in the eastern Mediterranean (Fig. 5.10 top bar). The abundance of the less opportunistic *U. mediterranea* remains relatively stable over the entire investigated interval, whereas the more opportunistic *U. peregrina* is dominant before and after the 8.5- 8.0 ka BP period and decreases drastically during the time of maximum EBF abundance (Fig 5.5). Both *Uvigerina* species are adapted to relatively high organic matter fluxes (De Rijk et al., 2000). However, *U. peregrina* is known to feed on seasonal pulses of freshly deposited phytodetritus arguing for high seasonal river fluxes triggering pronounced seasonal phytoplankton blooms in the time periods before and after the interruption (Koho et al., 2008). Highest SIIBF abundance occurs in the oldest part of the studied interval, where maximum *Bolivina* and *Brizalina* abundances indicate eutrophic conditions and EBF abundance is as low as 6 %. After 8 ka BP, SIIBF increase again but do not reach proportions exceeding 50%, whereas EBF abundance remains more stable. The

lower trophic conditions in the younger part of the sapropel S1 time interval mirror a general decrease in organic matter fluxes. This long-term trophic change corresponds to the decrease in Northern Hemisphere summer insolation resulting in reduced temperatures and precipitation in the Mediterranean region and northern Africa ultimately leading to the termination of sapropel S1 formation in the EMS (e.g., Emeis et al., 2000; Rohling et al., 2002; Weldeab et al., 2014).

The reproduction of benthic foraminifera in the oligotrophic Mediterranean deep-sea basins likely responds to phytoplankton blooms following maxima in precipitation and coastal runoff (mainly the Po river in our study area) supplying large amounts of nutrients to coastal surface waters (Caroppo et al., 2006; Zonneveld et al., 2012). Proxy records show that precipitation was high over the northern borderlands of the eastern Mediterranean Sea and the Italian mainland during S1 formation (Ariztegui et al., 2000; Giraudi et al., 2011; Kotthoff et al., 2008; Rolph et al., 2004) likely leading to enhanced coastal runoff and nutrient input into the Gulf of Taranto. In contrast to the severe environmental changes in bathyal and abyssal environments of the EMS with temporary anoxia and benthic ecosystem collapse (Schmiedl et al., 2010) persistently high benthic foraminiferal abundance and diversity on the shelf of the Gulf of Taranto prove that local oxygen concentrations never dropped below a critical threshold during times of sapropel S1 formation (Fig 5.3 and 5.4). This is plausible since persistent bottom water anoxia during S1 formation is commonly reported for water depths below 1800 m (De Lange et al., 2008; Schmiedl et al., 2010).

Concluding, our benthic foraminiferal record from the Gulf of Taranto shelf corroborates earlier findings of a mutli-century climate cooling occurring between 8.5 and 8.0 ka BP that is punctuated by the sharp 8.2 ka event (Rohling and Pälike, 2005). The cooling reflected in many proxy records started well before the 8.47 ± 0.3 ka BP meltwater flood from lakes Agassiz and Ojibway (Fig 5.10 A) (Barber et al., 1999).

Lake level low stands in central Italy (Fig. 5.10) (Giraudi et al., 2011) suggest a long-lasting period of dry conditions in the central Mediterranean around the 8.2 ka event. Clay mineral data from GeoB15403-4 seem to contradict this finding. Elevated Kaol/Chl ratios between ~8.2 ka BP and 8.1 ka BP suggest enhanced sediment input from the southern Apennines, at the same time the relatively steady rise in Sm/Ill ratios suggests a decline in Po River sediment supply (Fig. 5.10 C and E) Tomadin 1979; 2000). In order to interpret these signals it has to be considered that precipitation-forced fluvial transport is not the only potential terrestrial sediment source in the Gulf of Taranto and that sediment mobilization can respond to non-linear thresholds in vegetation and soil exposure (Ehrmann et al., 2013). Peizhen et al. (2001) argue that oscillations between cold and dry and warm and wet climate favor the rapid incision and denudation of land surfaces.

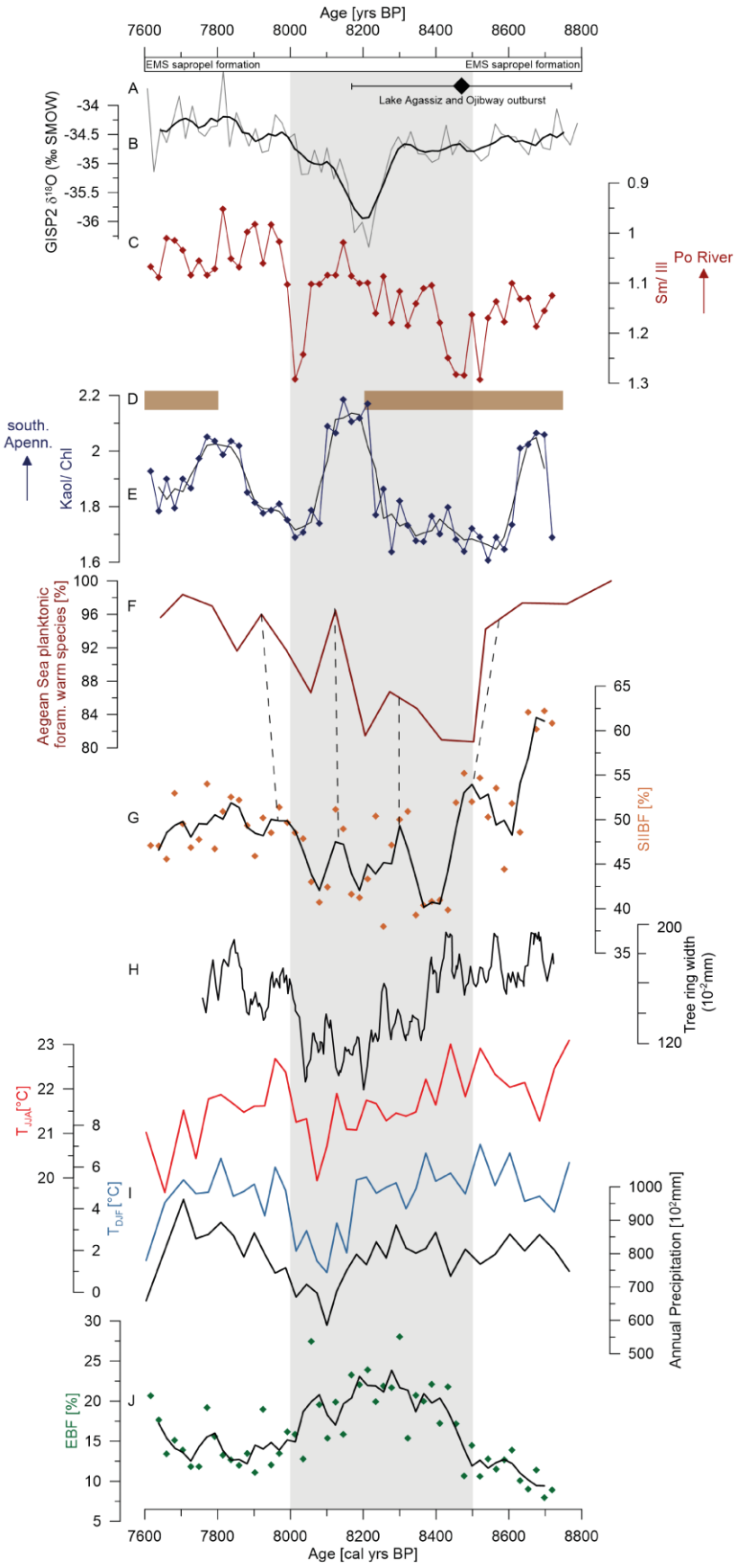

Figure 5.10. Comparison of records of northern high-latitude temperature, central European climate and Mediterranean environments for the time interval around the 8.2 ka cold event. A) Timing of the Lake Agassiz and Ojibway outburst (Barber et al., 1999). B) $\delta^{18}O$ record of Greenland ice core GISP2 (Grootes et al., 1997). Thick

black line represents a 5- point running average. C) Smectite/illite ratio of GeoB15403-4 with low values indicating elevated Po river flux. D) Central Italian lake level low stands (brown bars) from Lake Accesa and Lake Fucino (Giraudi et al., 2011). E) Kaolinite/chlorite ratio of GeoB15403-4 with high values indicating a southern Appenine provenance of sediments. F) Relative abundance of planktonic foraminifera species indicative for warm surface water temperatures in Aegean Sea core LC21 (Rohling et al., 2002). G) Relative abundance of shallow to intermediate infaunal benthic foraminifera (SIIBF, orange dots) of GeoB15403-4. Black line represents a 3-point running average. H) Compiled record of german tree ring width (Spurk et al., 2002; Rohling et al., 2005). I) Pollen-based summer (June to August) temperature (red), winter (December to February) temperature (blue) and annual precipitation (black) from the northern Aegean Sea (Pross et al., 2009). J) Relative abundance of epifaunal benthic foraminifera (EBF, green dots) of GeoB15403-4. Black line represents a 3-point running average.

Even though their study investigates different time scales, the early Holocene climate alternations combined with increased seasonality, as reconstructed from pollen records (Fig 5.10) (Pross et al., 2009), probably fostered pronounced physical weathering in winter and erosion in summer. Southern Apennine sediment mobilization is low during the 8.5-7.9 ka interval, but peaks at the time of lowest $\delta^{18}O$ values of GISP2. At 8.7 ka BP, when EBF and SIIBF indicate higher precipitation and nutrient flux, Apennine sediment input is high but drops around 8.6 ka BP possibly as a result of decreasing precipitation. A drier climate could have led to an increase in aeolian transport from the borderlands of the southern Adriatic Sea and the Gulf of Taranto assuming a partial deforestation according to observations from northern Greece (Pross et al., 2009). Declining precipitation and river runoff could have led to a diminished southern Apennine sediment supply until a threshold is reached where reduced vegetation cover during the coldest and driest conditions around 8.2 kar BP lead to a pronounced aeolian introduction of Apeninne clay particles into the south-western Adriatic and the Gulf of Taranto. After the pronounced dry and cold conditions around 8.2 ka BP, increasing precipitation could have led to more vegetation cover, less erosion and lower Kaol/Chl ratios until a certain threshold is reached around 7.9 ka BP and southern Appenine sediment flux rises again due to elevated precipitation rates during the sapropel boundary conditions. However, in addition to regional sources, dust input from North Africa may also contribute to the observed clay mineral signals in the Gulf of Taranto although present-day aeolian input from North Africa only plays a minor role (Jeromel et al., 2009). During the late Quaternary, the timing of dust fluxes from North African deserts into the central Aegean Sea and southeastern Ionian Sea followed a non-linear pattern responding to critical hydrological thresholds (Ehrmann et al., 2013). Lake records from northern Africa show low stands and dry conditions during the 8.2 ka event (Swezey et al., 1999) and the deposition of calcareous tufa documents a period of lower precipitation in the central Sahara and adjacent regions (Cremaschi et al., 2010).

Sm/Ill ratios representing the Po River sediment load show a more consistent trend, however, the lowest Po River supply occurs around ~8.5 ka BP and ~8.0 ka BP, at times when the

benthic ecosystem responded to changing food fluxes (Fig. 5.10 C). We do not have a coherent explanation for the observed clay mineral signal, but it may be attributed to vegetation changes in the river catchment and the enhanced seasonality of the early Holocene. Generally, dry summer conditions over the Po valley will lead to decreased riverine runoff and related drops in suspension load of the WAC. On the other hand, the persistence of particularly dry summer conditions during certain phases of the 8.2 ka event could lead to partial deforestation resulting in enhanced erosion and sediment mobilization during subsequent Alpine snowmelt and enhanced river runoff in spring. Furthermore, the different climate regimes of the large Po catchment are likely to dilute a pronounced seasonal signal since erosion in the Alpine region is pronounced after extreme winters, but erosion in the Po valley is greatly affected by extreme rainfall events after dry periods in summer (Bronick and Lal, 2005; Terranova et al., 2009; Van der Knijff et al., 2000).

5.5.2 Centennial-scale climate modulation of central Mediterranean oceanography during the 8.2 ka and 4.2 ka events

Underlying the climatic boundary conditions of the 8.2 ka interval are centennial-scale modulations of the hydrological regime. SIIBF variability during the 8.5–8.0 ka PB interval matches the abundance of planktonic foraminifera indicator species for warm water temperatures in the Aegean Sea (Fig. 5.10 F; supported by a highly resolved but less well dated core from the central Mediterranean; Rohling and Pälike, 2005), suggesting a link between SIIBF abundance and temperature. Elevated temperatures lead to more moisture generation hence elevated precipitation and river discharge triggering phytoplankton blooms in the Gulf of Taranto. Recently, Menke et al., (2017 b, under review) found a striking correlation between northern hemisphere temperatures and SIIBF abundance with quasi-periodic variabilities of 50 to 70 years for the past ~1000 years matching the AMO. They argue, that large-scale atmospheric processes modulate the overall hydrological regime, but the AMO paces summer rainfall and related impacts on marine environments on multi-decadal time scales. A study on multi-decadal climate variability of Mediterranean SST's revealed the same 70 yr periodicity suggesting stimulation by the AMO (Marullo et al., 2011). To what extent AMO driven processes had an impact on ecosystems during the 8.2 event cannot be resolved based on our data since reliable AMO reconstructions for time intervals prior to ~1500 yrs BP are not yet available. In addition, the limited data points of our dataset prevent from conducting statistically accurate time series analysis. The dominance of SIIBF during times of high sea-surface temperatures (evident from elevated abundances of planktonic warm species), however, argues for a similar connection between temperature-driven evaporation and precipitation, and marine trophic conditions also for the early Holocene (Fig. 5.10 F, G).

Benthic foraminifera stable isotope records reveal substantial differences between the 8.2 ka and the 4.2 ka intervals (Fig. 5.11). The most striking feature is the high-amplitude variability

and close correlation of epifaunal $\delta^{18}O$ and $\delta^{13}C$ across the 8.2 interval, which is absent across the 4.2 interval (Fig. 5.11 B and C). *Cibicidoides* and *Planulina* species are suspension feeders and preferentially inhabit an epifaunal microhabitat exposed to bottom water (Lutze and Thiel, 1989; Murray 2006), reliably recording its isotopic signal (e.g. Theodor et al., 2016 a). In the modern Adriatic Sea and the Gulf of Taranto low epifaunal $\delta^{18}O$ values of around 1.5 ‰ are indicative for shelf stations while the $\delta^{18}O$ values increase up to 3.5 at the deepest bathyal sites (Fig. 5.6). A similar depth-related $\delta^{18}O$ gradient has previously been reported for the shallow infaunal *U. mediterranea* from the same region (Grauel and Bernasconi, 2010) corroborating our own measurements. Site GeoB15403 is located on the outer shelf (water depth of 170 m) at the transition zone between surface waters and LIW and therefore is particularly prone to changes in water mass influence. Simultaneous fluctuations in $\delta^{18}O$ and $\delta^{13}C$ most likely reflect a switching between salty and nutrient poorer LIW (high $\delta^{18}O$ and high $\delta^{13}C$) and relatively fresh and nutrient-rich Adriatic water masses (low $\delta^{18}O$ and low $\delta^{13}C$) waters. The Gulf of Taranto displays substantial changes in seasonal circulation patterns comprising a reversal of the surface flow direction from a cyclonic to an anticyclonic mode (Pinardi et al., 2016). During the anticyclonic mode (Fig. 5.1 B) vertically stratified and oligotrophic water masses enter the gulf from the Ionian Sea. At present, this scenario occurs in fall (October) but during the cool boundary conditions of the 8.2 ka interval the circulation reversal could have occurred more often leading to an overall increase of Ionian Sea influence. A modified circulation pattern could also impact spatial oscillations of the Northern Ionian Cyclonic Gyre, which borders the Gulf of Taranto to the south (Fig. 5.1 A). The time intervals of high $\delta^{18}O$ and high $\delta^{13}C$ would then reflect periods with frequent entrainment of nutrient-poor Ionian waters at the time of foraminiferal calcification on the outer shelf of the Gulf of Taranto (Fig. 5.11 B and C). On the other hand, low $\delta^{18}O$ and low $\delta^{13}C$ would display times a cyclonic circulation, when Adriatic water masses carry large amounts of nutrients from the Po River into the study area, similar to the present-day situation.

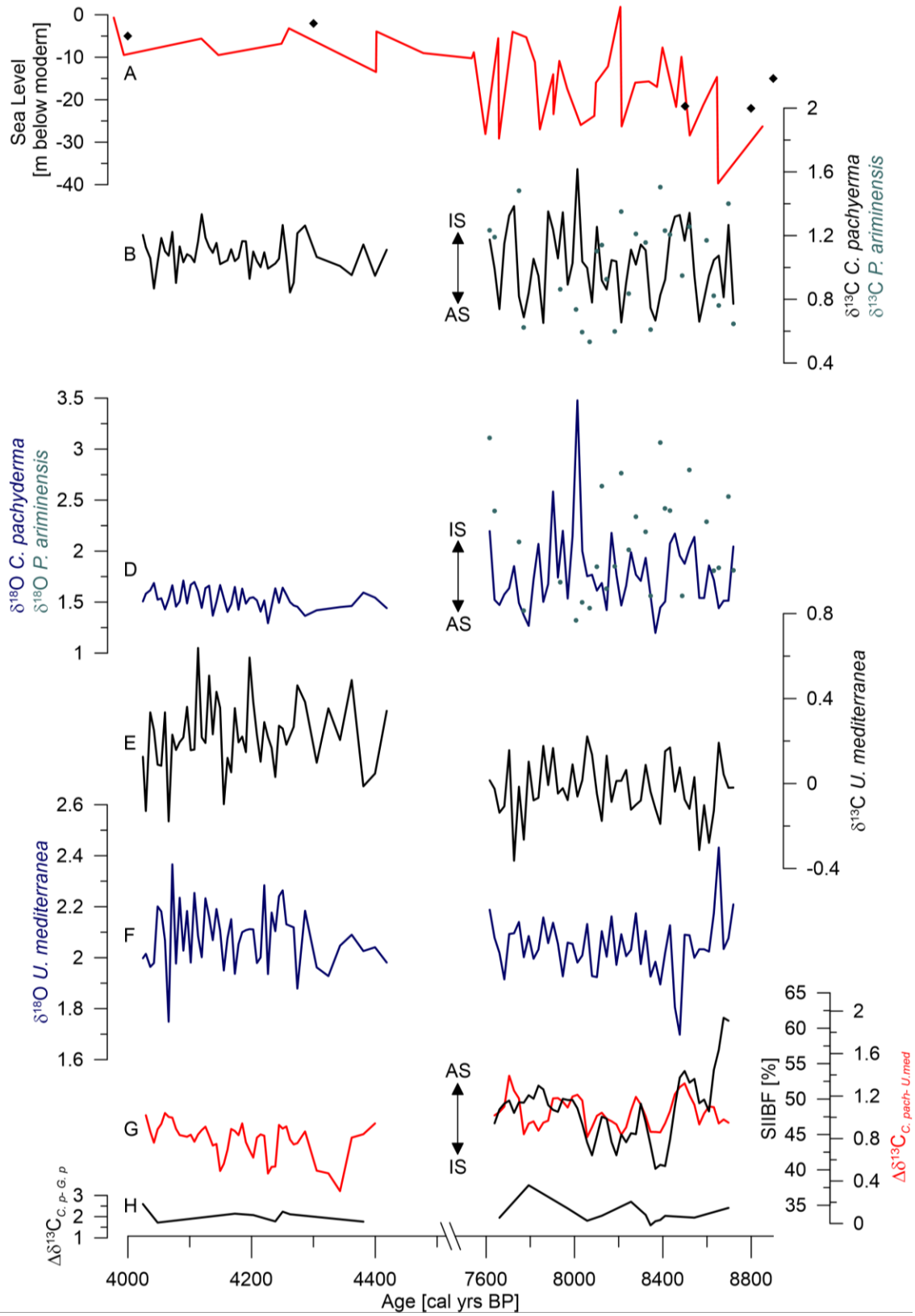

Figure 5.11. Comparison of stable isotope records of GeoB15403-4 as proxies for oceanographic and environmental variability in the Gulf of Taranto and Mediterranean sea level for the time intervals of the 4.2 ka and 8.2 ka events. All stable isotope data are reported in ‰VPDB. A) Mediterranean Sea level reconstruction (Grant et al., 2012) in m below modern level (red) and estimates of global Sea level (black dots; Alley et al., 2005). B) $\delta^{13}C$

record of *C. pachyderma* (black line) and *P. ariminensis* (green dots, in the 8.2 ka interval). C) $\delta^{18}O$ record of *C. pachyderma* (blue line) and *P. ariminensis* (green dots, in the 8.2 ka interval) as an indicator for LIW versus WAC dominance. D) $\delta^{13}C$ record (black line) of *U. mediterranea*. E) $\delta^{18}O$ record (blue line) of *U. mediterranea.* F) $\delta^{13}C$ difference between epifaunal *C. pachyderma* and shallow infaunal *U. mediterranea* (red line) and 3-point running average of the relative abundance of shallow to intermediate infaunal benthic foraminifera (SIIBF, black line). G) $\delta^{13}C$ difference between epifaunal *C. pachyderma* and deep infaunal *G. pseudospinescens.* Water mass provenance from the Adriatic Sea is marked AS and from the Ionian Sea is marked IS.

Alternatively, the strong variability of epifaunal $\delta^{18}O$ and $\delta^{13}C$ could reflect changes in the vertical extension of the nutrient-rich WAC at the core positions. During cold winters, dense waters of the WAC sink down into the deeper layers of the Gulf of Taranto (down to 300 m depth) bathing the outer shelf environments and thus also site GeoB15403-4 (Sellschopp and Alvarez, 2003). The coincidence of low $\delta^{13}C$ and low $\delta^{18}O$ bottom water conditions points to a nutrient-rich and relatively fresh water mass suggesting a direct influence of WAC at the study site.

Environmental boundary conditions during the 4.2 ka interval are much more stable, and nutrient-poor water masses are the dominant bottom waters (Fig. 5.11 C). Fluctuations in epibenthic $\delta^{13}C$ are much smaller during the 4.2 ka interval than during the 8.2 ka interval and overall values are higher (Fig. 5.11 B). This is plausible due to the lower overall nutrient fluxes compared to sapropel boundary conditions (e.g. Rohling et al., 2007). There is no correlation between epibenthic $\delta^{13}C$ and $\delta^{18}O$ arguing for more stable oceanographic conditions and where fluctuations in $\delta^{13}C$ are mainly driven by surface water production due to constant water mass dynamics (Fig 5.12).

While epifaunal benthic foraminifera record the bottom water isotopic signal, infaunal benthic foraminifera like *U. mediterranea* reflect the isotopic composition of the pore water $\delta^{13}C_{DIC}$ (McCorkle et al., 1990, 2008; Schmiedl et al., 2004) and are able to shift their microhabitat depth in response to food and oxygen availability (Linke and Lutze, 1993; Ohga and Kitazato, 1997). The $\Delta\ \delta^{13}C$ between epifaunal and shallow infaunal species hence allows for an estimation of organic matter flux rates (Theodor et al. 2016a, b). High $\Delta\ \delta^{13}C_{C.\ pach-\ U.\ med}$ values reflect times of increased organic matter fluxes most likely resulting from high surface water production at times of high precipitation and river discharge. Low values argue for lower organic matter availability due to less precipitation driven nutrient fluxes from land leading to less surface water productivity (Fig. 5.11 F red line). Peaks in $\Delta\ \delta^{13}C_{C.\ pach-\ U.\ med}$ coincide with peaks in SIIBF abundance (black line) indicating short lived shifts to pronounced eutrophic conditions within the overall mesotrophic conditions of the 8.2 Event. It is important to consider however, that during times of rapid phytodetritus deposition, negative offsets in $\delta^{13}C$ compared to the bottom water isotopic signature can even occur in shells of strictly epifaunal species

(Mackensen et al., 1993; Theodor et al., 2016a,b). This leads to a smoothing of the $\Delta\ \delta^{13}C$ record of epifaunal and infaunal species. It is possible that this effect has an influence on our isotopic record at times of maximum SIIBF abundance during the 8.2 ka interval.

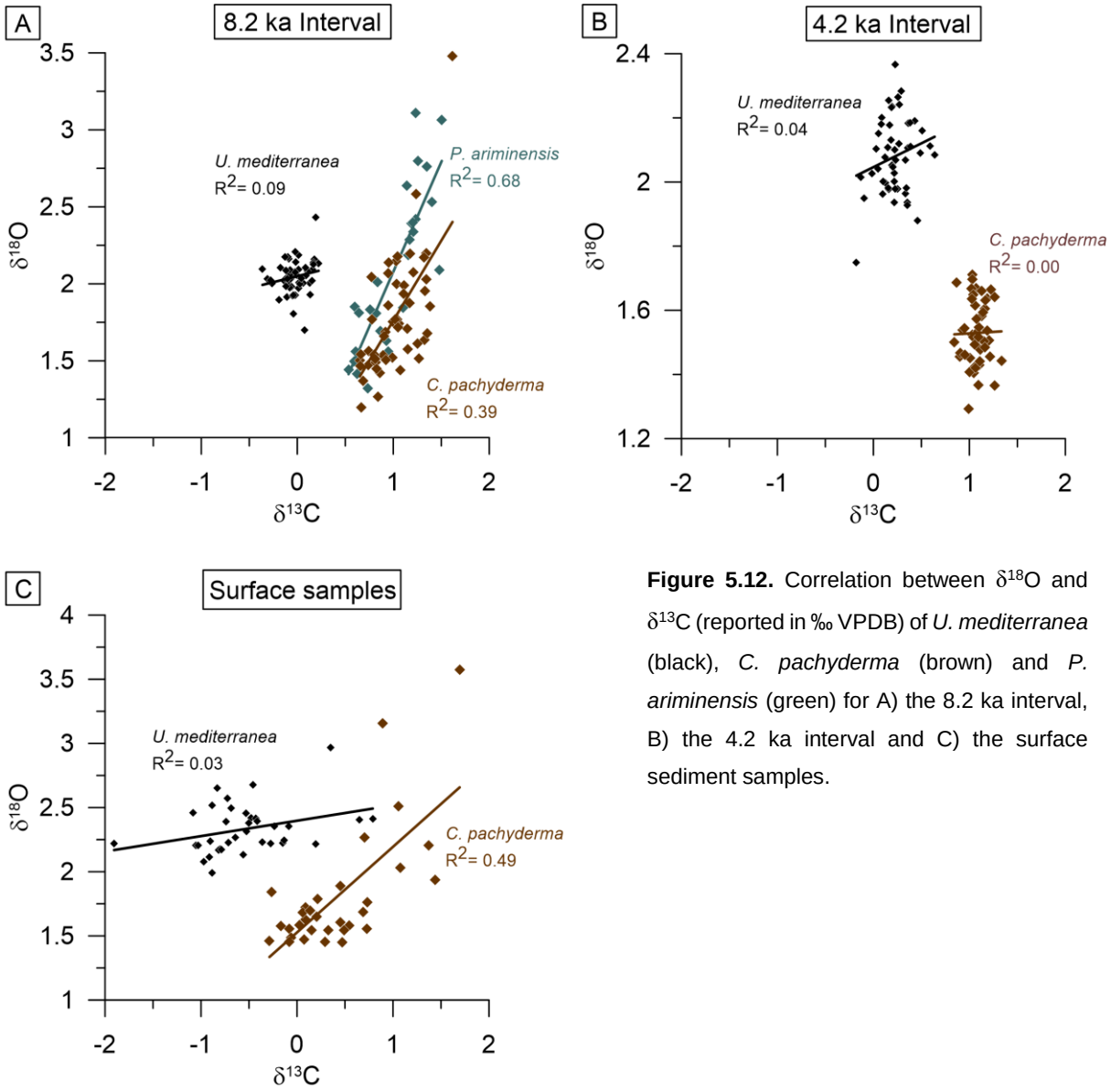

Figure 5.12. Correlation between $\delta^{18}O$ and $\delta^{13}C$ (reported in ‰ VPDB) of *U. mediterranea* (black), *C. pachyderma* (brown) and *P. ariminensis* (green) for A) the 8.2 ka interval, B) the 4.2 ka interval and C) the surface sediment samples.

During the 4.2 ka event, *U. mediterranea* $\delta^{13}C$ shows a higher range of fluctuations, but the $\Delta\ \delta^{13}C_{C.\ pach-\ U.\ med}$ varies on similar scales compared to the 8.2 ka interval (Fig. 5.11 D and F). This leads to the conclusion that during the more oligotrophic conditions of the 4.2 ka event, *U. mediterranea* was forced to migrate within the surface sediments in response to changing food availability (Theodor et al., 2016; Schmiedl et al., 2004). The overall more eutrophic sapropel boundary conditions of the 8.2 ka event prevented *U. mediterranea* from large changes in microhabitat depth.

The more unstable boundary conditions seen in the 8.2 ka interval could have been further amplified by the Holocene sea level evolution. High-resolution records of Mediterranean sea level are sparse, however multiple records agree on the general trend of sea level rise (Fig. 5.11 A) (Alley et al., 2005; Grant et al., 2012). Even though it can be argued whether the amplitude of change recorded for the 8.2 ka interval is realistic, fluctuations are much higher and melting snow and ice could have led to short- term sea level variations (Fig. 5.11 A right; Grant et al., 2012) in contrast to the 4.2 record, when sea level had already stabilized to near modern levels (Fig. 5.11 A left).

Combining all proxy evidence, we conclude that the 8.2 ka interval was exposed to greater fluctuations of precipitation, temperature, circulation and sea level, leading to more variable and unstable conditions than the relatively stable 4.2 ka interval. A pronounced 4.2 ka BP cooling or drying event as evident in records from the eastern Mediterranean borderlands and the Asian monsoon regions (Staubwasser et al., 2003; Weiss and Bradley, 2001) cannot be documented in our record.

5.5.3 Eutrophication of the Gulf of Taranto during the early Holocene and implications for the assessment of modern anthropogenic environmental impacts

Comparison of our early Holocene data with a benthic foraminiferal record from the same site shows that the observed anthropogenic eutrophication in the gulf during the past two centuries (Menke et al., 2017 b, under review) is of similar magnitude than natural eutrophication during the first part of sapropel S1 formation around 8.5 ka BP (Fig. 5.13). During the 8.2 ka event SIIBF reach a similarly low value of 40% as during the late Little Ice Age (LIA) when European climate was marked by a short interval of relatively dry and cold conditions (Fig. 5.13 B) (Bradley and Jones, 1993; Luterbacher et al., 2004; Wanner et al., 2008). Similarly, relatively high EBF abundances of ~24 % during the 8.2 ka event match those during the LIA (Fig. 5.13 D; with two very high EBF outliers during the 8.2 Event, possibly caused by the strong oceanographic fluctuations discussed in section 5.2). This comparison demonstrates that the human-induced eutrophication of shelf ecosystems of the Gulf of Taranto during the last two centuries was of similar magnitude as the eutrophication during sapropel boundary conditions. The modern nutrient fluxes in the Gulf of Taranto are linked to the densely populated Po valley, hence they reflect a local eutrophication signal decoupled from the orbital variation and large-scale hydrological changes that caused S1 formation (Degobbis et al., 2000; Rohling and Hilgen, 2007). However, modern anthropogenic eutrophication is not limited to the Po river plume, but a challenge throughout the entire Mediterranean Sea due to the densely populated borderlands (Karydis and Kitsiou, 2012).

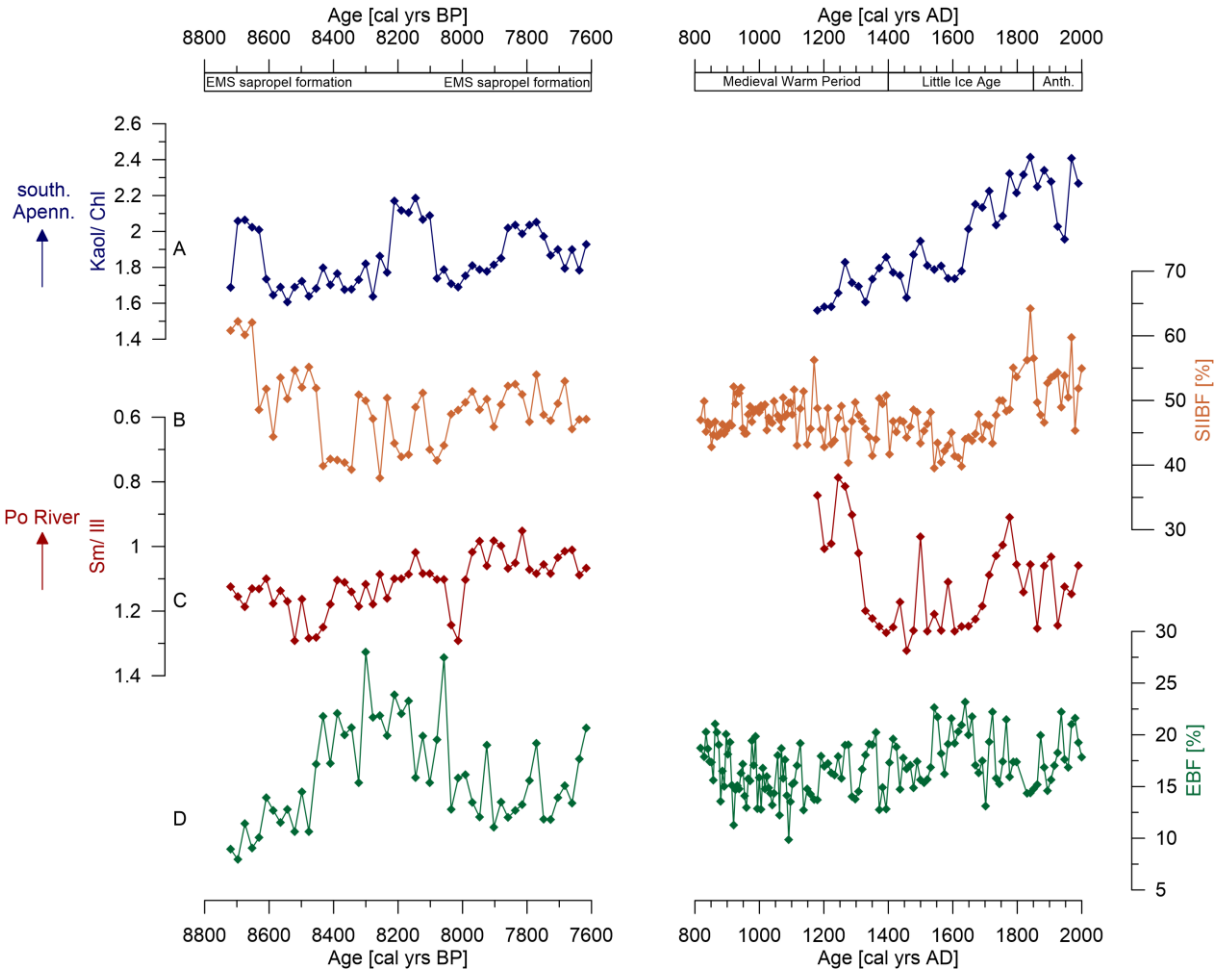

Figure 5.13. Comparison between proxy records for Italian hydrology and provenance of suspended sediment, and trophic conditions in the Gulf of Taranto for the intervals of the 8.2 ka event and the past millennium of GeoB15403- 4. Note the age on the x-axis is reported in yrs BP for the 8.2 ka interval and in AD for the last millennium. A) Kaolinite/chlorite ratio as proxy for a southern Apennine provenance of suspended sediment. B) Relative abundance of shallow to intermediate infaunal benthic foraminifera (SIIBF) as proxy for organic matter flux. C) Smectite/illite ratios as proxy for Po river derived suspended sediment. D) Relative abundance of epifaunal benthic foraminifera (EBF).

5.6 Conclusions

Our study provides detailed information on multi-decadal to centennial-scale variability of hydrology and trophic state of the Gulf of Taranto in the central Mediterranean Sea during the 8.2 and 4.2 ka events, two periods of pronounced northern hemisphere cooling and drought. High relative abundances of epifaunal benthic foraminifera (EBF) between ca. 8.5 and 8 ka BP indicate a shift towards more oligotrophic conditions corresponding to cooler and drier boundary conditions of the 8.2 ka event in the Mediterranean region. This climate caused a general reduction of river runoff and associated nutrient supply from the borderlands, ultimately leading to decreased food availability at shelf environments of the Gulf of Taranto. During this time, the relative abundance of shallow infaunal benthic foraminifera (SIIBF), which prefer

more eutrophic conditions, is low. In contrast, prior to 8.5 ka BP, SIIBF abundance is at a maximum corresponding to high nutrient fluxes and resulting eutrophic conditions, corresponding to the time interval of sapropel formation in the eastern Mediterranean Sea. Similarly, benthic ecosystems show a shift back to eutrophic conditions after 8 ka BP, however, the trophic level is lower when compared to the interval prior to 8.5 ka BP.

Persistently low amounts of deep infaunal benthic foraminifera (DIBF) prove that in contrast to bathyal and abyssal areas of the eastern Mediterranean Sea oxygen was not a limiting factor in shelf environments of the Gulf of Taranto during times of sapropel formation.

The clay mineral record reflects the generally dry climate boundary conditions during the 8.2 ka interval. Abrupt shifts in the clay mineral composition were possibly driven by short-term changes between cold-dry and warm-wet conditions involving thresholds in vegetation cover, soil erosion and aeolian and fluviatile sediment input.

Short-term changes in SIIBF abundance and the $\delta^{13}C$ difference between epifaunal *C. pachyderma* and shallow infaunal *U. mediterranea* likely document the response of central Mediterranean hydrology to the Atlantic Multidecadal Oscillation (AMO) as previously documented for the past millennium (Chapter 2). The variability of epibenthic foraminiferal stable isotope values is greater for the 8.2 ka interval than for the 4.2 ka interval. The positive correlation between $\delta^{18}O$ and $\delta^{13}C$ across the 8.2 ka interval argues for a switching between the presence of a salty and nutrient-poor water mass and a fresher and nutrient-rich water mass at the outer shelf of the Gulf of Taranto. The more unstable boundary conditions of the 8.2 ka interval are likely linked to the enhanced seasonality of the early Holocene. At times of particularly cold winters, enhanced vertical convection at intermediate water formation sites resulted in the entrainment of oligotrophic subsurface waters from the Ionian Sea into the Gulf of Taranto.

In contrast, the stable isotope values of epifaunal foraminifera are more stable during the 4.2 ka interval lacking a correlation between $\delta^{18}O$ and $\delta^{13}C$ values. This suggests the absence of substantial water mass shifts at outer shelf environments of the Gulf of Taranto during this time. The $\delta^{13}C$ record suggests overall lower organic matter fluxes during the 4.2 ka event than during the 8.2 ka event but indicates a comparable impact of the AMO on short-term trophic changes in the central Mediterranean region.

Comparison to a recent study conducted on the same sediment core suggests that human-induced eutrophication in the Gulf of Taranto since ~1800 AD reaches a similar magnitude as the eutrophic sapropel conditions of the early Holocene.

6 Conclusions and outlook

6.1 Conclusions

The aim of this study was to investigate the following three research hypotheses (as stated in chapter 1.1):

Due to high sedimentation rates in the Gulf of Taranto and its location, downwind of the Italian volcanic arc, tephrostratigraphy based on volcanic glass geochemistry provides a high-resolution, ^{14}C- independent stratigraphic framework for the age assessment of marine sediment cores.

Tephrostratigraphy based on geochemical fingerprinting of volcanic glass shards proved to be a reliable tool to establish and improve age models for marine sediment cores. Quantitative tephroanalysis of sediment samples from the uppermost 50 cm of gravity core GeoB15403-4 revealed the occurrence of two cryptotephras. Based on electron microprobe analysis it was possible to identify the source eruption of the two tephra layers, respectively. The peak in glass shard abundance at 1.5 cm depth was correlated to the 1944 AD eruption of the Somma-Vesuvius. The pronounced peak of glass shards with a rhyolitic composition at 36 cm suggests a primary tephra layer. Combining evidence from geochemical fingerprinting, the eruption type as well as the general time frame of AMS ^{14}C dates on planktonic foraminifera, allowed for identification of the 776 AD Monte Pilato eruption as the source for this cryptotephra.
The electron microprobe analyses revealed homogenous element distributions. Therefore, influences of several eruptions at the time of cryptotephra deposition as well as during post-depositional sediment reworking can be disregarded. The results show no evidence for the presence of several cryptotephras in the sediments of the area as suggested by previous studies using solely fluctuations in the abundance of tephra particles. This study underlines the importance of geochemical tephroanalysis in a highly geodynamic region like the Mediterranean Sea where numerous eruptions are recorded during the Holocene.

Italian hydrology, marine sedimentation and benthic ecosystem dynamics in the Gulf of Taranto are closely linked to changes in North Atlantic climate modes and are additionally forced by anthropogenic activity during the past millennium.

The Po river is the main driver of benthic ecosystem variability in the Gulf of Taranto, however, smaller rivers of the Apennines contribute to the nutrient supply of the West Adriatic Current

(WAC). The riverine organic matter and sediment influx, transported by the WAC into the gulf, leads to the development of a high-accumulation depocenter in the north-eastern part of the gulf, as reflected by a regional maximum of infaunal benthic foraminifera in recent times.
Clay mineral data and relative element distributions reveal a correlation of the Po river runoff with NAO strength for the past 300 years. The observed general increase in terrigenous fluxes at around ~1300 AD is coupled to a shift towards a persistently negative NAO. In contrast, the benthic shelf ecosystems responded to the northern Hemisphere temperature variability most likely due to positive anomalies resulting in enhanced precipitation, rising nutrient input into the Gulf of Taranto and associated organic matter fluxes to the sea floor. Spectral analysis of the faunal variability reveals a quasi-periodic variability of 50 to 70 years, arguing for an influence of the AMO on benthic ecosystem variability.
In conclusion, while the NAO determines the overall hydrological regime, variability of the AMO paces rainfall and marine ecosystem responses on multi-decadal timescales.
Increasing abundance of shallow to intermediate infaunal benthic foraminifera (SIIBF) since ~1800 AD display enhanced organic matter availability, probably a result of both rising temperatures and enhanced anthropogenic activity. Over the past decades, the SIIBF decline in abundance is likely a reflection of more strict regulations on fertilizers and reduction of riverine suspension loads due to the stabilization of river banks.

Multi-decadal to centennial climate changes are superimposed on the 8.2 ka and 4.2 ka events in the central Mediterranean. Associated variations in circulation and trophic conditions are amplified or attenuated depending on the respective Holocene orbital boundary conditions.

Between approximately 8.5 and 8.0 ka BP, high abundances of epifaunal benthic foraminifera (EBF) indicate a shift to more oligotrophic conditions corresponding to the cooler and drier conditions reported for the 8.2 ka event in the Mediterranean region. This cooler climate probably caused a decrease in river runoff and nutrient mobilization leading to a reduction of food availability in the Gulf of Taranto. Prior to 8.5 ka BP, SIIBF abundance is at its highest corresponding to the eutrophic conditions during early Holocene sapropel S1 formation in the eastern Mediterranean Sea. Although the dominance of SIIBF suggests generally eutrophic conditions, low amounts of deep infaunal benthic foraminifera (DIBF) prove, that in contrast to the lower bathyal and abyssal sub-basins of the eastern Mediterranean Sea at this time, oxygen was not a limiting factor on the deeper shelf of the Gulf of Taranto. After 8.0 ka BP, SIIBF indicate a shift back to more eutrophic conditions however abundance remains lower than before 8.5 ka BP.

The clay mineral record in the Gulf of Taranto mirrors the generally dry boundary conditions of the 8.2 ka event with abrupt shifts that were possibly driven by short-term changes between cold and dry and wet and warm conditions involving threshold responses in vegetation cover and soil erosion.

On shorter time-scales, SIIBF abundance and $\delta^{13}C$ difference between the epifaunal *C. pachyderma* and the shallow infaunal *U. mediterranea* likely document the response of the central Mediterranean hydrology to the AMO as previously documented for the past millennium. The strong isotopic variability and correlation between $\delta^{18}O$ and $\delta^{13}C$ during the 8.2 ka event argue for a switching between the dominance of a relatively saltier and nutrient-poor water mass and a relatively fresher and nutrient-rich water mass at the outer shelf of the Gulf of Taranto. This water mass variability was likely linked to the generally increased seasonality of the early Holocene and phases of particular cold winters during the 8.2 ka interval that promoted a vertical convection at sites of intermediate water formation and introduced subsurface waters from the Ionian Sea into the Gulf of Taranto. During the 4.2 ka interval stable isotope values are relatively constant and do not reflect a pronounced cold or dry event. The low variability and lacking correlation between epifaunal $\delta^{18}O$ and $\delta^{13}C$ suggests that subsurface water circulation was less variable at this time. The smaller $\delta^{13}C$ difference between *C. pachyderma and U. mediterranea* suggests generally lower organic matter fluxes to the seafloor when compared to the 8.2 ka interval. However, the inferred short-term trophic changes suggest a similar influence of the AMO on the trophic state of the Gulf of Taranto.

The comparison of the benthic ecosystem dynamics during the 8.2 ka interval and during the past millennium (see hypothesis 2) implies similar magnitudes of natural eutrophication during early Holocene sapropel boundary conditions and human-induced eutrophication since ~1800 AD.

6.2 Outlook

This study provides new insights to short-term climate, ecosystem and water mass variability in the Gulf of Taranto. The stable carbon and oxygen isotope signals of epifaunal foraminifera from the Gulf of Taranto and the western Adriatic Sea were used as modern equivalents. In the Gulf of Taranto, cryptotephrostratigraphy based on volcanic glass geochemistry proved to be a useful tool to enhance the accuracy of the age model and bears minimal uncertainty compared to tephra identification based solely on quantitative approaches. Geochemical fingerprinting of glass shards in several sediment cores from different locations in the Gulf of Taranto and adjacent regions would provide conclusive evidence for tephra distribution and give more detailed insights into ash transport. Based on improved stratigraphic frameworks the reported uniformity of sediment rates and depositional dynamics in the eastern Gulf of Taranto could be further tested.

Variations of the benthic foraminifera faunal composition and clay mineral ratios in the Gulf of Taranto are closely linked to Po river discharge and related variations in nutrient and sediment load of the WAC during the past millennium. Comparing the results from the Gulf of Taranto to sediment records from the south-western and mid-western Adriatic Sea could provide further evidence for this link and give insights into spatial gradients and temporal offsets.

The integration of benthic foraminiferal stable isotope records from sites in the northern Ionian and the southern Adriatic Sea would enable to conclusively identify water mass provenance and flow patterns during the 8.2 ka event. This is of great interest against the background of recent climate warming and its potential consequences for Mediterranean circulation, since it would allow for a more detailed characterization of water mass dynamics during periods of short-term climate change.

This study demonstrated that the 4.2 ka drought event had only little influence on marine environments of the central Mediterranean Sea. On the other hand, this event had a severe impact on the hydrology and thus human populations along the eastern Mediterranean borderlands. The integrated evaluation of proxy records from a core transect through the eastern Mediterranean Sea would be useful for identifying the spatial and temporal dynamics of the 4.2 ka event in the marine realm.

Proxy records, like the ones derived in this study, can be used for comparison to results from modeling experiments. The high-resolution record from the Gulf of Taranto could help to validate synthetic sediment cores and test the uniqueness of simulated temporal sediment and biogeochemical patterns.

7 References

Abrantes, F., Lebreiro, S., Rodrigues, T., Gil, I., Bartels-Jónsdóttir, H., Oliveira, P., Kissel, C., and Grimalt, J., 2005, Shallow-marine sediment cores record climate variability and earthquake activity off Lisbon (Portugal) for the last 2000 years: Quaternary Science Reviews, v. 24, no. 23, p. 2477-2494.

Aksu, A. E., Abrajano, T., Mudie, P. J., and Yaşar, D., 1999, Organic geochemical and palynological evidence for terrigenous origin of the organic matter in Aegean Sea sapropel S1: Marine Geology, v. 153, no. 1, p. 303-318.

Albert, P., Tomlinson, E., Smith, V., Di Roberto, A., Todman, A., Rosi, M., Marani, M., Muller, W., and Menzies, M., 2012, Marine-continental tephra correlations: volcanic glass geochemistry from the Marsili Basin and the Aeolian Islands, Southern Tyrrhenian Sea, Italy: Journal of Volcanology and Geothermal Research, v. 229, p. 74-94.

Albert, P. G., Tomlinson, E. L., Smith, V. C., Di Traglia, F., Pistolesi, M., Morris, A., Donato, P., De Rosa, R., Sulpizio, R., and Keller, J., 2017, Glass geochemistry of pyroclastic deposits from the Aeolian Islands in the last 50 ka: A proximal database for tephrochronology: Journal of Volcanology and Geothermal Research, v. 336, p. 81-107.

Alley, R. B., Clark, P. U., Huybrechts, P., and Joughin, I., 2005, Ice-sheet and sea-level changes: science, v. 310, no. 5747, p. 456-460.

Alley, R. B., Mayewski, P. A., Sowers, T., Stuiver, M., Taylor, K. C., and Clark, P. U., 1997, Holocene climatic instability: A prominent, widespread event 8200 yr ago: Geology, v. 25, no. 6, p. 483-486.

Alpert, P., Baldi, M., Ilani, R., Krichak, S., Price, C., Rodó, X., Saaroni, H., Ziv, B., Kishcha, P., Barkan, J., Mariotti, A., and Xoplaki, E., 2006, Chapter 2 Relations between climate variability in the Mediterranean region and the tropics: ENSO, South Asian and African monsoons, hurricanes and Saharan dust, in Lionello, P., Malanotte-Rizzoli, P., and Boscolo, R., eds., Developments in Earth and Environmental Sciences, Volume 4, Elsevier, p. 149-177.

Antoine, D., Morel, A., and André, J. M., 1995, Algal pigment distribution and primary production in the eastern Mediterranean as derived from coastal zone color scanner observations: Journal of Geophysical Research: Oceans, v. 100, no. C8, p. 16193-16209.

Ariztegui, D., Asioli, A., Lowe, J., Trincardi, F., Vigliotti, L., Tamburini, F., Chondrogianni, C., Accorsi, C., Mazzanti, M. B., and Mercuri, A., 2000, Palaeoclimate and the formation of sapropel S1: inferences from Late Quaternary lacustrine and marine sequences in the central Mediterranean region: Palaeogeography, Palaeoclimatology, Palaeoecology, v. 158, no. 3, p. 215-240.

Arnò, V., Principe, C., Rosi, M., Santacroce, R., Sbrana, A., and Sheridan, M., 1987, Eruptive history: Somma-Vesuvius, v. 114, p. 53-103.

Artegiani, A., Paschini, E., Russo, A., Bregant, D., Raicich, F., and Pinardi, N., 1997, The Adriatic Sea General Circulation. Part I: Air–Sea Interactions and Water Mass Structure: Journal of Physical Oceanography, v. 27, no. 8, p. 1492-1514.

Arz, H. W., Lamy, F., and Pätzold, J., 2006, A pronounced dry event recorded around 4.2 ka in brine sediments from the northern Red Sea: Quaternary Research, v. 66, no. 3, p. 432-441.

Bakker, P., Clark, P. U., Golledge, N. R., Schmittner, A., and Weber, M. E., 2017, Centennial-scale Holocene climate variations amplified by Antarctic Ice Sheet discharge: Nature, v. 541, no. 7635, p. 72-76.

Bar-Matthews, M., Ayalon, A., Kaufman, A., and Wasserburg, G. J., 1999, The Eastern Mediterranean paleoclimate as a reflection of regional events: Soreq cave, Israel: Earth and Planetary Science Letters, v. 166, no. 1, p. 85-95.

Barale, V., Jaquet, J.-M., and Ndiaye, M., 2008, Algal blooming patterns and anomalies in the Mediterranean Sea as derived from the SeaWiFS data set (1998–2003): Remote Sensing of Environment, v. 112, no. 8, p. 3300-3313.

Barber, D., Dyke, A., Hillaire-Marcel, C., Jennings, A., Andrews, J., Kerwin, M., Bilodeau, G., McNeely, R., Southon, J., and Morehead, M., 1999, Forcing of the cold event of 8,200 years ago by catastrophic drainage of Laurentide lakes: Nature, v. 400, no. 6742, p. 344-348.

Barberi, F., Macedonio, G., Pareschi, M., and Santacroce, R., 1990, Mapping the tephra fallout risk: an example from Vesuvius, Italy: Nature, v. 344, no. 6262, p. 142-144.

Barmawidjaja, D., Van der Zwaan, G., Jorissen, F., and Puskaric, S., 1995, 150 years of eutrophication in the northern Adriatic Sea: evidence from a benthic foraminiferal record: Marine Geology, v. 122, no. 4, p. 367-384.

Beccaluva, L., Bianchini, G., Bonadiman, C., Coltorti, M., Milani, L., Salvini, L., Siena, F., and Tassinari, R., 2007, Intraplate lithospheric and sublithospheric components in the Adriatic domain: Nephelinite to tholeiite magma generation in the Paleogene Veneto volcanic province, southern Alps: Geological Society of America Special Papers, v. 418, p. 131-152.

Beniston, M., Rebetez, M., Giorgi, F., and Marinucci, M., 1994, An analysis of regional climate change in Switzerland: Theoretical and applied climatology, v. 49, no. 3, p. 135-159.

Béranger, K., Mortier, L., Gasparini, G.-P., Gervasio, L., Astraldi, M., and Crépon, M., 2004, The dynamics of the Sicily Strait: a comprehensive study from observations and models: Deep Sea Research Part II: Topical Studies in Oceanography, v. 51, no. 4, p. 411-440.

Bertagnini, A., Di Roberto, A., and Pompilio, M., 2011, Paroxysmal activity at Stromboli: lessons from the past: Bulletin of volcanology, v. 73, no. 9, p. 1229-1243.

Biscaye, P., 1964, Distinction between Kaolinite and Chlorite in recent sediments by X-ray diffraction: American Mineralogist, v. 49, no. 9-1, p. 1281-&.

Biscaye, P. E., 1965, Mineralogy and sedimentation of recent deep-sea clay in the Atlantic Ocean and adjacent seas and oceans: Geological Society of America Bulletin, v. 76, no. 7, p. 803-832.

Boldrin, A., Miserocchi, S., Rabitti, S., Turchetto, M., Balboni, V., and Socal, G., 2002, Particulate matter in the southern Adriatic and Ionian Sea: characterisation and downward fluxes: Journal of Marine Systems, v. 33, p. 389-410.

Bond, G., Kromer, B., Beer, J., Muscheler, R., Evans, M. N., Showers, W., Hoffmann, S., Lotti-Bond, R., Hajdas, I., and Bonani, G., 2001, Persistent solar influence on North Atlantic climate during the Holocene: Science, v. 294, no. 5549, p. 2130-2136.

Bond, G., Showers, W., Cheseby, M., Lotti, R., Almasi, P., Priore, P., Cullen, H., Hajdas, I., and Bonani, G., 1997, A pervasive millennial-scale cycle in North Atlantic Holocene and glacial climates: science, v. 278, no. 5341, p. 1257-1266.

Bonino, G., Castagnoli, G. C., Callegari, E., and Zhu, G.-M., 1993, Radiometric and tephroanalysis dating of recent Ionian sea cores: Il Nuovo Cimento C, v. 16, no. 2, p. 155-162.

Bourne, A., Lowe, J., Trincardi, F., Asioli, A., Blockley, S., Wulf, S., Matthews, I., Piva, A., and Vigliotti, L., 2010, Distal tephra record for the last ca 105,000 years from core PRAD 1-2 in the central Adriatic Sea: implications for marine tephrostratigraphy: Quaternary Science Reviews, v. 29, no. 23, p. 3079-3094.

Bradley, R., and Jones, P., 1993, 1993:'Little Ice Age'summer temperature variations: their nature and relevance to recent global warming trends. The Holocene 3, 367-376.

Bronick, C. J., and Lal, R., 2005, Soil structure and management: a review: Geoderma, v. 124, no. 1, p. 3-22.

Brown, G. t., and Brindley, G., 1980, X-ray diffraction procedures for clay mineral identification: Crystal structures of clay minerals and their X-ray identification, v. 5, p. 305-359.

Budillon, G., Bue, N. L., Siena, G., and Spezie, G., 2010, Hydrographic characteristics of water masses and circulation in the Northern Ionian Sea: Deep Sea Research Part II: Topical Studies in Oceanography, v. 57, no. 5, p. 441-457.

Cacho, I., Grimalt, J. O., Canals, M., Sbaffi, L., Shackleton, N. J., Schönfeld, J., and Zahn, R., 2001, Variability of the western Mediterranean Sea surface temperature during the last 25,000 years and its connection with the Northern Hemisphere climatic changes: Paleoceanography, v. 16, no. 1, p. 40-52.

Caroppo, C., Turicchia, S., and Margheri, M. C., 2006, Phytoplankton assemblages in coastal waters of the northern Ionian Sea (eastern Mediterranean), with special reference to cyanobacteria: Journal of the Marine Biological Association of the United Kingdom, v. 86, no. 5, p. 927-937.

Castagnoli, G. C., Bonino, G., Caprioglio, F., Provenzale, A., Serio, M., and Guang-Mei, Z., 1990, The carbonate profile of two recent Ionian Sea cores: Evidence that the sedimentation rate is constant over the last millennia: Geophysical Research Letters, v. 17, no. 11, p. 1937-1940.

Chen, L., Zonneveld, K. A., and Versteegh, G. J., 2011, Short term climate variability during “Roman Classical Period” in the eastern Mediterranean: Quaternary Science Reviews, v. 30, no. 27, p. 3880-3891.

Chester, R., Baxter, G., Behairy, A., Connor, K., Cross, D., Elderfield, H., and Padgham, R., 1977, Soil-sized eolian dusts from the lower troposphere of the eastern Mediterranean Sea: Marine Geology, v. 24, no. 3, p. 201-217.

Chevalier, M., Brewer, S., and Chase, B. M., 2017, Qualitative assessment of PMIP3 rainfall simulations across the eastern African monsoon domains during the mid-Holocene and the Last Glacial Maximum: Quaternary Science Reviews, v. 156, p. 107-120.

Cimerman, F., and Langer, M. R., 1991, Mediterranean foraminifera.

Corliss, B. H., 1985, Microhabitats of benthic foraminifera within deep-sea sediments: Nature, v. 314, no. 6010, p. 435-438.

Costa, A., Macedonio, G., and Folch, A., 2006, A three-dimensional Eulerian model for transport and deposition of volcanic ashes: Earth and Planetary Science Letters, v. 241, no. 3, p. 634-647.

Cramp, A., and O'Sullivan, G., 1999, Neogene sapropels in the Mediterranean: a review: Marine Geology, v. 153, no. 1, p. 11-28.

Cremaschi, M., Zerboni, A., Spötl, C., and Felletti, F., 2010, The calcareous tufa in the Tadrart Acacus Mt.(SW Fezzan, Libya): an early Holocene palaeoclimate archive in the central Sahara: Palaeogeography, Palaeoclimatology, Palaeoecology, v. 287, no. 1, p. 81-94.

Croudace, I. W., Rindby, A., and Rothwell, R. G., 2006, ITRAX: description and evaluation of a new multi-function X-ray core scanner: Geological Society, London, Special Publications, v. 267, no. 1, p. 51-63.

Cullen, H. M., Hemming, S., Hemming, G., Brown, F., Guilderson, T., and Sirocko, F., 2000, Climate change and the collapse of the Akkadian empire: Evidence from the deep sea: Geology, v. 28, no. 4, p. 379-382.Cyr, A. J., Granger, D. E., Olivetti, V., and Molin, P., 2010, Quantifying rock uplift rates using channel steepness and cosmogenic nuclide–determined erosion rates: Examples from northern and southern Italy: Lithosphere, v. 2, no. 3, p. 188-198.

D'Antonio, M., Tilton, G. R., and Civetta, L., 1996, Petrogenesis of Italian Alkaline Lavas Deduced from Pb-Sr-Nd Isotope Relationships: Earth processes: reading the isotopic code, p. 253-267.

Dansgaard, W., Johnsen, S., Clausen, H., Dahl-Jensen, D., Gundestrup, N., Hammer, C., Hvidberg, C., Steffensen, J., Sveinbjörnsdottir, A., and Jouzel, J., 1993, Evidence for general instability of past climate from a 250-kyr ice-core record: Nature, v. 364, no. 6434, p. 218-220.

Davì, M., De Rosa, R., and Barca, D., 2009, A LA-ICP-MS study of minerals in the Rocche Rosse magmatic enclaves: evidence of a mafic input triggering the latest silicic eruption of Lipari Island (Aeolian Arc, Italy): Journal of Volcanology and Geothermal Research, v. 182, no. 1, p. 45-56.

Davies, S. M., Abbott, P. M., Pearce, N. J., Wastegård, S., and Blockley, S. P., 2012, Integrating the INTIMATE records using tephrochronology: rising to the challenge: Quaternary Science Reviews, v. 36, p. 11-27.

Davies, S. M., Branch, N. P., Lowe, J. J., and Turney, C. S., 2002, Towards a European tephrochronological framework for Termination 1 and the Early Holocene: Philosophical Transactions of the Royal Society of London A: Mathematical, Physical and Engineering Sciences, v. 360, no. 1793, p. 767-802.

Davies, S. M., Wohlfarth, B., Wastegård, S., Andersson, M., Blockley, S., and Possnert, G., 2004, Were there two Borrobol Tephras during the early Lateglacial period: implications for tephrochronology?: Quaternary Science Reviews, v. 23, no. 5, p. 581-589.

De Lange, G. J., Thomson, J., Reitz, A., Slomp, C. P., Principato, M. S., Erba, E., and Corselli, C., 2008, Synchronous basin-wide formation and redox-controlled preservation of a Mediterranean sapropel: Nature Geoscience, v. 1, no. 9, p. 606-610.

De Rijk, S., Jorissen, F., Rohling, E., and Troelstra, S., 2000, Organic flux control on bathymetric zonation of Mediterranean benthic foraminifera: Marine Micropaleontology, v. 40, no. 3, p. 151-166.

De Rijk, S., Troelstra, S., and Rohling, E., 1999, Benthic foraminiferal distribution in the Mediterranean Sea: Journal of Foraminiferal Research, v. 29, no. 2, p. 93-103.

De Vivo, B., Rolandi, G., Gans, P., Calvert, A., Bohrson, W., Spera, F., and Belkin, H., 2001, New constraints on the pyroclastic eruptive history of the Campanian volcanic Plain (Italy): Mineralogy and Petrology, v. 73, no. 1-3, p. 47-65.

Dee, D. P., Uppala, S., Simmons, A., Berrisford, P., Poli, P., Kobayashi, S., Andrae, U., Balmaseda, M., Balsamo, G., and Bauer, P., 2011, The ERA-Interim reanalysis: Configuration and performance of the data assimilation system: Quarterly Journal of the royal meteorological society, v. 137, no. 656, p. 553-597.

Degobbis, D., Gilmartin, M., and Orio, A. A., 1986, The relation of nutrient regeneration in the sediments of the northern Adriatic to eutrophication, with special reference to the Lagoon of Venice: Science of the total environment, v. 56, p. 201-210.

Degobbis, D., Precali, R., Ivancic, I., Smodlaka, N., Fuks, D., and Kveder, S., 2000, Long-term changes in the northern Adriatic ecosystem related to anthropogenic eutrophication: International Journal of Environment and Pollution, v. 13, no. 1-6, p. 495-533.

Delworth, T. L., and Mann, M. E., 2000, Observed and simulated multidecadal variability in the Northern Hemisphere: Climate Dynamics, v. 16, no. 9, p. 661-676.

DeMenocal, P., Ortiz, J., Guilderson, T., Adkins, J., Sarnthein, M., Baker, L., and Yarusinsky, M., 2000, Abrupt onset and termination of the African Humid Period:: rapid climate responses to gradual insolation forcing: Quaternary Science Reviews, v. 19, no. 1–5, p. 347-361.

Desprat, S., Goñi, M. a. F. S., and Loutre, M.-F., 2003, Revealing climatic variability of the last three millennia in northwestern Iberia using pollen influx data: Earth and Planetary Science Letters, v. 213, no. 1, p. 63-78.

Dilek, Y., 2006, Collision tectonics of the Mediterranean region: causes and consequences: Geological Society of America Special Papers, v. 409, p. 1-13.

Di Renzo, V., Di Vito, M., Arienzo, I., Carandente, A., Civetta, L., D'antonio, M., Giordano, F., Orsi, G., and Tonarini, S., 2007, Magmatic history of Somma–Vesuvius on the basis of new geochemical and isotopic data from a deep borehole (Camaldoli della Torre): Journal of Petrology, v. 48, no. 4, p. 753-784.

Donders, T. H., Wagner-Cremer, F., and Visscher, H., 2008, Integration of proxy data and model scenarios for the mid-Holocene onset of modern ENSO variability: Quaternary Science Reviews, v. 27, no. 5, p. 571-579.

Drever, J. I., and Zobrist, J., 1992, Chemical weathering of silicate rocks as a function of elevation in the southern Swiss Alps: Geochimica et Cosmochimica Acta, v. 56, no. 8, p. 3209-3216.

Drysdale, R., Zanchetta, G., Hellstrom, J., Maas, R., Fallick, A., Pickett, M., Cartwright, I., and Piccini, L., 2006, Late Holocene drought responsible for the collapse of Old World civilizations is recorded in an Italian cave flowstone: Geology, v. 34, no. 2, p. 101-104.

Dugmore, A., 1989, Icelandic volcanic ash in Scotland: The Scottish Geographical Magazine, v. 105, no. 3, p. 168-172.

Duplessy, J., Shackleton, N., Fairbanks, R., Labeyrie, L., Oppo, D., and Kallel, N., 1988, Deepwater source variations during the last climatic cycle and their impact on the global deepwater circulation: Paleoceanography, v. 3, no. 3, p. 343-360.

Ehrmann, W., Schmiedl, G., Hamann, Y., Kuhnt, T., Hemleben, C., and Siebel, W., 2007, Clay minerals in late glacial and Holocene sediments of the northern and southern Aegean Sea: Palaeogeography, Palaeoclimatology, Palaeoecology, 249, 36-57.

Ehrmann, W., Seidel, M., and Schmiedl, G., 2013, Dynamics of Late Quaternary North African humid periods documented in the clay mineral record of central Aegean Sea sediments: Global and planetary change, v. 107, p. 186-195.

Emeis, K.-C., Sakamoto, T., Wehausen, R., and Brumsack, H.-J., 2000, The sapropel record of the eastern Mediterranean Sea—results of Ocean Drilling Program Leg 160: Palaeogeography, Palaeoclimatology, Palaeoecology, v. 158, no. 3, p. 371-395.

Enfield, D. B., Mestas-Nuñez, A. M., and Trimble, P. J., 2001, The Atlantic multidecadal oscillation and its relation to rainfall and river flows in the continental US: Geophysical Research Letters, v. 28, no. 10, p. 2077-2080.

Fabiano, M., Danovaro, R., and Fraschetti, S., 1995, A three-year time series of elemental and biochemical composition of organic matter in subtidal sandy sediments of the Ligurian Sea (northwestern Mediterranean): Continental Shelf Research, v. 15, no. 11-12, p. 1453-1469.

Ferrarese, S., Cassardo, C., Elmi, A., Genovese, R., Longhetto, A., Manfrin, M., and Richiardone, R., 2008, Response of temperature and sea surface circulation to a Sirocco wind event in the Adriatic basin: A model simulation: Journal of Marine Systems, v. 74, no. 1, p. 659-671.

Focardi, S., Specchiulli, A., Spagnoli, F., Fiesoletti, F., and Rossi, C., 2009, A combinated approach to investigate the biochemistry and hydrography of a shallow bay in the South Adriatic Sea: the Gulf of Manfredonia (Italy): Environmental monitoring and assessment, v. 153, no. 1, p. 209-220.

Fontanier, C., Jorissen, F., Licari, L., Alexandre, A., Anschutz, P., and Carbonel, P., 2002, Live benthic foraminiferal faunas from the Bay of Biscay: faunal density, composition, and microhabitats: Deep Sea Research Part I: Oceanographic Research Papers, v. 49, no. 4, p. 751-785.

Forni, F., Lucchi, F., Peccerillo, A., Tranne, C., Rossi, P., and Frezzotti, M., 2013, Stratigraphy and geological evolution of the Lipari volcanic complex (central Aeolian archipelago): Geological Society, London, Memoirs, v. 37, no. 1, p. 213-279.

Frisia, S., Borsato, A., Preto, N., and McDermott, F., 2003, Late Holocene annual growth in three Alpine stalagmites records the influence of solar activity and the North Atlantic Oscillation on winter climate: Earth and Planetary Science Letters, v. 216, no. 3, p. 411-424.

Frisia, S., Borsato, A., Spötl, C., Villa, I. M., and Cucchi, F., 2005, Climate variability in the SE Alps of Italy over the past 17 000 years reconstructed from a stalagmite record: Boreas, v. 34, no. 4, p. 445-455.

Galay, V., 1983, Causes of river bed degradation: Water resources research, v. 19, no. 5, p. 1057-1090.

Giordani, P., and Angiolini, L., 1983, Chemical parameters characterizing the sedimentary environment in a NW Adriatic coastal area (Italy): Estuarine, Coastal and Shelf Science, v. 17, no. 2, p. 159-167.

Giraudi, C., Magny, M., Zanchetta, G., and Drysdale, R., 2011, The Holocene climatic evolution of Mediterranean Italy: A review of the continental geological data: The Holocene, v. 21, no. 1, p. 105-115.

Goudeau, M. L. S., Grauel, A. L., Bernasconi, S. M., and de Lange, G. J., 2013, Provenance of surface sediments along the southeastern Adriatic coast off Italy: An overview: Estuarine Coastal and Shelf Science, v. 134, p. 45-56.

Goudeau, M. L. S., Grauel, A. L., Tessarolo, C., Leider, A., Chen, L., Bernasconi, S. M., Versteegh, G. J. M., Zonneveld, K. A. F., Boer, W., Alonso-Hernandez, C. M., and De Lange, G. J., 2014, The Glacial-Interglacial transition and Holocene environmental changes in sediments from the Gulf of Taranto, central Mediterranean: Marine Geology, v. 348, p. 88-102.

Grant, K., Rohling, E., Bar-Matthews, M., Ayalon, A., Medina-Elizalde, M., Ramsey, C. B., Satow, C., and Roberts, A., 2012, Rapid coupling between ice volume and polar temperature over the past 150,000 years: Nature, v. 491, no. 7426, p. 744.

Grauel, A.-L., Goudeau, M.-L. S., de Lange, G. J., and Bernasconi, S. M., 2013a, Climate of the past 2500 years in the Gulf of Taranto, central Mediterranean Sea: A high-resolution climate reconstruction based on δ18O and δ13C of Globigerinoides ruber (white): The Holocene, v. 23, no. 10, p. 1440-1446.

Grauel, A., and Bernasconi, S., 2010, Core-top calibration of δ 18 O and δ 13 C of G. ruber (white) and U. mediterranea along the southern Adriatic coast of Italy: Marine Micropaleontology, v. 77, no. 3, p. 175-186.

Grauel, A. L., Leider, A., Goudeau, M. L. S., Muller, I. A., Bernasconi, S. M., Hinrichs, K. U., de Lange, G. J., Zonneveld, K. A. F., and Versteegh, G. J. M., 2013b, What do SST proxies really tell us? A high-resolution multiproxy (U-37(K '), TEX86H and foraminifera delta O-18) study in the Gulf of Taranto, central Mediterranean Sea: Quaternary Science Reviews, v. 73, p. 115-131.

Grazzini, C. V., and Pierre, C., 1991, High fertility in the Alboran Sea since the last glacial maximum: Paleoceanography, v. 6, no. 4, p. 519-536.

Grbec, B., and Morovic, M., 1997, Seasonal thermohaline fluctuations in the middle Adriatic Sea: Nuovo cimento della Società italiana di fisica. C, v. 20, no. 4, p. 561-576.

Grbec, B., Morović, M., Kušpilić, G., and Marasović, I., 2007, Climate regime shifts of the Adriatic Sea ecosystem: Rapport du 38e Congrès de la CIESM, v. 153.

Grimm, R., Maier-Reimer, E., Mikolajewicz, U., Schmiedl, G., Müller-Navarra, K., Adloff, F., Grant, K. M., Ziegler, M., Lourens, L. J., and Emeis, K.-C., 2015, Late glacial initiation of Holocene eastern Mediterranean sapropel formation: Nature communications, v. 6, p. 7099.

Grootes, P., and Stuiver, M., 1997, Oxygen 18/16 variability in Greenland snow and ice with 10− 3-to 105-year time resolution: Journal of Geophysical Research: Oceans, v. 102, no. C12, p. 26455-26470.

Grove, J. M., 2001, The onset of the Little Ice Age, History and Climate, Springer, p. 153-185.

Guichard, F., Carey, S., Arthur, M., Sigurdsson, H., and Arnold, M., 1993, Tephra from the Minoan eruption of Santorini in sediments of the Black Sea: Nature, v. 363, no. 6430, p. 610-612.

Guiot, J., and Corona, C., 2010, Growing season temperatures in Europe and climate forcings over the past 1400 years: PloS one, v. 5, no. 4, p. e9972.

Gupta, A. K., Anderson, D. M., and Overpeck, J. T., 2003, Abrupt changes in the Asian southwest monsoon during the Holocene and their links to the North Atlantic Ocean: Nature, v. 421, no. 6921, p. 354.

Gupta, B. K. S.: Modern foraminifera, Springer, 2002.

Herget, J., 2000, Holocene development of the River Lippe valley, Germany: a case study of anthropogenic influence: Earth Surface Processes and Landforms, v. 25, no. 3, p. 293-305.

Hilgen, F., Kuiper, K., Krijgsman, W., Snel, E., and van der Laan, E., 2007, Astronomical tuning as the basis for high resolution chronostratigraphy: the intricate history of the Messinian Salinity Crisis: Stratigraphy, v. 4, no. 2-3, p. 231-238.

Holmgren, K., Gogou, A., Izdebski, A., Luterbacher, J., Sicre, M.-A., and Xoplaki, E., 2016, Mediterranean Holocene climate, environment and human societies: Quaternary Science Reviews, v. 136, p. 1-4.

Holzhauser, H., Magny, M., and Zumbuühl, H. J., 2005, Glacier and lake-level variations in west-central Europe over the last 3500 years: The Holocene, v. 15, no. 6, p. 789-801.

Hammer, Ø., Harper, D., and Ryan, P., 2008, PAST-palaeontological statistics, ver. 1.89: Paleontological Museum, University of Oslo, Noruega.(También disponible en línea: http://folk. uio. no/ohammer/past/index. html).

Hammer, Ř., Harper, D., and Ryan, P., 2001, PAST: Paleontological Statistics Software Package for Education and Data Analysis–Palaeontol. Electron. 4: 9pp.

Hunt, J. B., and Hill, P. G., 2001, Tephrological implications of beam size—sample-size effects in electron microprobe analysis of glass shards: Journal of Quaternary Science, v. 16, no. 2, p. 105-117.

Hurrell, J. W., 1995, Decadal trends in the North Atlantic Oscillation: regional temperatures and precipitation: Science-AAAS-Weekly Paper Edition, v. 269, no. 5224, p. 676-678.

Hurrell, J. W., Kushnir, Y., and Visbeck, M., 2001, The north Atlantic oscillation: Science, v. 291, no. 5504, p. 603-605.

Hsü, K. J., Montadert, L., Bernoulli, D., Cita, M. B., Erickson, A., Garrison, R. E., Kidd, R. B., Mèlierés, F., Müller, C., and Wright, R., 1977, History of the Mediterranean salinity crisis: Nature, v. 267, no. 5610, p. 399-403.

Imbrie, J., Hays, J. D., Martinson, D. G., McIntyre, A., Mix, A. C., Morley, J. J., Pisias, N. G., Prell, W. L., and Shackleton, N. J., 1984, The orbital theory of Pleistocene climate: support from a revised chronology of the marine d18O record.

Jeromel, M., Malacic, V., and Rakovec, J., 2009, Weibull distribution of bora and sirocco winds in the northern Adriatic Sea/Weibullova distribucija bure i juga na sjevernom Jadranu: Geofizika, v. 26, no. 1, p. 85-101.

Jones, P. D., and Mann, M. E., 2004, Climate over past millennia: Reviews of Geophysics, v. 42, no. 2.

Jones, R. W., and Brady, H. B., 1994, The challenger foraminifera, Oxford University Press, USA.

Jorissen, F., Barmawidjaja, D., Puskaric, S., and Van der Zwaan, G., 1992, Vertical distribution of benthic foraminifera in the northern Adriatic Sea: the relation with the organic flux: Marine Micropaleontology, v. 19, no. 1-2, p. 131-146.

Jorissen, F., Fontanier, C., and Thomas, E.: Paleoceanographical Proxies Based on Deep-Sea Benthic Foraminiferal Assemblage Characteristics, 1 (07), doi: 10.1016, S1572-5480 (07), 01012-01013, 2007.

Jorissen, F. J., de Stigter, H. C., and Widmark, J. G., 1995, A conceptual model explaining benthic foraminiferal microhabitats: Marine micropaleontology, v. 26, no. 1-4, p. 3-15.

Jungclaus, J. H., Haak, H., Latif, M., and Mikolajewicz, U., 2005, Arctic–North Atlantic interactions and multidecadal variability of the meridional overturning circulation: Journal of climate, v. 18, no. 19, p. 4013-4031.

Justić, D., 1987, Long-term eutrophication of the northern Adriatic Sea: Marine Pollution Bulletin, v. 18, no. 6, p. 281-284.

Karydis, M., and Kitsiou, D., 2012, Eutrophication and environmental policy in the Mediterranean Sea: a review: Environmental monitoring and assessment, v. 184, no. 8, p. 4931-4984.

Keller, J.,2002, Lipari's fiery past: dating the medieval pumice eruption of Monte Pelato, in Proceedings International Conference ''The fire between air and water'', UNESCO-Regione Siciliana, Lipari2002, Volume 29.

Keller, J., Kraml, M., and Scheld, A., 1996, Late Quaternary tephrochronological correlation between deep-sea sediments and the land record in the Central Mediterranean, in Proceedings 30th International Geological Congress, Beijing1996, Volume 3, p. 204.

Keller, J., Ryan, W., Ninkovich, D., and Altherr, R., 1978, Explosive volcanic activity in the Mediterranean over the past 200,000 yr as recorded in deep-sea sediments: Geological Society of America Bulletin, v. 89, no. 4, p. 591-604.

Kleiven, H. K. F., Kissel, C., Laj, C., Ninnemann, U. S., Richter, T. O., and Cortijo, E., 2008, Reduced North Atlantic deep water coeval with the glacial Lake Agassiz freshwater outburst: science, v. 319, no. 5859, p. 60-64.

Knight, J. R., Folland, C. K., and Scaife, A. A., 2006, Climate impacts of the Atlantic multidecadal oscillation: Geophysical Research Letters, v. 33, no. 17.

Knudsen, M. F., Seidenkrantz, M.-S., Jacobsen, B. H., and Kuijpers, A., 2011, Tracking the Atlantic Multidecadal Oscillation through the last 8,000 years: Nature communications, v. 2, p. 178.

Koho, K., García, R., De Stigter, H., Epping, E., Koning, E., Kouwenhoven, T., and Van der Zwaan, G., 2008, Sedimentary labile organic carbon and pore water redox control on species distribution of benthic foraminifera: A case study from Lisbon–Setúbal Canyon (southern Portugal): Progress in Oceanography, v. 79, no. 1, p. 55-82.

Kotthoff, U., Pross, J., Müller, U. C., Peyron, O., Schmiedl, G., Schulz, H., and Bordon, A., 2008, Climate dynamics in the borderlands of the Aegean Sea during formation of sapropel S1 deduced from a marine pollen record: Quaternary Science Reviews, v. 27, no. 7, p. 832-845.

Kutterolf, S., Freundt, A., and Burkert, C., 2011, Eruptive history and magmatic evolution of the 1.9 kyr Plinian dacitic Chiltepe Tephra from Apoyeque volcano in west-central Nicaragua: Bulletin of volcanology, v. 73, no. 7, p. 811-831.

Kutterolf, S., Freundt, A., and Peréz, W., 2008, Pacific offshore record of plinian arc volcanism in Central America: 2. Tephra volumes and erupted masses: Geochemistry, Geophysics, Geosystems, v. 9, no. 2, p. n/a-n/a.

Kutterolf, S., Freundt, A., Perez, W., Wehrmann, H., and Schmincke, H.-U., 2007, Late Pleistocene to Holocene temporal succession and magnitudes of highly-explosive volcanic eruptions in west-central Nicaragua: Journal of Volcanology and Geothermal Research, v. 163, no. 1, p. 55-82.

Kutterolf, S., Schindlbeck, J., Anselmetti, F., Ariztegui, D., Brenner, M., Curtis, J., Schmid, D., Hodell, D., Mueller, A., and Pérez, L., 2016, A 400-ka tephrochronological framework for

Central America from Lake Petén Itzá (Guatemala) sediments: Quaternary Science Reviews, v. 150, p. 200-220.

Kuzucuoglu, C., Pastre, J.-F., Black, S., Ercan, T., Fontugne, M., Guillou, H., Hatté, C., Karabiyikoglu, M., Orth, P., and Türkecan, A., 1998, Identification and dating of tephra layers from Quaternary sedimentary sequences of Inner Anatolia, Turkey: Journal of Volcanology and Geothermal Research, v. 85, no. 1, p. 153-172.

Lahmeyer, J., 2006, Population statistics: Growth of the population per country in a historical perspective, including their administrative divisions and principal towns: Last updated, v. 30, no. 10, p. 2006.

Lajeunesse, P., 2012, Palaeoclimate: A history of outbursts: Nature Geoscience, v. 5, no. 12, p. 846.

Lamb, H. H., 2013, Climate: Present, Past and Future (Routledge Revivals): Volume 2: Climatic History and the Future, Routledge.

Le Maitre, R. W. B., Dudek, P., Keller, A., Lameyre, J., Le Bas, J., Sabine, M., Schmid, P., Sorensen, R., Streckeisen, H., and Woolley, A., 1989, A classification of igneous rocks and glossary of terms: Recommendations of the International Union of Geological Sciences, Subcommission on the Systematics of Igneous Rocks, International Union of Geological Sciences, v. 552.3 CLA.

Le Roy, M., Nicolussi, K., Deline, P., Astrade, L., Edouard, J.-L., Miramont, C., and Arnaud, F., 2015, Calendar-dated glacier variations in the western European Alps during the Neoglacial: the Mer de Glace record, Mont Blanc massif: Quaternary Science Reviews, v. 108, p. 1-22.

Lebreiro, S., Francés, G., Abrantes, F., Diz, P., Bartels-Jónsdóttir, H., Stroynowski, Z., Gil, I., Pena, L., Rodrigues, T., and Jones, P., 2006, Climate change and coastal hydrographic response along the Atlantic Iberian margin (Tagus Prodelta and Muros Ría) during the last two millennia: The Holocene, v. 16, no. 7, p. 1003-1015.

Linke, P., and Lutze, G., 1993, Microhabitat preferences of benthic foraminifera—a static concept or a dynamic adaptation to optimize food acquisition?: Marine micropaleontology, v. 20, no. 3-4, p. 215-234.

Lionello, P., Malanotte-Rizzoli, P., Boscolo, R., Alpert, P., Artale, V., Li, L., Luterbacher, J., May, W., Trigo, R., and Tsimplis, M., 2006, The Mediterranean climate: an overview of the main characteristics and issues, Elsevier.

Lipizer, M., Partescano, E., Rabitti, A., Giorgetti, A., and Crise, A., 2014, Qualified temperature, salinity and dissolved oxygen climatologies in a changing Adriatic Sea: Ocean Science, v. 10, no. 5, p. 771.

Lotze, H. K., Coll, M., and Dunne, J. A., 2011, Historical changes in marine resources, food-web structure and ecosystem functioning in the Adriatic Sea, Mediterranean: Ecosystems, v. 14, no. 2, p. 198-222.

Lowe, D. J., 2011, Tephrochronology and its application: a review: Quaternary Geochronology, v. 6, no. 2, p. 107-153.

Lowe, D. J., and Hunt, J. B., 2001, A summary of terminology used in tephra-related studies.

Lucchi, F., Keller, J., and Tranne, C., 2013, Regional stratigraphic correlations across the Aeolian archipelago (southern Italy): Geological Society, London, Memoirs, v. 37, no. 1, p. 55-81.

Lucchi, F., Tranne, C., De Astis, G., Keller, J., Losito, R., and Morche, W., 2008, Stratigraphy and significance of Brown Tuffs on the Aeolian Islands (southern Italy): Journal of Volcanology and Geothermal Research, v. 177, no. 1, p. 49-70.

Luterbacher, J., Dietrich, D., Xoplaki, E., Grosjean, M., and Wanner, H., 2004, European seasonal and annual temperature variability, trends, and extremes since 1500: Science, v. 303, no. 5663, p. 1499-1503.

Luterbacher, J., García-Herrera, R., Acker-On, S., Allen, R., Alvarez-Castro, M.-C., Benito, G., Booth, J., Buntgen, U., Cagatay, N., and Colombaroli, D., 2012, A review of 2000 years of paleoclimatic evidence in the Mediterranean.

Luterbacher, J., Rickli, R., Xoplaki, E., Tinguely, C., Beck, C., Pfister, C., and Wanner, H., 2001, The late Maunder minimum (1675–1715)–a key period forstudying decadal scale climatic change in Europe: Climatic Change, v. 49, no. 4, p. 441-462.

Luterbacher, J., Xoplaki, E., Casty, C., Wanner, H., Pauling, A., Küttel, M., Brönnimann, S., Fischer, E., Fleitmann, D., and Gonzalez-Rouco, F. J., 2006, Mediterranean climate variability over the last centuries: a review: Developments in Earth and environmental Sciences, v. 4, p. 27-148.

Lutze, G., and Thiel, H., 1989, Epibenthic foraminifera from elevated microhabitats; Cibicidoides wuellerstorfi and Planulina ariminensis: Journal of Foraminiferal Research, v. 19, no. 2, p. 153-158.

Mackensen, A., and Douglas, R. G., 1989, Down-core distribution of live and dead deep-water benthic foraminifera in box cores from the Weddell Sea and the California continental borderland: Deep Sea Research Part A. Oceanographic Research Papers, v. 36, no. 6, p. 879-900.

Mackensen, A., Hubberten, H. W., Bickert, T., Fischer, G., and Fütterer, D., 1993, The δ13C in benthic foraminiferal tests of Fontbotia wuellerstorfi (Schwager) relative to the δ13C of dissolved inorganic carbon in southern ocean deep water: implications for glacial ocean circulation models: Paleoceanography, v. 8, no. 5, p. 587-610.

Magny, M., De Beaulieu, J.-L., Drescher-Schneider, R., Vannière, B., Walter-Simonnet, A.-V., Miras, Y., Millet, L., Bossuet, G., Peyron, O., and Brugiapaglia, E., 2007, Holocene climate changes in the central Mediterranean as recorded by lake-level fluctuations at Lake Accesa (Tuscany, Italy): Quaternary Science Reviews, v. 26, no. 13, p. 1736-1758.

Malanotterizzoli, P., and Hecht, A., 1988, Large-scale properties of the eastern mediterranean-A review: Oceanologica Acta, v. 11, no. 4, p. 323-335.

Mann, M. E., Zhang, Z., Rutherford, S., Bradley, R. S., Hughes, M. K., Shindell, D., Ammann, C., Faluvegi, G., and Ni, F., 2009, Global signatures and dynamical origins of the Little Ice Age and Medieval Climate Anomaly: Science, v. 326, no. 5957, p. 1256-1260.

Marchetti, M., 2002, Environmental changes in the central Po Plain (northern Italy) due to fluvial modifications and anthropogenic activities: Geomorphology, v. 44, no. 3, p. 361-373.

Marchetti, R., Provini, A., and Crosa, G., 1989, Nutrient load carried by the River Po into the Adriatic Sea, 1968–1987: Marine Pollution Bulletin, v. 20, no. 4, p. 168-172.

Margari, V., Pyle, D., Bryant, C., and Gibbard, P., 2007, Mediterranean tephra stratigraphy revisited: results from a long terrestrial sequence on Lesvos Island, Greece: Journal of Volcanology and Geothermal Research, v. 163, no. 1, p. 34-54.

Marullo, S., Artale, V., and Santoleri, R., 2011, The SST multidecadal variability in the Atlantic–Mediterranean region and its relation to AMO: Journal of Climate, v. 24, no. 16, p. 4385-4401.

Matsuoka, N., 2008, Frost weathering and rockwall erosion in the southeastern Swiss Alps: Long-term (1994–2006) observations: Geomorphology, v. 99, no. 1, p. 353-368.

May, P. W., 1982, Climatological Flux Estimates in the Mediterranean Sea. Part I. Winds and Wind Stresses: Naval ocean research and development activity Stennis space center MS.

McCorkle, D. C., Bernhard, J. M., Hintz, C. J., Blanks, J. K., Chandler, G. T., and Shaw, T. J., 2008, The carbon and oxygen stable isotopic composition of cultured benthic foraminifera: Geological Society, London, Special Publications, v. 303, no. 1, p. 135-154.

McCorkle, D. C., Keigwin, L. D., Corliss, B. H., and Emerson, S. R., 1990, The influence of microhabitats on the carbon isotopic composition of deep-sea benthic foraminifera: Paleoceanography, v. 5, no. 2, p. 161-185.

McEvedy, C., and Jones, R., 1978, Atlas of world population history, Penguin Books Ltd, Harmondsworth, Middlesex, England.

Melki, T., 2011, Variation of deepwater convection in the western Mediterranean Sea (Gulf of Lion) during the last 28 ka: Quaternary international, v. 241, no. 1, p. 160-168.

Menke V., Ehrmann W., Milker Y.,2017 b Brzelinski S., Möbius J., Mikolajewicz U., Zolitschka B., Zonneveld K., Emeis K.C. and Schmiedl S., Combined North Atlantic and

anthropogenic forcing of changes in the marine environments in the Gulf of Taranto (Italy) during the last millennium: Under review in Climate of the Past.

Menke V., Kutterolf S., Sievers C., Schindlbeck J. and Schmiedl G., 2017 a, Cryptotephra from Lipari Volcano in the eastern Gulf of Taranto (Italy) – A ^{14}C- independent time marker for paleoclimatic studies: Under review in Quaternary Research

Mercone, D., Thomson, J., Croudace, I., Siani, G., Paterne, M., and Troelstra, S., 2000, Duration of S1, the most recent sapropel in the eastern Mediterranean Sea, as indicated by accelerator mass spectrometry radiocarbon and geochemical evidence: Paleoceanography, v. 15, no. 3, p. 336-347.

Meyers, P. A., 1994, Preservation of elemental and isotopic source identification of sedimentary organic matter: Chemical Geology, v. 114, no. 3-4, p. 289-302.

Milker, Y., and Schmiedl, G., 2012, A taxonomic guide to modern benthic shelf foraminifera of the western Mediterranean Sea: Palaeontologia electronica, v. 15, no. 2, p. 1-134.

Milligan, T. G., and Cattaneo, A., 2007, Sediment dynamics in the western Adriatic Sea: From transport to stratigraphy: Continental Shelf Research, v. 27, no. 3, p. 287-295.

Millot, C., and Taupier-Letage, I., 2005, Circulation in the Mediterranean sea: The Mediterranean Sea, p. 323-334.

Montone, P., Mariucci, M. T., Pondrelli, S., and Amato, A., 2004, An improved stress map for Italy and surrounding regions (central Mediterranean): Journal of Geophysical Research: Solid Earth, v. 109, no. B10.

Mozetič, P., Solidoro, C., Cossarini, G., Socal, G., Precali, R., Francé, J., Bianchi, F., De Vittor, C., Smodlaka, N., and Umani, S. F., 2010, Recent trends towards oligotrophication of the northern Adriatic: evidence from chlorophyll a time series: Estuaries and Coasts, v. 33, no. 2, p. 362-375.

Murray, J. W., 2003, An illustrated guide to the benthic foraminifera of the Hebridean shelf, west of Scotland, with notes on their mode of life: Palaeontologia Electronica, v. 5, no. 1, p. 31.

Murray, J.W., 2006, Ecology and applications of benthic foraminifera, Cambridge University Press.

Myers, P. G., and Rohling, E. J., 2000, Modeling a 200-yr interruption of the Holocene sapropel S 1: Quaternary Research, v. 53, no. 1, p. 98-104.

Neugebauer, I., Wulf, S., Schwab, M. J., Serb, J., Plessen, B., Appelt, O., and Brauer, A., 2017, Implications of S1 tephra findings in Dead Sea and Tayma palaeolake sediments for marine reservoir age estimation and palaeoclimate synchronisation: Quaternary Science Reviews, v. 170, p. 269-275.

Newhall, C. G., and Self, S., 1982, The volcanic explosivity index (VEI) an estimate of explosive magnitude for historical volcanism: Journal of Geophysical Research: Oceans, v. 87, no. C2, p. 1231-1238.

Ohga, T., and Kitazato, H., 1997, Seasonal changes in bathyal foraminiferal populations in response to the flux of organic matter (Sagami Bay, Japan): Terra Nova, v. 9, no. 1, p. 33-37.

Orlić, M., Kuzmić, M., and Pasarić, Z., 1994, Response of the Adriatic Sea to the bora and sirocco forcing: Continental Shelf Research, v. 14, no. 1, p. 91-116.

Paillard, D. L., L.; Yiou, P. , 1996, A Macintosh program performs time series analysis: Eos Trans. American Geophysical Union, v. 77, no. 3924, p. 379.

Paterne, M., Guichard, F., and Labeyrie, J., 1988, Explosive activity of the South Italian volcanoes during the past 80,000 years as determined by marine tephrochronology: Journal of Volcanology and Geothermal Research, v. 34, no. 3, p. 153-172.

Paterne, M., Guichard, F., Labeyrie, J., Gillot, P., and Duplessy, J.-C., 1986, Tyrrhenian Sea tephrochronology of the oxygen isotope record for the past 60,000 years: Marine Geology, v. 72, no. 3-4, p. 259-285.

Paterne, M., Labeyrie, J., Guichard, F., Mazaud, A., and Maitre, F., 1990, Fluctuations of the Campanian explosive volcanic activity (South Italy) during the past 190,000 years, as determined by marine tephrochronology: Earth and Planetary Science Letters, v. 98, no. 2, p. 166-174.

Pachauri, R. K., Meyer, L., Plattner, G.-K., and Stocker, T., 2015, IPCC, 2014: Climate change 2014: Synthesis report. Contribution of working groups I, II and III to the fifth assessment report of the intergovernmental panel on climate change, IPCC.

Peizhen, Z., Molnar, P., and Downs, W. R., 2001, Increased sedimentation rates and grain sizes 2-4 Myr ago due to the influence of climate change on erosion rates: Nature, v. 410, no. 6831, p. 891.

Petschick, R., Kuhn, G., and Gingele, F., 1996, Clay mineral distribution in surface sediments of the South Atlantic: sources, transport, and relation to oceanography: Marine Geology, v. 130, no. 3-4, p. 203-229.

Pinardi, N., Lyubartsev, V., Cardellicchio, N., Caporale, C., Ciliberti, S., Coppini, G., De Pascalis, F., Dialti, L., Federico, I., and Filippone, M., 2016, Marine Rapid Environmental Assessment in the Gulf of Taranto: a multiscale approach: Natural Hazards and Earth System Sciences, v. 16, no. 12, p. 2623.

Piochi, M., De Vivo, B., and Ayuso, R., 2006, The magma feeding system of Somma-Vesuvius (Italy) strato-volcano: new inferences from a review of geochemical and Sr, Nd, Pb and O isotope data: Developments in Volcanology, v. 9, p. 181-202.

Pongratz, J., Reick, C., Raddatz, T., and Claussen, M., 2008, A reconstruction of global agricultural areas and land cover for the last millennium: Global Biogeochemical Cycles, v. 22, no. 3.

Poulain, P.-M., 2001, Adriatic Sea surface circulation as derived from drifter data between 1990 and 1999: Journal of Marine Systems, v. 29, no. 1, p. 3-32.

Pross, J., Kotthoff, U., Müller, U., Peyron, O., Dormoy, I., Schmiedl, G., Kalaitzidis, S., and Smith, A., 2009, Massive perturbation in terrestrial ecosystems of the Eastern Mediterranean region associated with the 8.2 kyr BP climatic event: Geology, v. 37, no. 10, p. 887-890.

Psarra, S., Tselepides, A., and Ignatiades, L., 2000, Primary productivity in the oligotrophic Cretan Sea (NE Mediterranean): seasonal and interannual variability: Progress in Oceanography, v. 46, no. 2, p. 187-204.

Puškarić, S., Berger, G. W., and Jorissen, F. J., 1990, Successive appearance of subfossil phytoplankton species in Holocene sediments of the northern Adriatic and its relation to the increased eutrophication pressure: Estuarine, Coastal and Shelf Science, v. 31, no. 2, p. 177-187.

Pyne-O'Donnell, S., Cwynar, L., Vincent, J., Spear, R., and Froese, D., 2014, The Glacier Peak Tephra: A Continental-Scale Latest Pleistocene Time Horizon, in Proceedings AGU Fall Meeting Abstracts2014.

Rachev, N., and Purini, R., 2001, The Adriatic response to the bora forcing: A numerical study: Il Nuovo cimento della Società italiana di fisica. C. Geophysics and space physics, v. 24, no. 2, p. 303-311.

Rasmussen, T. L., 2005, Systematic paleontology and ecology of benthic foraminifera from the Plio-Pleistocene Kallithea Bay section, Rhodes, Greece: Cushman Foundation Special Publication, v. 39, p. 53-157.

Rasmussen, T. L., and Thomsen, E., 2005, Foraminifera and paleoenvironment of the Plio-Pleistocene Kallithea Bay section, Rhodes, Greece: Evidence for cyclic sedimentation and shallow-water sapropels: Cushman Foundation for Foraminiferal Research, Special Publication, v. 39, p. 15-51.

Reimer, P. J., 2004, IntCal04 terrestrial radiocarbon age calibration, 0-26 cal kyr BP: Radiocarbon, v. 46, p. 1029-1058.

Reimer, P. J., Bard, E., Bayliss, A., Beck, J. W., Blackwell, P. G., Ramsey, C. B., Buck, C. E., Cheng, H., Edwards, R. L., Friedrich, M., Grootes, P. M., Guilderson, T. P., Haflidason, H., Hajdas, I., Hatte, C., Heaton, T. J., Hoffmann, D. L., Hogg, A. G., Hughen, K. A., Kaiser, K. F., Kromer, B., Manning, S. W., Niu, M., Reimer, R. W., Richards, D. A., Scott, E. M., Southon, J. R., Staff, R. A., Turney, C. S. M., and van der Plicht, J., 2013, Intcal13

and Marine13 Radiocarbon Age Calibration Curves 0-50,000 Years Cal Bp: Radiocarbon, v. 55, no. 4, p. 1869-1887.

Renssen, H., Goosse, H., and Fichefet, T., 2002, Modeling the effect of freshwater pulses on the early Holocene climate: The influence of high-frequency climate variability: Paleoceanography, v. 17, no. 2.

Richter, T. O., Van der Gaast, S., Koster, B., Vaars, A., Gieles, R., de Stigter, H. C., De Haas, H., and van Weering, T. C., 2006, The Avaatech XRF Core Scanner: technical description and applications to NE Atlantic sediments: Geological Society, London, Special Publications, v. 267, no. 1, p. 39-50.

Rodolfi, G., 1988, Geomorphological mapping applied to land evaluation and soil conservation in agricultural planning: some examples from Tuscany (Italy).

Rögl, F., 1999, Mediterranean and Paratethys. Facts and hypotheses of an Oligocene to Miocene paleogeography (short overview): Geologica Carpathica, v. 50, no. 4, p. 339.

Rohling, E., and Hilgen, F., 2007, The eastern Mediterranean climate at times of sapropel formation: a review: Netherlands Journal of Geosciences/Geologie en Mijnbouw, no. Classic Papers.

Robinson, A. R., Leslie, W. G., Theocharis, A., and Lascaratos, A., 2001, Mediterranean sea circulation: Ocean currents: a derivative of the Encyclopedia of Ocean Sciences, p. 1689-1705

Rohling, E., Jorissen, F., and De Stigter, H., 1997, 200 year interruption of Holocene sapropel formation in the Adriatic Sea: Journal of Micropalaeontology, v. 16, no. 2, p. 97-108.

Rohling, E., Marino, G., and Grant, K., 2015, Mediterranean climate and oceanography, and the periodic development of anoxic events (sapropels): Earth-Science Reviews, v. 143, p. 62-97.

Rohling, E. J., Casford, J., Abu-Zied, R., Cooke, S., Mercone, D., Thomson, J., Croudace, I., Jorissen, F. J., Brinkhuis, H., and Kallmeyer, J., 2002, Rapid Holocene climate changes in the eastern Mediterranean, Droughts, food and culture, Springer, p. 35-46.

Rohling, E. J., and Pälike, H., 2005, Centennial-scale climate cooling with a sudden cold event around 8,200 years ago: Nature, v. 434, no. 7036, p. 975.

Rolph, T. C., Vigliotti, L., and Oldfield, F., 2004, Mineral magnetism and geomagnetic secular variation of marine and lacustrine sediments from central Italy: timing and nature of local and regional Holocene environmental change: Quaternary Science Reviews, v. 23, no. 14, p. 1699-1722.

Rossignol-Strick, M., 1983, African monsoons, an immediate climate response to orbital insolation: Nature, v. 304, no. 5921, p. 46-49.

Rossi, S., Auroux, C., and Mascle, J., 1983, The Gulf of Taranto (Southern Italy): seismic stratigraphy and shallow structure: Marine Geology, v. 51, no. 3-4, p. 327-346.

Rothwell, R. G., and Rack, F. R., 2006, New techniques in sediment core analysis: an introduction: Geological Society, London, Special Publications, v. 267, no. 1, p. 1-29.

Sangiorgi, F., and Donders, T. H., 2004, Reconstructing 150 years of eutrophication in the north-western Adriatic Sea (Italy) using dinoflagellate cysts, pollen and spores: Estuarine, Coastal and Shelf Science, v. 60, no. 1, p. 69-79.

Savini, A., and Corselli, C., 2010, High-resolution bathymetry and acoustic geophysical data from Santa Maria di Leuca Cold Water Coral province (Northern Ionian Sea—Apulian continental slope): Deep Sea Research Part II: Topical Studies in Oceanography, v. 57, no. 5, p. 326-344

Schacht, U., 2005, Alteration of volcanic glasses in marine sediments: laboratory experiments and field studies: Christian-Albrechts Universität Kiel.

Schindlbeck, J. C., Kutterolf, S., Freundt, A., Alvarado, G., Wang, K. L., Straub, S., Hemming, S., Frische, M., and Woodhead, J., 2016, Late Cenozoic tephrostratigraphy offshore the southern Central American Volcanic Arc: 1. Tephra ages and provenance: Geochemistry, Geophysics, Geosystems.

Schmiedl, G., De Bovée, F., Buscail, R., Charriere, B., Hemleben, C., Medernach, L., and Picon, P., 2000, Trophic control of benthic foraminiferal abundance and microhabitat in the bathyal Gulf of Lions, western Mediterranean Sea: Marine Micropaleontology, v. 40, no. 3, p. 167-188.

Schmiedl, G., Kuhnt, T., Ehrmann, W., Emeis, K. C., Hamann, Y., Kotthoff, U., Dulski, P., and Pross, J., 2010, Climatic forcing of eastern Mediterranean deep-water formation and benthic ecosystems during the past 22 000 years: Quaternary Science Reviews, v. 29, no. 23-24, p. 3006-3020.

Schmiedl, G., Pfeilsticker, M., Hemleben, C., and Mackensen, A., 2004, Environmental and biological effects on the stable isotope composition of recent deep-sea benthic foraminifera from the western Mediterranean Sea: Marine Micropaleontology, v. 51, no. 1, p. 129-152.

Schmincke, H.-U., and Sumita, M., 2013, Fire in the sea—Growth and destruction of submarine volcanoes: Geology, v. 41, no. 3, p. 381-382.

Schlitzer, R., Ocean Data View, odv.awi.de, 2017

Schulz, M., and Paul, A., 2002, Holocene climate variability on centennial-to-millennial time scales: 1. Climate records from the North-Atlantic realm, Climate development and history of the North Atlantic realm, Springer, p. 41-54.

Sellschopp, J., and Álvarez, A., 2003, Dense low-salinity outflow from the Adriatic Sea under mild (2001) and strong (1999) winter conditions: Journal of Geophysical Research: Oceans, v. 108, no. C9.

Sgarella, F., and Moncharmont Zei, M., 1993, Benthic foraminifera of the Gulf of Naples (Italy): systematics and autoecology: Bollettino della Società Paleontologica Italiana, v. 32, no. 2, p. 145-264.

Shackleton, N., 1987, Oxygen isotopes, ice volume and sea level: Quaternary Science Reviews, v. 6, no. 3, p. 183-190.

Siani, G., Sulpizio, R., Paterne, M., and Sbrana, A., 2004, Tephrostratigraphy study for the last 18,000 14 C years in a deep-sea sediment sequence for the South Adriatic: Quaternary Science Reviews, v. 23, no. 23, p. 2485-2500.

Simeoni, U., and Corbau, C., 2009, A review of the Delta Po evolution (Italy) related to climatic changes and human impacts: Geomorphology, v. 107, no. 1, p. 64-71.

Sivall, T., 1957, Sirocco in the Levant: Geografiska Annaler, v. 39, no. 2/3, p. 114-142.

Soon, W., Herrera, V. M. V., Selvaraj, K., Traversi, R., Usoskin, I., Chen, C.-T. A., Lou, J.-Y., Kao, S.-J., Carter, R. M., and Pipin, V., 2014, A review of Holocene solar-linked climatic variation on centennial to millennial timescales: Physical processes, interpretative frameworks and a new multiple cross-wavelet transform algorithm: Earth-Science Reviews, v. 134, p. 1-15.

Spurk, M., Leuschner, H. H., Baillie, M. G., Briffa, K. R., and Friedrich, M., 2002, Depositional frequency of German subfossil oaks: climatically and non-climatically induced fluctuations in the Holocene: The Holocene, v. 12, no. 6, p. 707-715.

Staubwasser, M., Sirocko, F., Grootes, P. M., and Segl, M., 2003, Climate change at the 4.2 ka BP termination of the Indus valley civilization and Holocene south Asian monsoon variability: Geophysical Research Letters, v. 30, no. 8.

Staubwasser, M., and Weiss, H., 2006, Holocene climate and cultural evolution in late prehistoric–early historic West Asia: Quaternary Research, v. 66, no. 3, p. 372-387.

Stefani, M., and Vincenzi, S., 2005, The interplay of eustasy, climate and human activity in the late Quaternary depositional evolution and sedimentary architecture of the Po Delta system: Marine Geology, v. 222, p. 19-48.

Stenseth, N. C., Ottersen, G., Hurrell, J. W., Mysterud, A., Lima, M., Chan, K. S., Yoccoz, N. G., and Ådlandsvik, B., 2003, Studying climate effects on ecology through the use of climate indices: the North Atlantic Oscillation, El Nino Southern Oscillation and beyond: Proceedings of the Royal Society of London B: Biological Sciences, v. 270, no. 1529, p. 2087-2096.

Stuiver, M., 1994, Atmospheric 14C as a proxy of solar and climatic change, The solar engine and its influence on terrestrial atmosphere and climate, Springer, p. 203-220.

Sutton, R. T., and Hodson, D. L., 2005, Atlantic Ocean forcing of North American and European summer climate: science, v. 309, no. 5731, p. 115-118.

Swezey, C., Lancaster, N., Kocurek, G., Deynoux, M., Blum, M., Price, D., and Pion, J.-C., 1999, Response of aeolian systems to Holocene climatic and hydrologic changes on the northern margin of the Sahara: a high-resolution record from the Chott Rharsa basin, Tunisia: The Holocene, v. 9, no. 2, p. 141-147.

Tanhua, T., Hainbucher, D., Schroeder, K., Cardin, V., Álvarez, M., and Civitarese, G., 2013, The Mediterranean Sea system: a review and an introduction to the special issue: Ocean Science, v. 9, no. 5, p. 789.

Taricco, C., Alessio, S., and Vivaldo, G., 2008, Sequence of eruptive events in the Vesuvio area recorded in shallow-water Ionian Sea sediments: Nonlinear Processes in Geophysics, v. 15, no. 1, p. 25-32.

Taricco, C., Ghil, M., Alessio, S., and Vivaldo, G., 2009, Two millennia of climate variability in the Central Mediterranean: Climate of the Past, v. 5, no. 5, p. 171-181.

Taricco, C., Vivaldo, G., Alessio, S., Rubinetti, S., and Mancuso, S., 2015, A high-resolution δ18O record and Mediterranean climate variability: Climate of the Past, v. 11, no. 3, p. 509-522.

Terranova, O., Antronico, L., Coscarelli, R., and Iaquinta, P., 2009, Soil erosion risk scenarios in the Mediterranean environment using RUSLE and GIS: an application model for Calabria (southern Italy): Geomorphology, v. 112, no. 3, p. 228-245.

Theodor, M., Schmiedl, G., Jorissen, F., and Mackensen, A., 2016a, Stable carbon isotope gradients in benthic foraminifera as proxy for organic carbon fluxes in the Mediterranean Sea: Biogeosciences, v. 13, no. 23, p. 6385.

Theodor, M., Schmiedl, G., and Mackensen, A., 2016b, Stable isotope composition of deep-sea benthic foraminifera under contrasting trophic conditions in the western Mediterranean Sea: Marine Micropaleontology, v. 124, p. 16-28.

Thornton, S., and McManus, J., 1994, Application of organic carbon and nitrogen stable isotope and C/N ratios as source indicators of organic matter provenance in estuarine systems: evidence from the Tay Estuary, Scotland: Estuarine, Coastal and Shelf Science, v. 38, no. 3, p. 219-233.

Tierney, J. E., Lewis, S. C., Cook, B. I., LeGrande, A. N., and Schmidt, G. A., 2011, Model, proxy and isotopic perspectives on the East African Humid Period: Earth and Planetary Science Letters, v. 307, no. 1, p. 103-112.

Tomadin, L., 1979, Clay mineralogy of recent sediments around the Po River delta: G. Geol, v. 43, p. 249-275.

Tomadin, L., 2000, Sedimentary fluxes and different dispersion mechanisms of the clay sediments in the Adriatic Basin: Rendiconti Lincei, v. 11, no. 3, p. 161-174.

Tomasino, M., and Valle, F. D., 2000, Natural climatic changes and solar cycles: an analysis of hydrological time series: Hydrological sciences journal, v. 45, no. 3, p. 477-489.

Tomlinson, E. L., McMillan, P. F., Zhang, M., Jones, A. P., and Redfern, S. A., 2007, Quartz-bearing C–O–H fluid inclusions diamond: Retracing the pressure–temperature path in the mantle using calibrated high temperature IR spectroscopy: Geochimica et Cosmochimica Acta, v. 71, no. 24, p. 6030-6039.

Tomlinson, E. L., Smith, V. C., Albert, P. G., Aydar, E., Civetta, L., Cioni, R., Çubukçu, E., Gertisser, R., Isaia, R., and Menzies, M. A., 2015, The major and trace element glass compositions of the productive Mediterranean volcanic sources: tools for correlating distal tephra layers in and around Europe: Quaternary Science Reviews, v. 118, p. 48-66.

Trincardi, F., Correggiari, A., and Roveri, M., 1994, Late Quaternary transgressive erosion and deposition in a modern epicontinental shelf: the Adriatic semienclosed basin: Geo-marine letters, v. 14, no. 1, p. 41-51.

Trouet, V., Esper, J., Graham, N. E., Baker, A., Scourse, J. D., and Frank, D. C., 2009, Persistent positive North Atlantic Oscillation mode dominated the medieval climate anomaly: science, v. 324, no. 5923, p. 78-80.

Tsimplis, M. N., and Bryden, H. L., 2000, Estimation of the transports through the Strait of Gibraltar: Deep Sea Research Part I: Oceanographic Research Papers, v. 47, no. 12, p. 2219-2242.

Tsimplis, M. N., Zervakis, V., Josey, S. A., Peneva, E. L., Struglia, M. V., Stanev, E. V., Theocharis, A., Lionello, P., Malanotte-Rizzoli, P., and Artale, V., 2006, Changes in the oceanography of the Mediterranean Sea and their link to climate variability: Developments in Earth and Environmental Sciences, v. 4, p. 227-282.

Turchetto, M., Boldrin, A., Langone, L., Miserocchi, S., Tesi, T., and Foglini, F., 2007, Particle transport in the Bari canyon (southern Adriatic Sea): Marine Geology, v. 246, no. 2, p. 231-247.

Turney, C. S., and Brown, H., 2007, Catastrophic early Holocene sea level rise, human migration and the Neolithic transition in Europe: Quaternary Science Reviews, v. 26, no. 17, p. 2036-2041.

Turney, C. S., Lowe, J. J., Davies, S. M., Hall, V., Lowe, D. J., Wastegård, S., Hoek, W. Z., and Alloway, B., 2004, Tephrochronology of Last Termination sequences in Europe: a protocol for improved analytical precision and robust correlation procedures (a joint SCOTAV–INTIMATE proposal): Journal of Quaternary Science, v. 19, no. 2, p. 111-120.

Van der Knijff, J., Jones, R., and Montanarella, L., 2000, Soil erosion risk assessment in Europe, European Soil Bureau, European Commission Belgium.

Van der Plas, L., and Tobi, A., 1965, A chart for judging the reliability of point counting results: American Journal of Science, v. 263, no. 1, p. 87-90.

Venkatarathnam, K., and Ryan, W. B., 1971, Dispersal patterns of clay minerals in the sediments of the eastern Mediterranean Sea: Marine Geology, v. 11, no. 4, p. 261-282.

Versteegh, G., De Leeuw, J., Taricco, C., and Romero, A., 2007, Temperature and productivity influences on U37K′ and their possible relation to solar forcing of the Mediterranean winter: Geochemistry, Geophysics, Geosystems, v. 8, no. 9.

Vinci, A., 1985, Distribution and chemical composition of tephra layers from Eastern Mediterranean abyssal sediments: Marine Geology, v. 64, no. 1-2, p. 143-155.

Vivaldo, G., Taricco, C., Alessio, S., and Ghil, M., 2009, Accurate dating of Gallipoli Terrace (Ionian Sea) sediments: Historical eruptions and climate records: PAGES-Past Global Changes, v. 17, no. 1, p. 8-9.

Vogel, H., Zanchetta, G., Sulpizio, R., Wagner, B., and Nowaczyk, N., 2010, A tephrostratigraphic record for the last glacial–interglacial cycle from Lake Ohrid, Albania and Macedonia: Journal of Quaternary Science, v. 25, no. 3, p. 320-338.

Wanner, H., Beer, J., Bütikofer, J., Crowley, T. J., Cubasch, U., Flückiger, J., Goosse, H., Grosjean, M., Joos, F., and Kaplan, J. O., 2008, Mid-to Late Holocene climate change: an overview: Quaternary Science Reviews, v. 27, no. 19, p. 1791-1828.

Weiss, H., and Bradley, R. S., 2001, What drives societal collapse?: Science, v. 291, no. 5504, p. 609-610.

Weiss, H., Courty, M.-A., Wetterstrom, W., Guichard, F., Senior, L., Meadow, R., and Curnow, A., 1993, The genesis and collapse of third millennium north Mesopotamian civilization: Science-New York then Washington, v. 261, p. 995-995.

Weldeab, S., Menke, V., and Schmiedl, G., 2014, The pace of East African monsoon evolution during the Holocene: Geophysical Research Letters, v. 41, no. 5, p. 1724-1732.

Weninger, B., Alram-Stern, E., Bauer, E., Clare, L., Danzeglocke, U., Jöris, O., Kubatzki, C., Rollefson, G., Todorova, H., and van Andel, T., 2006, Climate forcing due to the 8200 cal yr BP event observed at Early Neolithic sites in the eastern Mediterranean: Quaternary Research, v. 66, no. 3, p. 401-420.

Wohlfarth, B., Blaauw, M., Davies, S., Andersson, M., Wastegård, S., Hormes, A., and Possnert, G., 2006, Constraining the age of Lateglacial and early Holocene pollen zones and tephra horizons in southern Sweden with Bayesian probability methods: Journal of Quaternary Science, v. 21, no. 4, p. 321-334.

Wortel, M., and Spakman, W., 2000, Subduction and slab detachment in the Mediterranean-Carpathian region: Science, v. 290, no. 5498, p. 1910-1917.

Wulf, S., Kraml, M., Brauer, A., Keller, J., and Negendank, J. F., 2004, Tephrochronology of the 100ka lacustrine sediment record of Lago Grande di Monticchio (southern Italy): Quaternary International, v. 122, no. 1, p. 7-30.

Wulf, S., Kraml, M., and Keller, J., 2008, Towards a detailed distal tephrostratigraphy in the Central Mediterranean: the last 20,000 yrs record of Lago Grande di Monticchio: Journal of Volcanology and Geothermal Research, v. 177, no. 1, p. 118-132.

Wulf, S., Kraml, M., Kuhn, T., Schwarz, M., Inthorn, M., Keller, J., Kuscu, I., and Halbach, P., 2002, Marine tephra from the Cape Riva eruption (22 ka) of Santorini in the Sea of Marmara: Marine Geology, v. 183, no. 1, p. 131-141.

Wüst, G., 1960, Die Tiefenzirkulation des Mittelländischen Meeres in den Kernschichten des Zwischen- und des Tiefenwassers: Deutsche Hydrografische Zeitschrift, v. 13, no. 3, p. 105-131.

Wüst, G.,1961, On the vertical circulation of the Mediterranean Sea: Journal of Geophysical Research, v. 66, no. 10, p. 3261-3271.

Xoplaki, E., Luterbacher, J., and Gonzales-Roucho, J., 2006, Mediterranean summer temperature and winter precipitation, large-scale dynamics, trends: Nuovo Cimento della Societa Italiana di Fisica. C, Geophysics and Space Physics, v. 29, no. 1, p. 45-54.

Zahn, R., Winn, K., and Sarnthein, M., 1986, Benthic foraminiferal δ13C and accumulation rates of organic carbon: Uvigerina peregrina group and Cibicidoides wuellerstorfi: Paleoceanography, v. 1, no. 1, p. 27-42.

Zanchetta, G., Regattieri, E., Isola, I., Drysdale, R., Bini, M., Baneschi, I., and Hellstrom, J., 2016, The so-called “4.2 event” in the central Mediterranean and its climatic teleconnections: Alpine and Mediterranean Quaternary, v. 29, no. 1, p. 5-17.

Zanchetta, G., Sulpizio, R., Roberts, N., Cioni, R., Eastwood, W. J., Siani, G., Caron, B., Paterne, M., and Santacroce, R., 2011, Tephrostratigraphy, chronology and climatic events of the Mediterranean basin during the Holocene: an overview: The Holocene, v. 21, no. 1, p. 33-52.

Zonneveld, K., 2008, Report and preliminary results of R/V POSEIDON Cruise P339 [POS339], Piräus-Messina, 16 June-2 July 2006. CAPPUCCINO-Calabrian and Adriatic palaeoproductivity and climatic variability in the last two millenia.

Zonneveld, K. A., Chen, L., Elshanawany, R., Fischer, H. W., Hoins, M., Ibrahim, M. I., Pittauerova, D., and Versteegh, G. J., 2012, The use of dinoflagellate cysts to separate human-induced from natural variability in the trophic state of the Po River discharge plume over the last two centuries: Marine pollution bulletin, v. 64, no. 1, p. 114-132.

Zonneveld, K. A., Chen, L., Möbius, J., and Mahmoud, M. S., 2009, Environmental significance of dinoflagellate cysts from the proximal part of the Po-river discharge plume (off southern Italy, Eastern Mediterranean): Journal of Sea Research, v. 62, no. 4, p. 189-213.

Zonneveld, K. A., and Siccha, M., 2016, Dinoflagellate cyst based modern analogue technique at test—A 300year record from the Gulf of Taranto (Eastern Mediterranean): Palaeogeography, Palaeoclimatology, Palaeoecology, v. 450, p. 17-37.

Internet references:

https://www.diercke.de/content/ (last accessed 28.10.2017)
https://oceancolor.gsfc.nasa.gov/SeaWiFS (last accessed 28.10.2017)
https://www.coastcolour.org/products.html (last accessed 28.10.2017)
https://www.gebco.net (last accessed 26.5.2017)
https://www.ngdc.noaa.gov/stp/solar/ssndata.html (last accessed 28.10.2017)
http://www.esrl.noaa.gov/psd/gcos_wgsp/Timeseries/NAO/ (last accessed 4.10.2017)
http://calib.org/marine/ (last accessed 28.10.2017)

Appendix

Appendix I

Table A.1. Grouping of benthic foraminifera according to their environmental preferences after Gupta (2002), Jorissen et al. (1995), Jorissen et al. (2007), Murray (2006) and references therein. All foraminifera species that were grouped are also marked in Appendix Table A.2.4., A.2.5, A.2.6 and A.2.9.

Epifaunal Benthic Foraminifera (EBF)	Shallow to Intermediate Infaunal Benthic Foraminifera (SIIBF)	Deep Infaunal Benthic Foraminifera (DIBF)
Adelosina spp. *Affinterina spp.* *Articulina mucronata* *Biloculina spp.* *Cibicides spp.* *Cornuspira spp.* *Cycloforina spp.* *Eponides spp.* *Miliolinella spp.* *Lachlanella spp.* *Nummoloculina sp1.* *Nubecularia spp.* *Peneroplis pertusus* *Plandiscorbis rarescens* *Planorbulina mediterranensis* *Planulina ariminensis* *Planorbulina sp.* *Pseudotriloculina sp1.* *Pyrgo spp.* *Quinqueloculina spp.* *Sigmoilina spp.* *Siphonaperta spp.* *Spiroloculina spp.* *Spirophtalmidium spp.* *Triloculina spp.* *Trisegmentina compressa*	*Brizalina spp.* *Bolivina spp.* *Bulimina spp.* *Cassidulina spp.* *Globocassidulina subglobosa* *Melonis spp.* *Pullenia spp.* *Rectuvigerina spp.* *Uvigerina spp.*	*Chilostomella oolina* *Fursenkoina spp.* *Globobulimina spp.* *Stainforthia spp.*

Appendix II

Appendix II is available on the attached CD and consists of:

Appendix Table A.2.1. Major element data of all single glass shard measurements of GeoB15403-4 normalized to 100wt% water free. Additionally the respective analytical total per measurement is given. If possible, averages are given per sample and glass shard species with respective intra sample variation describing the range of single measurements. Sample marked with a grey field and bold letters represents the sample with the highest amount of cryptotephra.

Appendix Table A.2.2. EMP monitor measurements of samples from GeoB15403-4.

Appendix Table A.2.3. Averaged major element data as well as point counting results of analysed samples of core GeoB15403-4; std describes the range of single measurements.

Appendix Table A.2.4. Counted numbers of benthic foraminifera of gravity core GeoB15403-4. Colors display species that were grouped according to their microhabitat preferences with green marking Epifaunal Benthic Foraminifera (EBF), orange marking Shallow to Intermediate Infaunal Benthic Foraminifera (SIIBF) and blue marking Deep Infaunal Benthic Foraminifera (DIBF).

Appendix Table A.2.5. Counted numbers of benthic foraminifera of multi core GeoB15406-4. Colours display species that were grouped according to their microhabitat preferences with green marking Epifaunal Benthic Foraminifera (EBF), orange marking Shallow to Intermediate Infaunal Benthic Foraminifera (SIIBF) and blue marking Deep Infaunal Benthic Foraminifera (DIBF).

Appendix Table A.2.6. Results of stable isotope measurements on tests of benthic foraminifera of multi core GeoB15406-4.

Appendix Table A.2.7. Counted numbers of benthic foraminifera of surface sediment samples from the western Adriatic Sea and the Gulf of Taranto. Colors display species that were grouped according to their microhabitat preferences with green marking Epifaunal Benthic Foraminifera (EBF), orange Shallow to Intermediate Infaunal Benthic Foraminifera (SIIBF) marking and blue marking Deep Infaunal Benthic Foraminifera (DIBF).

Appendix Table A.2.8. Results of the clay mineral measurements of the upper 19.5 cm of multi core GeoB15403-6.

Appendix Table A.2.9. Results of Carbon and Nitrogen measurements of bulk sediment samples of GeoB15403-4. One outlier was excluded from data interpretation and is marked in red.

Appendix Table A.2.10. Ca/Ti results from X-ray fluorescence (XRF) core scanning of gravity core GeoB15403-4.

Appendix Table A.2.11. Counted numbers of benthic foraminifera of gravity core GeoB15403-4 for the 8.2 ka interval. Colours display species that were grouped according to their microhabitat preferences with green marking Epifaunal Benthic Foraminifera (EBF), orange marking Shallow to Intermediate Infaunal Benthic Foraminifera (SIIBF) and blue marking Deep Infaunal Benthic Foraminifera (DIBF).

Appendix Table A.2.12. Number of benthic foraminifera taxa, Dominance (D) and Shannon Wiener diversity (H) calculated with PAST (PAleonological STatistics) after Hammer et al. (2001) and Hammer et al. (2008) of gravity core GeoB15403-4 for the 8.2 ka interval.

Appendix Table A.2.13. Results of stable isotope measurements on tests of living (bengal rose stained) foraminifera of surface sediment samples from the western Adriatic Sea and the Gulf of Taranto.

Appendix Table A.2.14. Results of stable isotope measurements on tests of benthic foraminifera from the 4.2 ka interval of GeoB15403-4.

Appendix Table A.2.15. Results of stable isotope measurements on tests of benthic foraminifera from the 8.2 ka interval of GeoB15403-4. One measurement marked in red was excluded from data interpretation due to a very low amount of sample material and thus low confidence level of the measurement.

Appendix Table A.2.16. Results of the clay mineral measurements of the 8.2 ka interval of gravity core GeoB15403-4.

Danksagung

Ich möchte mich zutiefst bei allen Menschen bedanken, die mich während der Entstehung dieser Arbeit begleitet haben.

An erster Stelle möchte ich mich bei Gerhard Schmiedl für die stete Unterstützung bedanken. Angefangen bei der Projektfindung und Beantragung des Stipendiums, über die fachliche Betreuung während der Laborarbeit, bis hin zu den fachlichen Diskussionen und Anregungen während des Verfassens der Manuskripte und der Dissertation.

Bei Uwe Mikolajewicz bedanke ich mich für die kritischen Fragen und wertvollen Anregungen und dafür, dass er sich stets Zeit für einen Blick auf meine Daten genommen hat.

Kay Christian Emeis möchte ich für die konstruktiven Anmerkungen während der Panel Meetings sowie für die Unterstützung bei der Organisation der Laborarbeit, bei der Beantragung von Stipendien und bei dem Verfassen dieser Arbeit danken.

Yvonne Milker danke ich ganz besonders für ihr stets offenes Ohr und ihre Hilfe bei sämtlichen technischen und fachlichen Fragen, egal ob diese morgens um 7 Uhr oder samstags vormittags gestellt wurden.

Bei Marc Theodor möchte ich mich für seine Unterstützung, die fachlichen Diskussionen und natürlich die geduldige Begutachtung meiner Uvigerinen bedanken.

Karin Zonneveld danke ich für die Bereitsstellung des Probenmaterials. Bei Werner Ehrmann bedanke ich mich für die Messungen der Tonminerale sowie die angeregten Diskussionen. Jürgen Möbius danke ich für die zahlreichen Diskussionen und Anmerkungen. Steffen Kutterolf und Julie Schnidlbeck danke ich für die durchführung der Mikrosondenmessungen und die gute Zusammenarbeit. Bei Andreas Mackensen und Nils Andersen möchte ich mich für die Durchführung der Isotopenmessungen bedanken. Niko Lahajnar und Frauke Langenberg danke ich für die Unterstützung und Durchführung der geochemischen Messungen. Bernd Zolitschka danke ich für die Durchführung der XRF scans.

Bei meinen beiden Bürokollegen Swaantje Brzelinski und Helge Arne Winkelbauer möchte ich mich für ihre Unterstützung bedanken und dafür, dass Sie so manchen langen Abreitstag kurzweilig erscheinen ließen.

Darüber hinaus danke ich der gesamten Arbeitsgruppe für ihre fachliche Unterstützung und die zahlreichen Gespräche, vor allem Ulrich Kotthoff, Sabine Prader, Katharina Müller-Navarra und Dorothea Bunzel.

Zu guter Letzt möchte ich mich bei meiner Familie für ihre moralische und finanzielle Unterstützung bedanken. Vor allem bei Marie, Petra, Hilde, Helmi, Irene und Walter. In Gedenken daran, dass mein Vater in dieser Zeit so plötzlich verstorben ist und die Abgabe

dieser Arbeit nicht mehr miterleben kann. Bei Baird möchte ich mich für seine Unterstützung in der Endphase der Arbeit bedanken und für sein Verständnis für meine langen Monologe über die Arbeit sowie für meine Prioritätensetzung in den letzten Monaten vor der Abgabe.
Der besondere Dank gilt natürlich Kristin und Maya. Maya danke ich für ihre stete gute laune und ihr Verständnis für meine arbeitsreichen Tage auch am Wochenende. Kristin danke ich für ihr uneingeschränkte Unterstützung, dafür das Sie mich mit gesundem Essen versorgt hat wenn mir auch eine Tiefkühlpizza gereicht hätte, für ihr offenes Ohr während meiner endlosen Monologe beim Verfassen der Manuskripte, für Ihr Verständis für meine immer straffer werdenden Zeitpläne und ganz besonders natürlich für ihre Freundschaft!

Eidesstattliche Versicherung:
Declaration on oath

Hiermit erkläre ich des Eides statt, dass ich die vorliegende Dissertationsschrift selbst verfasst und keine anderen Hilfsmittel als die angegebenen Quellen und Hilfsmittel benutzt habe.

I hereby declare, on oath, that I have written the present dissertation by my own and have not used other than the acknowledged resources and aids.

Hamburg, den

Valerie Menke